Elucidating the Molecular Architecture of the α_{1D}-AR:PDZ-Protein Macromolecular Complex

Dorathy-Ann Alyssa Harris

A dissertation submitted in partial fulfillment of the
requirements for the degree of

Doctor of Philosophy

University of Washington

2019

Reading Committee:

Chris Hague, Chair

Alexey Merz

Nephi Stella

Program Authorized to Offer Degree
Pharmacology

University of Washington

Abstract

Elucidating the Molecular Architecture of the α_{1D}-AR:PDZ-Protein Macromolecular Complex

Dorathy-Ann Alyssa Harris

Chair of the Supervisory Committee:
Christopher Hague
Department of Pharmacology

G Protein-Coupled Receptors (GPCRs) are seven transmembrane proteins that are the targets for over 30% of all medications currently on the market. Adrenergic Receptors (ARs) are one type of GPCR that responds to the endogenous catecholamines norepinephrine (NE) and epinephrine(Epi). In the AR family, there are three types: α_1-, α_2-, and β-ARs. Within each of these subfamilies are three subtypes and the Hague lab focuses one of these receptors: the α_{1D}-AR. The α_{1D}-AR is an interesting receptor in that it is very difficult to study due to its intracellular localization. There are no known cell lines that express endogenous α_{1D}-ARs and within 48 hours after removing epithelial cell expressing the α_{1D}-AR at the membrane, the receptor becomes localized to the endoplasmic reticulum (ER).

Studying the α_{1D}-AR is clinically important as there are many disorders that are influenced by this receptor. For example, it can impact urine flow in older males, due to benign prostate hypertrophy (BPH). The α_{1D}-AR is also vital in the circulatory system in repairing blood vessels after injury as well as stimulus-induced movement. Also of note is the role the α_{1D}-AR plays in both schizophrenia and post-traumatic stress disorder (PTSD, Raskind et. al. 2018). It has been noted that treatment with antagonists will decrease the reoccurrence of nightmares in veterans with PTSD. However, most antagonists have major toxic side effects that are associated with taking these medications. Thus, it is vital to determine how the α_{1D}-AR signals with its PDZ and

non PDZ proteins as a potential to create new therapeutics for PTSD, schizophrenia, BPH, and cardiovascular disease.

Previously, the Hague laboratory determined that there may be a cell line that endogenously expresses the α_{1D}-AR. Through mass spectrometry, it was determined that SW480 cells (a colorectal cancer cell line; CRC) express interacting proteins that have been previously shown to interact with the α_{1D}-AR. Thus, I proposed to determine if this cell line *does* endogenously express the α_{1D}-AR.

Unfortunately, it was determined that the α_{1D}-AR is *not* present in SW480 cells; instead the most common receptor discovered was the α_{1B}-AR. This was apparently inconsistent with the only other paper (Masur et. al. 2001) that attempted to characterize the ARs present in SW480 cells and their role in cancer. When we attempted to use traditional methods, such as radioligand binding, we were also unable to detect this receptor. Thus, we concluded that the EPIC Dynamic Mass Redistribution (DMR) technology is able to detect previously imperceptible, low density receptors.

The Hague laboratory has also determined that the α_{1D}-AR must form a homodimeric macromolecular structure to even retain plasma membrane localization. Specifically, the α_{1D}-AR interacts with the PSD95/DLG1/Zo-1 (PDZ) domain proteins syntrophin and Scribble (SCRIB) via a PDZ-ligand on its C-terminus (CT) in all human cell lines screened to date. This interaction was unique as no other GPCRs interacted with syntrophins or Scribble.

Interestingly, in only one of the cell lines screened, it was also discovered that there are three additional proteins that interact with the α_{1D}-AR. These proteins are calcium/calmodulin-dependent protein kinase (CASK), human disks large 1 (hDLG1), and LIN7A. Previous research has shown that hDLG1 and LIN7A can also associate with another membrane-associated guanylate kinase (MAGUK) protein, MPP7. Thus, I proposed to biochemically determine the

architecture of the α_{1D}-AR:PDZ protein complex and determine the functional purpose of these PDZ proteins.

Based on our data, it appears that SCRIB binds the α_{1D}-AR with the highest affinity (0.07 μM), particularly PDZ domains 1/4 (0.78 and 1.38 μM, respectively). Syntrophins bound with the next highest affinity (0.56 μM) followed by hDLG1 (0.72 μM). CASK did bind, but at very low affinity (2.13 μM) and neither LIN7A nor MPP7 appeared to bind. It is yet unclear how the hDLG1 tripartite complex interacts with the α_{1D}-AR, whether it be as a transport or scaffolding complex.

All the PDZ proteins that seem to interact with the α_{1D}-AR are basolateral proteins and involved in either scaffolding or localization. To determine which membrane the α_{1D}-AR is actually localized to, we needed to find a reliable three-dimensional (3D) methodology to use as a model to conduct our experiments. I proposed to use several different methods; a hydrogel method (such as Corning Life Science's Matrigel) and a non-adherent method (such as Corning Life Science's Spheroid Microplate) to find the most consistent methodology for forming our 3D structures.

Matrigel proved to be inconsistent for our model cell type; HEK293T cells. This is likely due to the length of time necessary to form the spheroid and lumen. However, the spheroid microplate proved to be efficient and fast in the formation of our spheroids. Interestingly, I noticed the α_{1D}-AR at the surface of the membrane, something that is not seen in two-dimensional (2D) cells. I was determined to see if this correlated to an increase in pharmacodynamic properties, and indeed, it *did* show a significant increase in both EC_{50} and Emax. Our data, combined, seems to indicate an intricate macromolecular complex of PDZ and non-PDZ proteins that are vital for polarization of the cells and localization to the proper membrane. These data open a whole new

field of questions in fundamental cell biology and open the door to novel therapeutics that can target any number of new sites.

TABLE OF CONTENTS

LIST OF FIGURES

LIST OF TABLES

ACKNOWLEDGEMENTS

I would like to thank Dr. Christopher Hague for all his mentorship, help, and guidance throughout my undergraduate and graduate career. I would also like to thank Eric Janezic for all his help both with experiments and with his mentorship and friendship. I want to thank Dr. Chris Hague, Dr. Nephi Stella, Dr. John Scott, and Dr. Alexy Merz for being on my supervisory committee. I would also like to thank all past and current Hague Lab members for all their hard work and support. I would like to thank my family and friends for their continual support and encouragement in me and my work, in particular my parents, James and Brenda Harris, and Jenna Grillo. I would also like to thank Ashlynn and Jazz for offering suggestions in writing and emotional support. Lastly, I want to thank my husband and partner in crime, Abrian Brewder, for constantly loving and encouraging my growth, both inside and outside of work.

DEDICATION

I dedicate this work to my parents and my husband. Without their support, guidance, and love, this work would not have been possible.

Chapter I – Introduction and Background

G Protein-Coupled Receptors

Interestingly, the idea that drugs bind to specific sites and/or receptors on cell surfaces can be traced back to Paul Ehrlich (1854-1915) in Germany who used dyes to visualize biological structures (Drews, 2004). Since then, four major classes of receptors have been identified that signal after binding an endogenous ligand. These include tyrosine kinase receptors, nuclear receptors, ion channels, and G Protein-Coupled Receptors (GPCRs) (Figure 1.1). Tyrosine kinase receptors are high affinity, cell-surface receptors for growth factors, cytokines, and hormones. With an extracellular N-terminal region, and an intracellular C-terminal region (Hubbard. 1999), these receptors are key regulators of endocrine signaling, development, and cancer (Zwick et. al. 2001). Nuclear receptors are vital for sensing steroid and thyroid molecules to regulate the expression of specific genes and are thus transcription factors (Evans. 1988, Olefsky. 2001). Ion channels are pore-forming membrane proteins that allow for the passage of ions to establish a resting membrane potential (Hille 1985).

GPCRs are characterized by their seven transmembrane (TM) spanning domains. Historically, GPCRs have been a major target for medications and are still the target of ~34% of all current FDA approved medications with 475 drugs that act at 108 unique GPCRs (Hauser et. al. 2017). GPCRs are among of the most diverse receptors and sense signaling molecules such as light, odorants, lipids, proteins, and sugars (Venkatakrishnan et. al. 2013).

Around 4% of human DNA encodes GPCRs; a startling amount. This encodes around 340 genes and 1000 human receptors, each of which tends to be highly specific for their ligands (Bockaert et. al. 2003). Of the various types of GPCRs, they are classified into 4 families – Rhodopsin receptor family (Class A), Secretin /Adhesion receptor family (Class B), Glutamate/Pheromone

receptor family (Class C), and the Frizzled/Taste 2 receptor family (Figure 1.2, Largerstrom et. al. 2008). Of the various families, the Rhodopsin receptor family is the largest and contains a conserved structure.

The structure of a typical GPCR consists of the N-terminus (NT), three extracellular loops (ECL1-ECL3), the TM regions (of which there are 7), three intracellular loops (ICL1-ICL3), an intracellular amphipathic helix (H8), and a C-terminus (CT, Largerstrom et. al. 2008).

The TM region consists of seven α-helices. The extracellular region of the membrane is important in receptor stability due to the presence of disulfide bridges, particularly one in TM3 that connects to EL2. This structure is conserved among most GPCRs. This disulfide bridge anchors the receptor to the extracellular matrix (ECM) and limits the extent of structural changes with receptor activation (Wheatley et. al. 2011). As such, it is suggested that TM3 is important in maintaining the fold of the receptor, both before and after receptor activation. Depending on the size of the ligand, it will penetrate the binding pocket at different depths and can even bind to some ECLs (Venkatakrishnan et. al. 2013). However, TM3, TM6, and TM7 (also highly structurally conserved) form a scaffold for the ligand-binding pocket, which conveys ligand specificity.

The intracellular region and the cytoplasmic ends of the TM regions bind the downstream heterotrimeric G proteins, GPCR kinases, and arrestins (Venkatakrishnan et. al. 2013). Interestingly, a short amphipathic helix (H8) is present in several class A GPCR structures and may be important in G protein binding despite its lack of contact with the G protein.

GPCRs bind heterotrimeric G proteins, comprised of a beta (β), gamma (γ), and an alpha (α) subunit. When a ligand binds, the GPCR undergoes a conformational change, which exposes the GDP/GTP binding site on the α-subunit (Bockaert et. al. 2003). When exposed, GDP is exchanged for GTP and the α-subunit dissociates from both the receptors and the β– and γ–

subunits. The β– and γ– subunits can activate other signaling mechanisms, but the α-subunit determines the major signaling event for the GPCR.

Adrenergic Receptors

Adrenergic Receptors (ARs) are part of the Rhodopsin-like receptor class that responds to the endogenous catecholamines norepinephrine (NE) and epinephrine (Epi). There are three classes of adrenergic receptors: α_1-ARs, which signal through $G\alpha_{q/11}$; α_2-ARs, which signal through $G\alpha_{i/o}$; and β–ARs, which signal through $G\alpha_s$ (Figure 1.3, Strosberg, 1993). In each of the classes of receptors, there are three subclasses of receptors characterized by structural and functional differences (Rosenbaum et. al. 2009). The α_1-ARs include the α_{1A}-AR, α_{1B}-AR, and α_{1D}-AR. The α_2-ARs include α_{2A}-AR, α_{2B}-AR, and α_{2C}-AR. The β–ARs include β1-AR, β2-AR, and β–3AR (Interestingly, β2 and β3 can also couple to $G\alpha_{i/o}$ in addition to $G\alpha_s$, Perez et. al. 2006). These receptors are vital in the function and maintenance of both the neuroendocrine and cardiovascular systems and are the targeted by some of the most commonly prescribed medications in the United States (Molinoff 1984, Fuentes et. al. 2018). For example, α_2-ARs are expressed abundantly on sympathetic presynaptic nerve terminals, where they play a critical role in the negative-feedback loop regulating NE release. Thus, medications targeting α_2-ARs are used often to treat hypertension (agonists), impotence, and depression (antagonists, Perez et. al. 2006). β-ARs are expressed in the heart, kidney, stomach, bronchioles, and adipose tissue and can be used as a target for heart failure, bronchodilation (agonists), arrhythmia, coronary heart disease (CAD), glaucoma, and stage fright (antagonists, Perez et. al. 2006).

Lastly, α_1-ARs are responsible for smooth muscle contraction and vasoconstriction (Schmitz et. al. 1981, Piascik et. al. 2001). These receptors can be found in the skin, gastrointestinal (GI)

system, prostate, urinary bladder, brain, kidney, uterus, and bronchioles (Schmitz et. al. 1981, Piascik et. al. 2001, Chou et. al. 2003). Medications targeting α_1-ARs include agonists for vasoconstriction, hypotension, decongestants, and weight loss while antagonists are used for vasodilation, hypertension, antipsychotics, post-traumatic stress disorder (PTSD) and benign prostatic hypertrophy (BPH, Piascik et. al. 2001).

Adrenergic Receptors in Cancer

Every year, there are about 439 new cancer incidences among every 100,000 people in the United States and is the leading cause of death (National Cancer Institutes, Lu'o'ng et. al. 2012). Some of the most common, and deadly, forms of cancer include breast cancer, colorectal cancer (CRC), renal cancer and prostate cancer and will take the lives of about 140,000 people in the United States alone (National Cancer Institutes). In particular, CRC is the third and fourth most common cancer among women and men, respectively and the leading cause of cancer-related deaths worldwide (Parkin et. al. 2005, Jemal et. al. 2010, Chin et. al. 2015)

Medications do exist to target various adrenergic receptors in several of these cancer types including breast, endometrium, ovarian, urothelial, colorectal, lung, and thyroid cancer (Rains et. al. 2017). Historically, the most studied ARs for cancer are the β-ARs and it seems that antagonists to these receptors can provide a beneficial clinical effect for patients (Lu'o'ng et. al. 2012, Chin et. al. 2015). Stress-upregulation of catecholamine stimulation to β-ARs, particularly β1/2-ARs, accelerate the progression of various cancers, such as CRCs and breast cancer (Wang et. al. 2015, Chin et. al. 2015, Rains et. al. 2017). Additionally, β-antagonists appear to exert their anti-cancer effects via the β2-AR, which induces cell cycle arrest and suppressed cell viability when activated by endogenous catecholamines (Lu'o'ng et. al. 2012, Chin et. al. 2015, Wang et. al. 2015).

There have been limited studies performed examining the effects of medications targeting α2-ARs in cancer patients. Due to the inhibitory effect on sympathetic NE release produced by α_2-AR stimulation it would be logical to predict that α_2-AR agonists may diminish tumor growth by indirectly blocking β-AR activation (Lamkin et. al. 2014). However, published studies have produced conflicting results. For example, prolonged treatment with the highly selective α_2-AR agonist (dexmedetomidine, DEX) increased tumor growth and metastasis (Pinero et. al. 2012, Szpunar et. al. 2013, Castillo et. al. 2017), indicating additional studies are necessary to establish the role of catecholamines and adrenergic receptors in regulating tumor growth.

Another adrenergic receptor family that is largely unstudied in the field of oncology includes the α_1-ARs, despite its prominent expression in liver, prostatic, renal and ovarian cancer biopsies as observed by histological staining (The Human Protein Atlas). Interestingly, a previous study suggests α_1-AR subtypes may perform specific roles, where long-term activation of the α_{1A}-AR subtype decreases cancer incidence, whereas the α_{1B}-AR enhances (Collette et. al. 2014). Additionally, signal-transduction cross-talk between the α_{1D}-AR and the transient receptor potential vanilloid type 1 (TRPV1) increases prostate cancer proliferation rate (Morelli et. al. 2014). Thus, it is clear that additional studies are needed.

The α_{1D}-Adrenergic Receptor

The α_1-AR family of GPCRs contains 3 subtypes (the α_{1A}-AR, α_{1B}-AR, and α_{1D}-AR) but only one of these subtypes, the α_{1D}-AR, contains a Type I PDZ ligand (amino acid sequence: REDTI). This receptor is found in the prostate, coronary arteries, and the hippocampus and thus is important in memory, hypertension, CAD (Jensen et. al. 2015) benign prostate hypertrophy, bladder obstruction (Lepor. 2007, Schwinn et. al. 2009), schizophrenia, and post-traumatic stress disorder (Clark et. al. 2006, Olson et. al. 2011 Simon et. al. 2017). While these disorders are

varied, they represent important clinical drug targets. Deleterious side effects (orthostatic hypotension and reflex tachycardia) are often observed with chronic use of non-selective α1-AR antagonists.

Of all the adrenergic receptors, the α_{1D}-AR has been one of the most difficult to study, primarily because endogenous functional α_{1D}-ARs have yet to be identified in any human cell line. Additionally, α_{1D}-AR cDNA transfection results in the receptor's intracellular sequestration and weak functional responses. This is because while the α_{1A}-AR and α_{1B}-AR localize to the plasma membrane, the α_{1D}-AR is contained within the endoplasmic reticulum (Figure 1.4 A-C, Hague et. al. 2004, Fan et. al. 2009). Interestingly, the Hague lab has discovered that by truncating the N-terminus of the receptor (Figure 1.4 D), it is possible for the receptor to localize to the membrane, which increases the pharmacodynamic properties of the receptor.

In a series of elegant experiments, Fan et. al. (2009) showed the sequestration of the α_{1D}-AR inside cells within 48 hours post aortic dissection from a rat. These experiments may provide a key clue as to why this sequestration occurs with the α_{1D}-AR as within 48 hours post dissection there is a loss of cell polarity.

Since 2006, the Hague lab has made significant progress in understanding the cellular and molecular mechanisms regulating α_{1D}-AR expression. First, it was discovered the α_{1D}-AR uses the Type I PDZ-ligand (REDTI) located on its C-terminal domain (CT) to binds the syntrophin family of PDZ proteins (α, β1, and/or β2). In the decade that followed, tandem-affinity purification/mass spectrometry (TAP/MS) demonstrated that syntrophins recruit multiple members of the dystrophin-associated protein complex (DAPC) to the α_{1D}-AR, including utrophin, dystrobrevin, dystrophin (Lyssand et. al. 2008), and α-catulin (Lyssand et. al. 2010). Then in 2015, the multi-PDZ domain scaffold Scribble (SCRIB) was discovered to be an additional member of the complex (Camp et. al. 2015). Interestingly, SCRIB contains 4 PDZ

domains, indicating that it might bind up to four α_{1D}-ARs at the membrane. This presents the opportunity for precise molecular scaffolding of the receptor at specific microdomains in polarized cells. Remarkably, we demonstrated that α_{1D}-ARs are organized as homodimers, with one α_{1D}-AR protomer bound to the DAPC:syntrophin complex, and the other bound to SCRIB. Proteomic screening of α_{1D}-AR across 6 human cancer cell lines revealed the α_{1D}-AR ubiquitously interacts with syntrophins and SCRIB. However, in one cell type, SW480 colon carcinoma cells, the α_{1D}-AR interacted with 3 additional PDZ proteins: human Disks Large 1 (hDLG1), calcium/calmodulin-dependent serine protein kinase (CASK), and LIN7A (Table 1.1, Camp et. al. 2015). This surprising discovery, that the α_{1D}-AR can interact with no less than 5 PDZ proteins in a single human cell line, implies the α_{1D}-AR may be simultaneously expressed as multiple, functionally distinct macromolecular complexes (Figure 1.5).

PDZ Proteins and the α_{1D}-AR Complex

Thus far, proteins that we have identified to interact with the α_{1D}-AR include syntrophins (Lyssand et. al. 2006), SCRIB, hDLG1, LIN7A, and CASK (Camp et. al. 2015). The PDZ domains of each of these proteins is expected to bind the Type I PDZ ligand located on the distal CT of the α_{1D}-AR (REDTI). Interestingly, CASK is predicted to bind Type II PDZ ligands, raising the possibility that it is being indirectly recruited to the complex by one of the other PDZ interactors (Bezprovanny et. al. 2001). PDZ domains typically bind the last 4-6 amino acids on the CT of a protein. The PDZ domain structure has a globular module formed by six β strands and two α helices, which forms a CT peptide binding groove. Type I PDZ domain bind the S/T-X-Φ target sequence (in which Φ is a hydrophobic residue) and type II PDZ domains bind the Φ-X-Φ target sequence. These proteins are vital for localization, transport, and expression of

various proteins (Fuh et. al. 2000, Bezprozvanny et. al. 2001, Tonikian et. al. 2008, Lee et. al. 2010).

PDZ domains are protein-protein recognition modules that play a critical role in the organization of signaling complexes through transport, localization, and assembly of supramolecular complexes (Harris et. al. 2001). These PDZ domains have also shown prevalence in regulating the transport of membrane proteins during the process of cell polarization, and thereby regulate the signaling of key medical targets. Thus, potential exists for PDZ proteins to one day become a target for novel medications (Dev 2004, Ivarson et. al. 2013).

Syntrophins comprise three unique, genetically distinct isoforms (α, β, γ), Each are core components dictating the architecture of neuromuscular junctions due to their essential role in scaffolding the dystrophin-associated protein complex (DAPC). Structurally, syntrophins contain two pleckstrin homology (PH) domains, a PDZ domain that can facilitate homo- and heterodimerization with other PDZ proteins, and a syntrophin unique (SU) domain (Adams et. al. 1993, Ehmsen et. al. 2002).

Loss-of-function mutations in the DAPC lead to the development of the lethal muscle-wasting disorder, Duchenne muscular dystrophy (MD, Ehmsen et. al. 2002). The DAPC is thought to play a primary structural role in the neuromuscular junction by linking structural rearrangements of the actin cytoskeleton system to cellular movement along the extracellular matrix (Peterof et. al. 1993). The largest member of the complex, Dystrophin, is a 427 kDa protein containing an NT actin-binding domain, a central rod domain, and a cysteine-rich CT that facilitates formation of the DAPC (Jung et. al. 1995, Ehmsen et. al. 2002). Another member of the complex, dystrobrevin, has two isoforms (α- and β-dystrobrevin) and is highly expressed in brain, skeletal, and cardiac muscle with low levels in the liver, lung, and pancreas. The NT portion of dystrobrevin has been shown to link the sarcoglycan-sarcospan to the DAPC (Yoshida et. al.

2000). Utrophin is a homologue of dystrophin but is expressed in a reciprocal manner, despite having many of the same protein-binding properties (Blake et. al. 1996).

hDLG1 is a promiscuous PDZ protein that forms multiple tripartite complexes. The first, found expressed at the apical membrane of polarized cells, includes hDLG1:LIN7A: MPP7. hDLG1 also forms two additional tripartite complexes that express at the basolateral membrane; hDLG1, lethal giant larvae (LGL), and SCRIB (and acts primarily as a scaffolding complex) and hDLG1, LIN7A, and CASK (and acts as either a scaffolding or transport complex) (Lozovatsky et. al. 2009). Thus, it may be possible that hDLG1 anchors to the α_{1D}-AR as tripartite complex, presumably to direct trafficking of the receptor to a distinct membrane in polarized cells. Additionally, SCRIB, MPP7, CASK, and hDLG1 are categorized as membrane-associated guanylate kinases (MAGUKs), and comprise of a PDZ-SH3-GUK tandem domain at the C-terminal of the protein. Mutations in MAGUK proteins are linked to many human diseases including cancer, psychiatric disorders, and intellectual disabilities (Hseuh. 2006, Gardoni. 2008, Ivanova et. al. 2011). These proteins play important roles in cell polarity establishment and maintenance, cell adhesions, and intracellular signal transductions.

The PDZ protein MPP7 was not pulled down with the other PDZ proteins in our proteomic screen (Table 1.1, Camp et. al. 2015). Many MAGUK proteins, such as MPP7, also contain an L27 domain (Lozovatsky et. al. 2009). MPP7 contains 2 L27 domains, L27N and L27C (Stuke et. al. 2007)). Stuke et. al. (2007) suggests that CASK and MPP7 compete for the same binding site on hDLG1 and, depending on the levels of CASK in various cell lines, could be hard to detect (Stuke et. al. 2007). This could explain why we did not detect it in our proteomic screens.

2D vs. 3D Cell Culture

Historically, two-dimensional (2D) cell culture has predominated the field, particularly due to the availability and use of human cells to study disease and assess the characteristics of therapeutic agents (Duval et. al. 2017). This approach provides numerous benefits, such as low cost of maintenance, ease of use and manipulation, and ease of use in high throughput screens. There are just as many drawbacks to this methodology, however. These cells lack a third-dimension (3D) structure, meaning the cells lack polarization, cell-cell adhesion events and communication, and a cell-ECM interaction that mimics an *in vivo* environment (Table 1.2, Rodriguez-Boulan et. al. 1989, Duval et. al. 2017, Boussommier et. al. 2018).

Conversely, animal models provide a traditional substitute to 2D cell culture. These models address many of the concerns of 2D cell culture, principally the inability to have a full model organism (Boussommier et. al. 2018). A major drawback to this model is that it can prove to be highly expensive, time consuming, and lacks the same anatomy and physiology as humans (Hartung, 2008, Hoarau-Vechot et. al. 2018).

An alternative to both of these methodologies is using 3D cell culture (Figure 1.6, Table 1.2). These methods provide a system that deviates less from *in vivo* responses by providing cell-cell and cell-ECM contact as through the formation of polarized cells (Duval et. al. 2017). Polarity refers to the asymmetric distribution of proteins that allow the cells to form organized membrane subdomains for specialized functions including secretion, filtration, absorption, and sensory function (Rodriguez-Boulan et. al. 1989). The formation of polarity is established by an intricate network of protein-protein interactions (Ahlstrom et. al. 2014).

There are many protein complexes that control epithelial polarity, but there are three major classifications in which these complexes are organized (Figure 1.7). The first is the Crumbs complex, which is comprised of Crumbs (Crb) proteins, proteins associated with Lin-7

1(PALS1) and PALS1-associated with tight junction protein (PATJ) and leads to the formation of the apical membrane (Pieczynski et. al. 2011).

The second major complex is the Par complex which is comprised of proteins partitioning defective-3 (Par3), partitioning defective-6 (Par-6) and aPCK. The Par complex is a cornerstone of apico-basolateral polarity by regulating the formation of the tight junctions (TJ). The last major complex is the Scribble complex, which is comprised mostly of SCRIB, hDLG1 and lethal giant larvae (Lgl). Typically, the SCRIB protein complex localizes to the basolateral membrane, although an additional heterotrimeric protein complex containing hDLG1, MPP7, and LIN7A has been observed at the apical membrane, where it impacts the formation of adherins junctions (Bohl et. al. 2007, Stucke et. al. 2007). A complex of hDLG1, CASK, and LIN7A has been observed at the basolateral membrane and may play a role in transporting receptors to the membrane (Lozovatsky et. al. 2009, Lin et. al. 2013). In general, the apical membrane forms first and antagonism by basolateral proteins leads to the switch that forms the basolateral membrane (Ahlstrom et. al. 2014).

There have been several 3D cell model systems to study polarized cells. The most traditional method for studying 3D cell culture was to use Madin-Darby Canine Kidney (MDCK) cells. This cell line has been used for a variety of studies including cell polarity, cell-cell adhesions, cell motility, and growth factor responses (O'Brien et. al. 2002).

The most common current model system is spheroid formation. There are many techniques in this category such as microfluidics (such as Organs-on a chip), hydrogels (such as Corning Life Science's Matrigel), hanging-drop culture, and non-adherent surface methods (Hartung, 2008, Duval et. al. 2017, Hoarau-Vechot et. al. 2018).

The hanging-drop method was originally used to study bacteria in a confined and control environment. The cells accumulate at the tip of the drop and will eventually form a spheroid

(Hoarau-Vechot et. al. 2018). In contrast, the organ-on-a-chip allows for formation of organoid-like environments that can be linked to determine the effects of drugs on various organ systems (Zhang et. al. 2018). Hydrogels form the cell-ECM interaction though the presence of laminin in the gel, which forces the lumen to form in the center of the spheroid (Hoarau-Vechot et. al. 2018). Lastly, the non-adherent surface method includes ultra-low attachment plates (ULA). These 96 well rounded-bottom plates are coated with a hydrogel that prevents the adherence of the cells, which instead, form a spheroid (Bergeron et. al. 2017).

Epithelial to Mesenchymal Cell Transitions

An epithelial to mesenchymal transition (EMT) is a biological process that allows a polarized epithelial cell affixed to the ECM to undergo a biochemical change to the mesenchymal cell phenotype for migratory events, whether these be during embryonic morphogenesis or in disease states (Kalluri et. al. 2009, Thiery et. al. 2009, Ahlstrom 2014). There are three major classifications of EMTs, each of which correlates to distinct biological settings (Figure 1.8).

EMT Type 1 is typically observed during developmental phases, such as implantation, embryo formation, and organ growth (Kalluri et. al. 2009, Kim et. al. 2018). This type of EMT does not have an invasive phenotype or lead to organ fibrosis. Unique to this type of EMT is the diverse cell types that may then undergo a mesenchymal to epithelial transition (MET), to then form a secondary and even tertiary epithelial cells that form the basis for various organs (Kim et. al. 2018).

Type 2 EMTs are associated with wound repair, tissue regeneration, and organ fibrosis. These EMTs are usually associated with an immune response following trauma and inflammatory injury (Kalluri et. al. 2009, Stone et. al. 2016). Fibrosis is essentially un-abated tissue repair that

is caused by persistent inflammation which allows for myofibroblast persistence (Stone et. al. 2016, Kim et. al. 2018).

Lastly, Type 3 EMTs are largely a carcinogenic form in which cancerous cells highjack the normal biological process to lead to metastasis (Kalluri et. al. 2009, Heerboth et. al. 2015). Overexpression of various EMT signatures change the epithelial polarity so that the tumor cells may acquire mesenchymal cell traits that leads to the migration from a primary tumor to a secondary location (Kim et. al. 2018).

The process of undergoing an EMT involves several important factors. First, disruption of cell-cell adhesion molecules such as E-Cadherins (adherens junctions) and occludins (tight junctions) in the lateral membrane (Ahlstrom et. al. 2014). Next, there needs to be a disruption in the cell-ECM adhesion in which the interaction between integrins and fibronectin/laminin/collagen is severed (Ahlstrom et. al. 2014). Lastly, the polarity of the cell must be disrupted by inactivating the molecules that establish cell polarity (Ahlstrom et. al. 2014).

Abbreviations: GPCR, G Protein-Coupled Receptor; ECL, extracellular loops; ICL, intracellular loops; ECM, extracellular matrix; AR, Adrenergic Receptor; NE, norepinephrine; Epi, epinephrine; CAD, coronary artery disease; GI, gastrointestinal; PDZ, X; 2D, two-dimensional; 3D, three-dimensional; Crb, Crumbs; PALS1, proteins associated with Lin-7 1; PATJ, PALS1-associated with tight junction protein; TJ, tight junctions; SCRIB, Scribble; hDLG1, human disks large 1; Lgl, lethal giant larvae; ULA, ultra-low attachment; TAP/MS, tandem-affinity purification/mass spectrometry; MPPs, palmitoylated membrane proteins; DEX, X; TRPV1, X; CRC, colorectal cancers; MD, muscular dystrophy; CASK, X; NT, N-terminal.

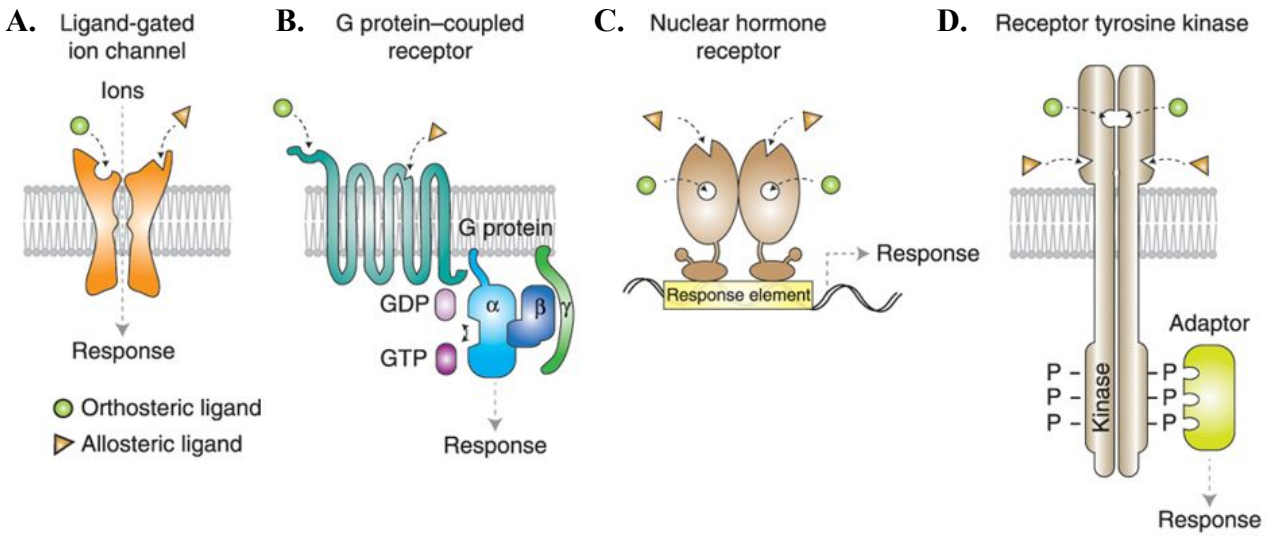

Figure 1.1. Various types of signaling receptors. A. Ligand-gated ion channels. B. G protein-coupled receptors. C. Nuclear hormone receptor. D. Tyrosine kinase receptor. Smet et. al. 2014.

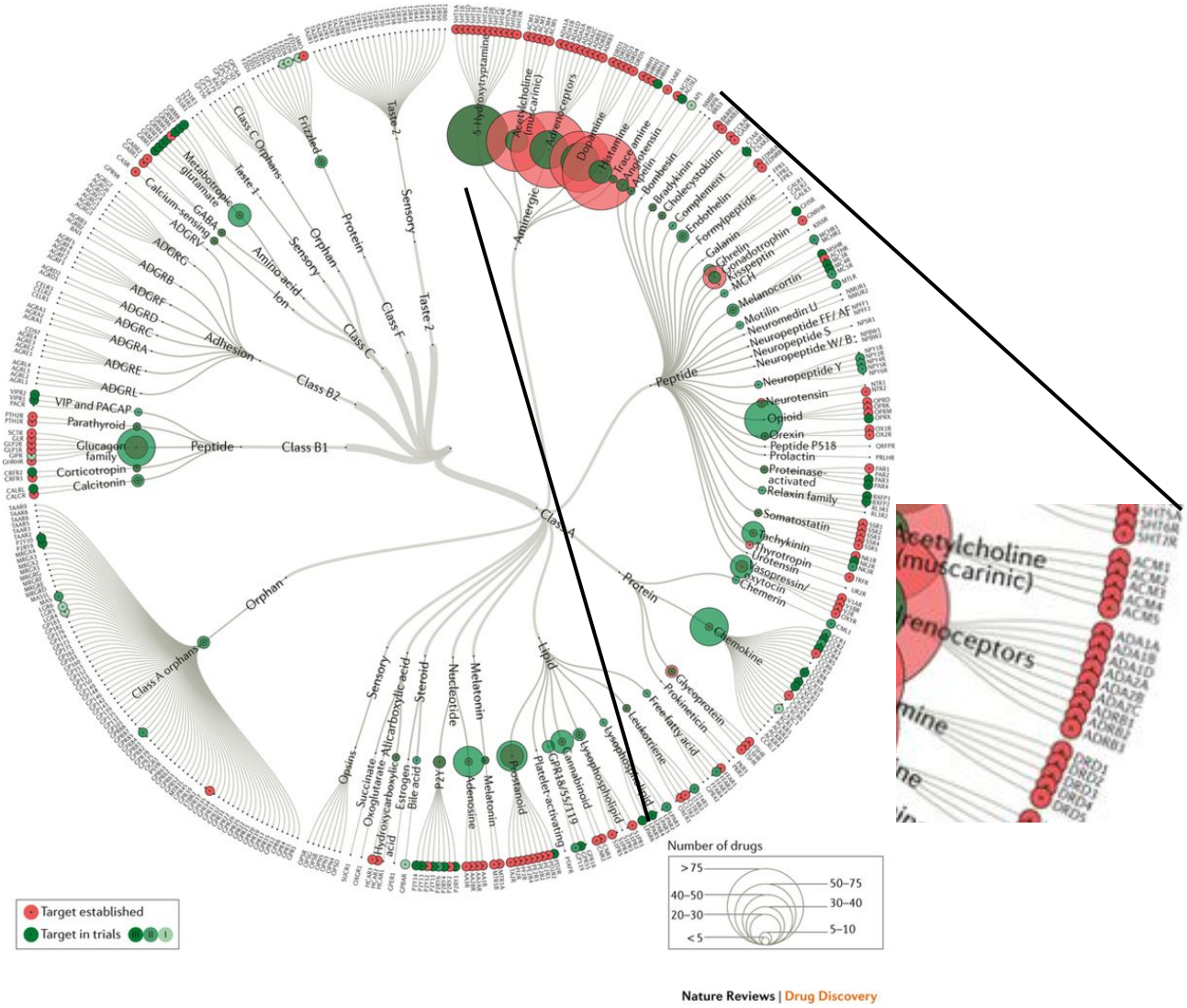

Figure 1.2. Classes of GPCRs. Inset shows the various subtypes of adrenoceptors. Hauser et. al. 2017.

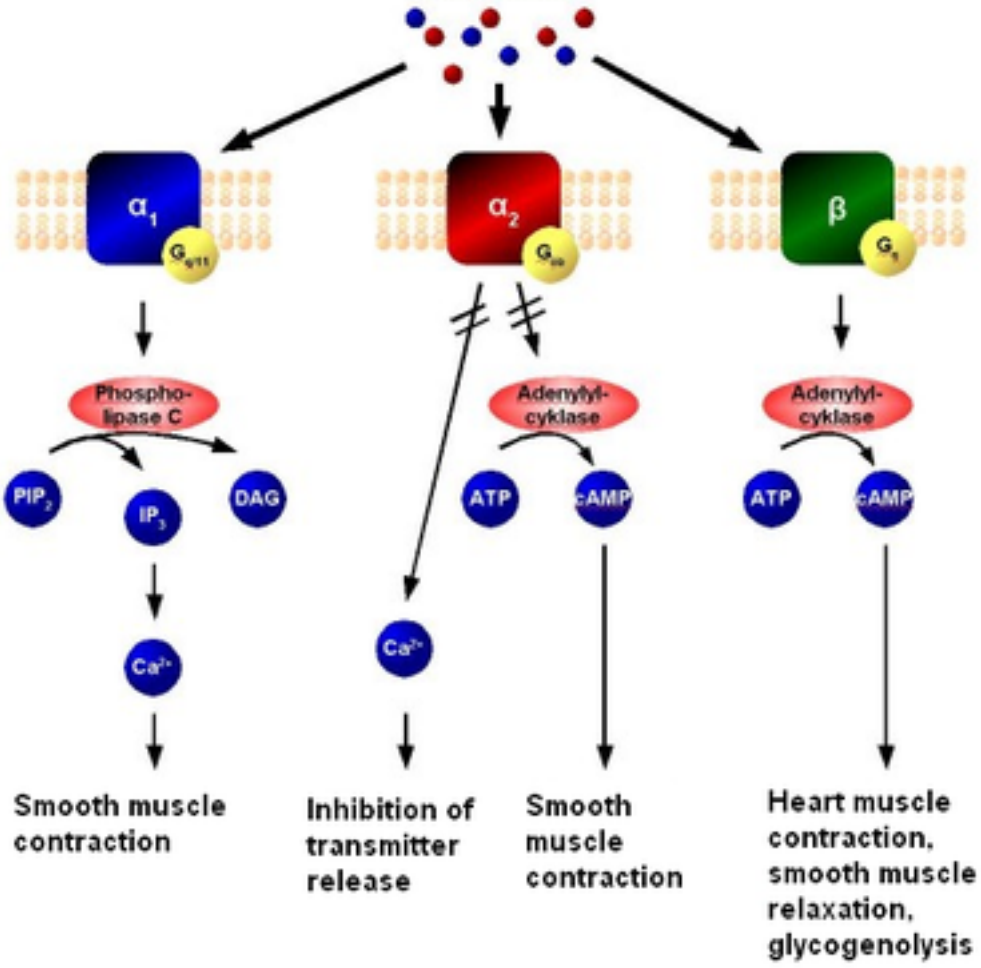

Figure 1.3. Adrenergic Receptors and their Downstream Signaling Cascades. Various adrenergic receptor subtypes, their downstream signaling cascades, and the physiological functions. Gordon 2018.

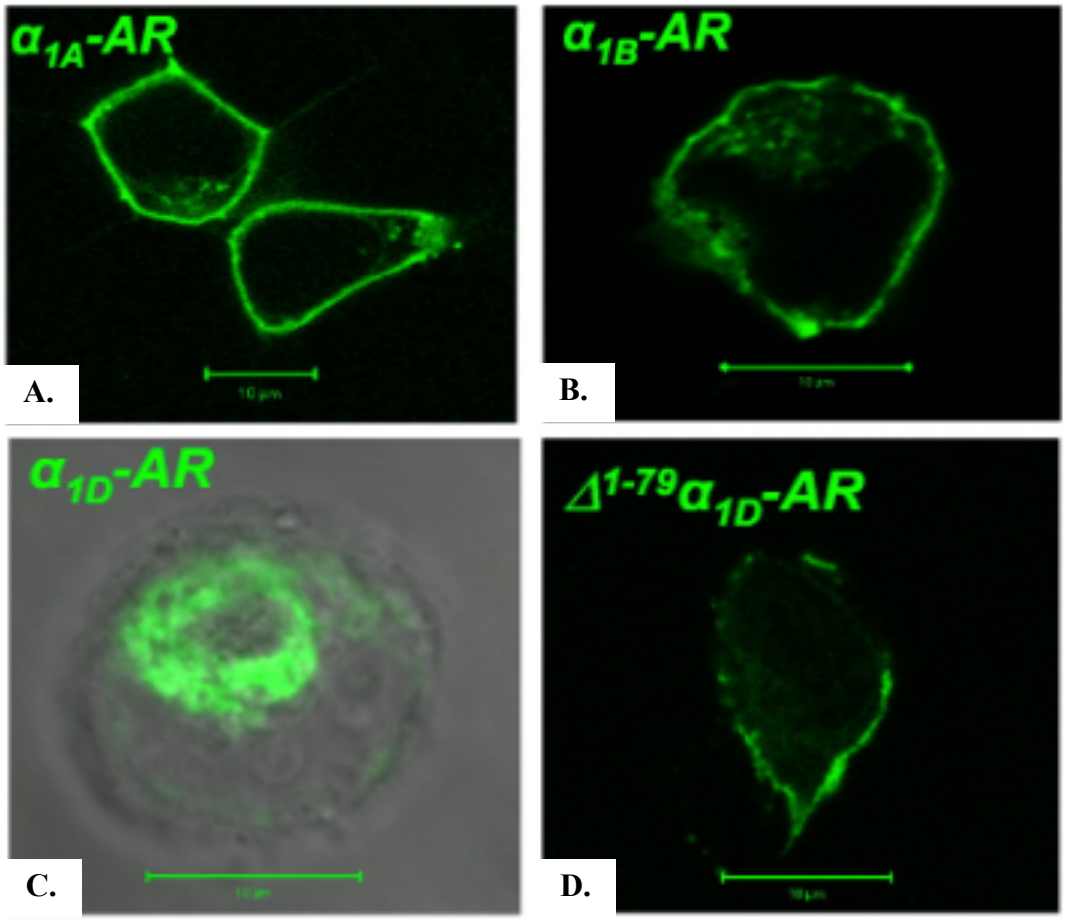

Figure 1.4. Expression of α_1-ARs in the cell. A. GFP-tagged α_{1A}-AR expresses at the membrane of cells. B. GFP tagged α_{1B}-AR expresses at the membrane of cells. C. GFP-tagged full-length α_{1D}-AR is sequestered into the endoplasmic reticulum. D. N-terminal truncation returns the GFP-tagged α_{1D}-AR to the membrane. Hague et. al. 2004.

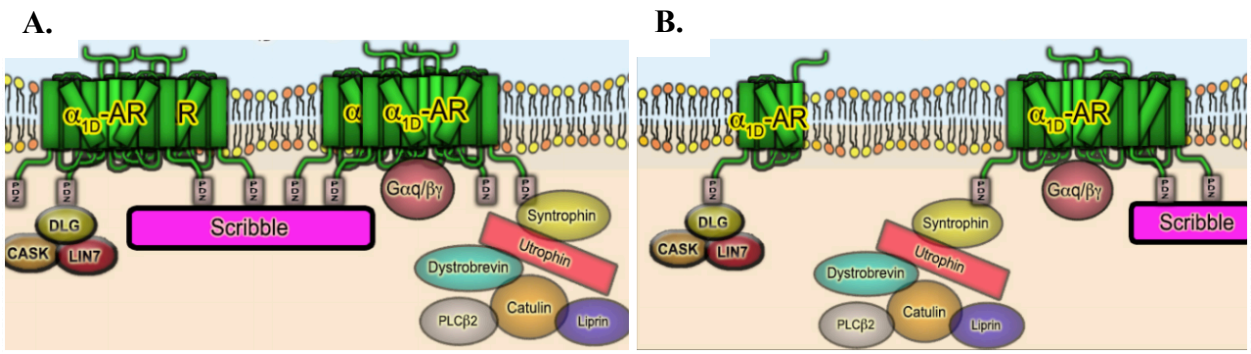

Figure 1.5. Potential architectures of the α_{1D}-AR and its interacting proteins. The α_{1D}-AR can bind to hDLG, CASK, LIN7A, syntrophin, and SCRIB. A. One large macromolecular network of PDZ and non PDZ proteins. B. Multiple complexes binding PDZ and non PDZ proteins.

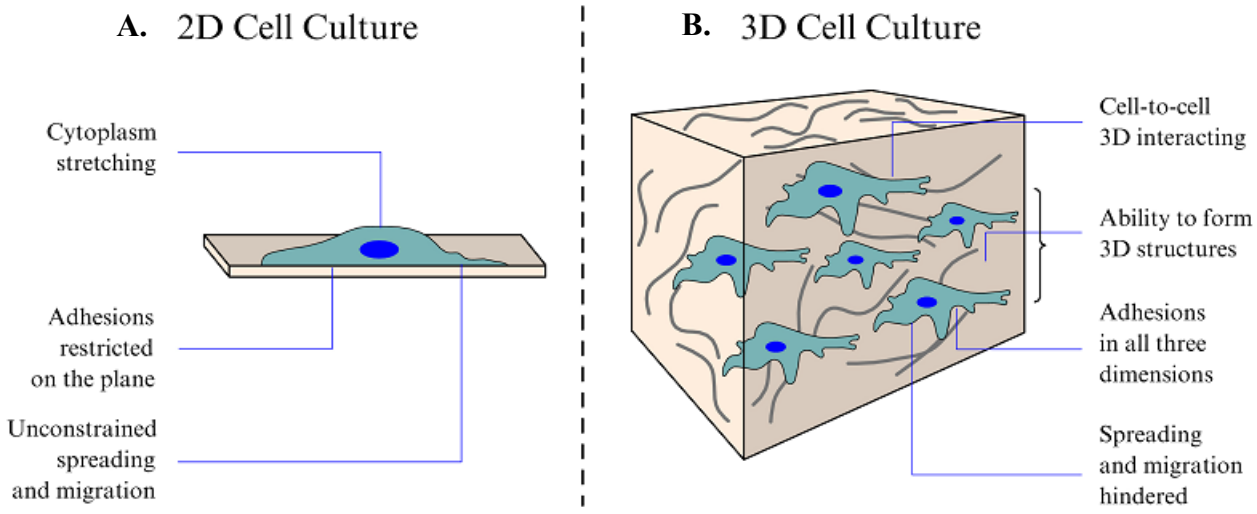

Figure 1.6. 2D vs. 3D Cell Culture. A. 2D cell culture showing a cell affixed to one plane. B. An example of 3D cell culture showing the ability of cells to interact with each other in a physiologic manner. Ustyugov et. al. 2018.

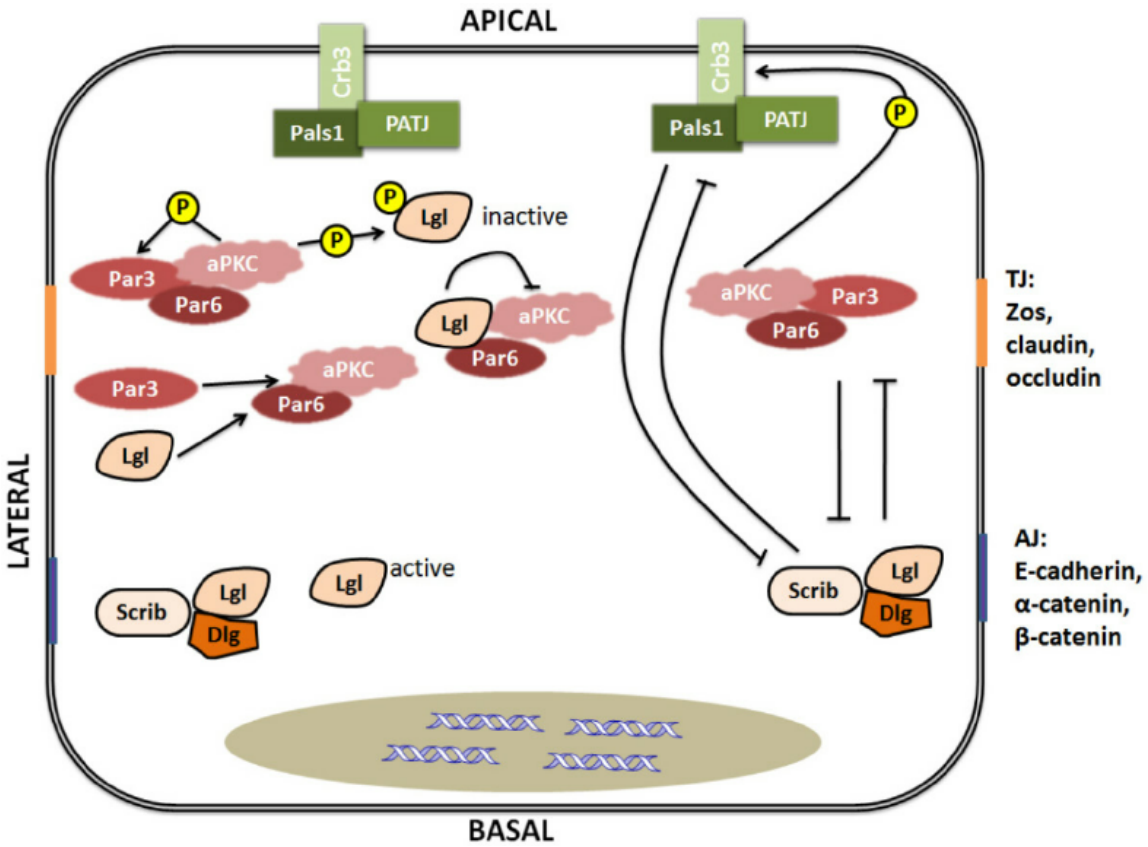

Figure 1.7. Proteins responsible for apico-basolateral polarity formation in epithelial cells. The cell shown the location of the apical membrane (which faces the lumen), the basal membrane (which faces the ECM), and the lateral membrane (which contains tight junctions (TJ) and adherins junctions (AJ) and is responsible for cell-cell contact). Inside the cell is the proteins responsible for polarity. Cao et. al. 2015.

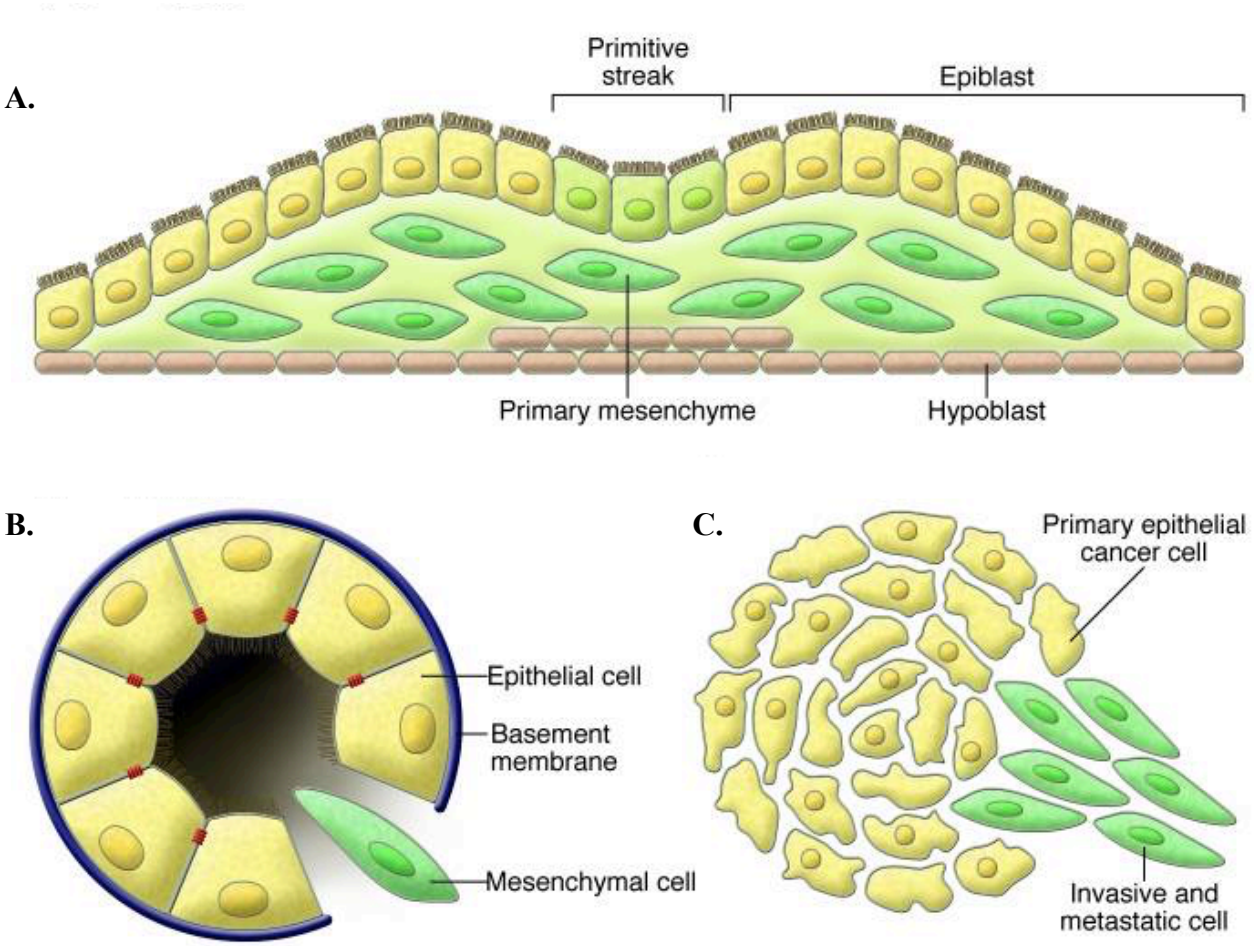

Figure 1.8. Types of Epithelial to Mesenchymal Transition. A. Type 1 EMT, primarily active in embryogenesis. B. Type 2 EMT, found in organ fibrosis and wound repair. C. Type 3 EMT found in cancer cells. Kalluri et. al. 2009.

Cell Type	ADRA1D		PDZ Proteins			Non-PDZ Proteins		
tissue	%Cov	#UP	Name	%Cov	#UP	Name	%Cov	#UP
HEK293T	15.4	9	SCRIB	10.7	12	CTNNAL1	1.1	1
kidney			SYNTB1	27.9	11	DMD	3.0	10
			SYNTB2	42.4	19	DTNA	17.6	5
						UTRN	17.0	10
HeLa	10.0	4	SCRIB	13.5	8	CTNNAL1	13.6	8
cervix			SNTA	6.3	4	DTNA	4.0	9
			SNTB1	27.7	13	DTNB	17.3	8
			SNTB2	37.6	26	UTRN	20.3	62
A529	2.6	2	SCRIB	2.3	2	DMD	8.5	4
lung			SNTB2	32.4	17	DTNB	6.3	4
						MAPK1	4.7	2
						UTRN	11.3	36
MCF-7	9.8	3	SCRIB	4.9	6	DMD	7.4	4
breast			SNTB2	27.4	15	DTNA	26.1	9
						DTNB	7.9	5
						MAPK1	9.2	4
						MAPK3	9.8	3
						UTRN	15.7	48
A375	2.6	2	SCRIB	2.8	2	DMD	4.5	2
skin			SNTB2	9.6	28	DTNA	8.7	4
						DTNB	5.0	3
						UTRN	9.6	28

SW480	8.6	5	CASK	5.1	4	CTNNAL1	10.9	7
colon			DLG1	7.2	5	DT	11.0	3
			LIN7A	7.7	1	DTNB	17.1	9
			SCRIB	8.8	12	PPFIA1	11.1	8
			SNTB1	37.0	20	PPFIBP1	12.9	9
			SNTB2	43.9	26	UTRN	22.5	76

Table 1.1. ADRA1D proteomic analysis in different human cell lines. Data shown include cell type and source tissue, percent peptide coverage (%Cov), number of unique peptides (#UP), PDZ and non-PDZ proteins detected.

	2D Cell Culture	3D Cell Culture	Animal Models
Advantages	Cost Well established Quick High throughput Ease of use Easy downstream processing	More relevant cell model Better simulation of living organisms High throughput	Can model disease states Can show multiple organ systems
Disadvantages	Non-physiologic cell structures Less biologically relevant	Added expense More complex structure Batch differences Must be optimized for individual labs	Many diseases are human-specific Differences in physiology Not high throughput Expensive Time consuming

Table 1.2. Advantages and Disadvantages to 2D cell culture, 3D cell culture, and animal models.

CHAPTER II – Pharmacological Characterization of α_1-AR Subtypes in SW480 and Other Cancer Cells

2.1 Introduction

Recent studies have shown that catecholamine signaling may play a role in cancer development and metastasis. Specifically, chronic β-AR activation drives primary tumor growth and metastasis by increasing the production of angiogenetic factors, enhancing invasion of cancer cells through the stimulation of an epithelial to mesenchymal transition (EMT), and/or affecting cancer cell viability and resistance to apoptosis (Cole et. al. 2012). Due to this, β-AR antagonists have improved the clinical outcomes for human cancer patients. These studies suggest that, among the molecular mechanisms involved in catecholamine signaling, β-ARs represent a promising target to treat cancer.

However, the effect of α-ARs in cancer pathogenesis is poorly understood. It has been reported that there is an increase in α-ARs seen in some cancer cell lines (Collette et. al. 2011). Interestingly, doxazosin and terazosin, α1-AR antagonists, can induce tumor cell apoptosis (Anglin et. al. 2002, Partin et al., 2003). Unfortunately, it remains unclear whether these effects occur through α1-AR and/or non–α1-AR–dependent mechanisms (Kyprianou et. al. 2009). This question is particularly relevant when considering the three known subtypes of α1-AR (α_{1A}, α_{1B}, α_{1D}) and their differential coupling in various cell types. For example, in mouse models, chronic activation of α_{1A}-ARs reduces cancer incidence and prolongs life span, whereas chronic α_{1B}-AR activation typically produces deleterious effects on multiple organ systems (Wang et. al. 2000, Zuscik et. al. 2000, Papay et. al. 2002, Doze et. al. 2009, Collette et. al. 2014). As such, understanding the effects of chronic α1-AR activation in specific cancer subtypes is essential.

Our laboratory studies macromolecular complexes formed by distinct α1-AR subtypes and how complex architecture influences α1-AR signaling and physiologic function. We recently showed that α1-AR subtypes associate with selective intracellular molecular scaffolds that dictate their pharmacodynamic and signaling characteristics (Lyssand et. al. 2008, 2010, Camp et. al. 2015). Interestingly, proteomic screening indicates cell-type–specific α1-AR:PDZ-protein complexes are formed in human SW480 colorectal cancer cells (CRCs), suggesting α1-ARs may couple to noncanonical, G protein–independent signal transduction mechanisms in this cell line (Camp et al., 2015).

2.2 Materials and Methods

Reagents and Constructs. Human α_{1B}-AR cDNAs were subcloned in pSNAPf (New England Biolabs, Ipswich, MA) using In-Fusion HD cloning technology (Clontech, Mountain View, CA), as described in Kountz et al. (2016). The 5-methylurapidil (U101), BMY 7378 HCl (B134), clonidine HCl (C7897), (±) cyclazosin HCl (C247), dopamine HCl (H8502), doxazosin mesylate (D9815), histamine (H7125), (-)-isoproterenol HCl (I6504), (R)-(-)-niguldipine HCl (N162), phenylephrine hydrochloride (P6126), prazosin HCl (P7791), phentolamine HCl (P7547), phenoxybenzamine HCl (B019), (±)-propranolol HCl (P0884), serotonin HCl (H9523), tamsulosin HCl (T1330), and terazosin HCl (T4680) were purchased from Sigma-Aldrich (St. Louis, MO). Rauwolscine HCL was from Tocris (Bristol, UK). The [7-methoxy-3H]-prazosin and myo-[2-3H(N)]-inositol were from Perkin-Elmer. SNAP-782 substrate (S9142S) was from New England Biolabs (Corning, NY). Epic 384-well glass-bottomed biosensor plates were from Corning.

Cell Culture and Transfections. Human SW480 colon carcinoma cells, HCT116 colorectal cancer cells, MDAMB231 metastatic breast cancer cells, and U251 glioblastoma cells were grown in Dulbecco's modified Eagle's medium (DMEM) supplemented with 10% fetal bovine serum and 2 mM L-glutamine. For SNAP–α_{1B}-AR studies, cells were transfected with 1 mg/ml polyethylenimine and indicated concentrations of cDNA constructs, and then assayed 48 hours post-transfection.

Label-Free Dynamic Mass Redistribution Assays. Label-free DMR assays were performed using a method derived from previously documented studies (Fang et. al. 2006, 2007). SW480 cells (passage number 3–10) were seeded at ~500 k/well in Corning Epic sensor microplates and cultured for 24 hours in DMEM plus fetal bovine serum. On the day of the experiment, cells were washed three times with Hanks' balanced salt solution (HBSS) buffer and transferred to the Corning Epic BT reader, which was permanently housed in a Thermo cell culture incubator at 37°C with 5% CO2, as this magnified the amplitude of recorded DMR responses. Cells were incubated with antagonists dissolved in HBSS for at least 1 hour prior to adding agonist to ensure that equilibrium between antagonist and receptor had been reached, during which baseline DMR measurements were recorded. All compounds were added using a Sorenson Biosciences 96-well Benchtop Pipettor. Agonist DMR responses were recorded for 1 hour. Raw data were exported to Microsoft Excel using Epic Analyzer Software and then imported into GraphPad Prism software to calculate agonist (potency, intrinsic activity) and antagonist (affinity) properties. Agonist concentration–response curves were fit using variable slope nonlinear regression to determine potency (EC50) and Hill slope. The y-axis values on raw DMR data and agonist DMR concentration–response curves represent the shift in light wavelength in picometers (pm) as a result of DMR. Schild Plot analyses were performed when appropriate using a method derived

from that first described in Arunlakshana and Schild (1959). Schild data were calculated for each experimental n (each having four replicates), and final Schild plots were calculated as the mean ± S.E.M. of each experimental value. Schild plots were fit using linear regression analysis. Nonlinear regression analysis was also used to determine whether antagonist Schild slopes were significantly different than 1. Apparent affinity (pKB) was calculated using the equation pKB = log (DR-1) − log [B]. Control experiments were performed, demonstrating antagonists used in this study did not stimulate significant DMR responses.

Quantitative Reverse-Transcriptase Polymerase Chain Reaction Assays. Total RNA was isolated from SW480 cells using NucleoSpin RNA isolation kit, according to manufacturer's instructions (Macherey-Nagel). One-step quantitative reverse-transcriptase polymerase chain reactions (qRT-PCR) were carried out in a final volume of 20 μL that included the following: 2 μL template RNA (25 ng final concentration), 0.8 μL forward and reverse primer (10 μM final concentration), 0.4 μL ROX reference dye, 10 μL 2× one-step SYBR RT-PCR buffer, and 5.2 μL RNase-free H2O using the One Step SYBR PrimeScript RT-PCR kit (Clontech). Primers used for qRT-PCR analysis were as follows: α_{1A} forward, 5′-TGCCAGATCAACGAGGAGC-3′, and reverse, 5′-GGCGTTTTTCCGATGGATGC-3′; α_{1B} forward, 5′-CTTTCACGAGGACACCCTTAGC-3′, and reverse, 5′-GCCCAACGTCTTAGCTGCTT-3′; α_{1D} forward, 5′-CTCCAGCCTGTCGCACAAG-3′, and reverse, 5′-TGTAGTCGGCCAATTCGTAGG-3′; β2 forward, 5′-TGGTGTGGATTGTGTCAGGC-3′, and reverse, 5′-GGCTTGGTTCGTGAAGAAGTC-3′; and adenine phosphoribosyltransferase (APRT) forward, 5′-GGCCGCATCGACTACATCG-3′, and reverse, 5′-CTCAGCCTTCCCGTACTCC-3′.

qRT-PCR Reactions: 42°C for 5 minutes; 95°C for 5 seconds; and 60°C for 20 seconds. Melt curve data were collected from 60°C to 95°C at a ramping rate of 0.2°C per second. qRT-PCRs were performed in quadruplicate on a Stratagene Mx3000 Real Time PCR system. Relative expression values of each genes of interest were normalized to the expression value of housekeeping gene APRT.

Radioligand-Binding Assays. Cell membranes were prepared from cultured SW480 cells via scraping and polytron grinding three times for 30 seconds. Lysates were resuspended in ice-cold phosphate-buffered saline (PBS). Protein concentration was determined with an Eppendorf D30 BioPhotometer. A total of 100 µL PBS containing 100 µg resuspended cell lysates was incubated with 100 µL varying concentrations of [3H]-prazosin for 30 minutes at 37°C with gentle shaking, in the absence (representing total [3H]-prazosin bound) or presence of 100 µM nonselective α-AR antagonist phentolamine (representing nonspecific [3H]-prazosin bound). Samples were then subjected to Brandel vacuum filtration (Brandel, Gaithersburg, MD). Filters were incubated with 5 mL liquid scintillation fluid and counted with a Tri-Carb 2200 CA liquid scintillation analyzer (Packard Instrument, Rockville, MD). Data were converted from cpm to fmol/mg protein (http://www.graphpad.com/quickcalcs/radcalcform/), and specific bound was calculated as total bound − nonspecific bound. Specific bound data were fit with one-site specific binding saturation analysis using GraphPad Prism 6 software. Data are expressed as mean ± S.E.M.

Phosphoinositol Hydrolysis Assays. SW480 cells were prelabeled with 1 mCi/mL [3H]-myo-inositol. After 48 hours, cells were stimulated with 100 µM phenylephrine for 1 hour in HBSS buffer plus 10 mM LiCl. Total inositol phosphates were purified via Dowex ion exchange

chromatography using the method described in Lyssand et al. (2008). Data were analyzed with GraphPad Prism 6 software and expressed as mean ± S.E.M.

SNAP Protein Gels. SW480 cells were transfected with empty SNAP vector or SNAP-tagged α_{1B}-AR cDNA using the previously described polyethylenimine transfection method. Forty-eight hours after transfection, cells were lysed with 50 mM Tris-HCl, 150 mM NaCl, 1% Nonidet P-40, and 0.1% Tween 20 buffer. A total of 0.5 μM BG-782 substrate and 1 mM dithiothreitol was added to lysates, and samples were incubated for 30 minutes at 37°C in the dark. Approximately 10 μg cell lysates was run on 8–10% gels using SDS-PAGE. Gels were imaged using the LI-COR Odyssey Scanner. Protein band size was determined by comparison with PageRuler Prestained NIR Protein Ladder (Thermo #26635).

Cell Proliferation and Viability. Cells grown in DMEM supplemented with 10% fetal bovine serum were harvested using trypsin and seeded in DMEM supplemented with 1% fetal bovine serum in 96-well plates (5000 cells/well). Twenty-four hours later, cells were treated by adding drugs to the cell culture media, as previously described (Cherry et al., 2016). Three days later, cell proliferation was measured using 5-bromo-2′-deoxy-uridine cell proliferation enzyme-linked immunosorbent assay (colorimetric) kit (Roche, Indianapolis, IN) and cell viability using water soluble tetrazolium salt-1 (1:20; Roche, Pleasanton, CA) following manufacturer's protocols.

2.3 Results

To our knowledge, only one study has examined AR expression and function in SW480 cells (Masur et. al. 2001). Specifically, using flow cytometry and primary antibodies targeting AR subtypes, this study suggested that SW480 cells express both α2- and β-ARs, and little to no α1-

ARs (Figure 2.1). However, our previous research detected the presence of PDZ interacting proteins that are only known to interact with the α_{1D}-AR. To determine if a cell line endogenously expresses α_{1D}-AR, we subjected SW480 cells to label-free DMR assays, which measure agonist-stimulated changes in cell shape as a functional output. This highly quantitative technology detects deflections in the wavelength of polarized light reflected through glass-bottom microsensor plates (Camp et. al. 2016). Up to 1 pm changes in wavelength are reliably detected, thereby permitting detection of minute changes in cell shape stimulated by endogenous ARs.

We first examined SW480 DMR responses stimulated by AR subtype-selective agonists in real-time for 60 minutes. Raw DMR tracings are displayed in Figure 2.2 A-E, which were then used to construct agonist concentration curves at t=60 minutes (Figure 2.2 F) to calculate agonist potencies and intrinsic activities (Table 2.1). As shown in Figure 2.2A, the endogenous catecholamine norepinephrine (NE) stimulated strong positive DMR responses in a concentration-dependent manor, presumably through the activation of β- and α2-ARs previously demonstrated to be expressed by this cell type (Masur et. al. 2001). Accordingly, the β-AR–selective agonist isoproterenol (ISO, Figure 2.2B) and the α2-AR partial agonist clonidine (CLN, Figure 2.2C) stimulated weaker DMR responses than those observed with NE. CLN was the most potent adrenergic agonist (Table 2.1). Serotonin (5-HT) (Figure 2.2E) and histamine (data not shown) produced no significant DMR responses, suggesting members of these essential G protein–coupled receptor (GPCR) families are not endogenously expressed by SW480 cells.

Unexpectedly, the α1-AR–selective agonist phenylephrine (PHE) stimulated positive DMR responses (Figure 2.1 D) with higher intrinsic activity (0.68) than both CLN and ISO suggesting that functional α1-ARs are present in SW480 cells, in direct contrast to the findings of previous studies (Masur et. al. 2001).

Because DMR assays are thought to measure the summation of all cell signaling events, the possibility exists that the observed PHE effects were a result of non-α1-AR signaling mechanisms. PHE has been reported to activate β-ARs in human vascular beds (Torp et. al. 2001), rabbit left ventricle (Wagner et. al. 1974), and guinea pig ventricles (Chess-Williams et. al., 1990), depending on the relative density of α-ARs versus β-ARs expressed. Thus, we assayed the efficacy of AR subtype-selective antagonists to block PHE-stimulated DMR responses. If the observed PHE DMR events are occurring via direct α1-AR stimulation, we expect α1-AR antagonists to inhibit PHE responses at concentrations in the range of their reported nanomolar affinities.

Saturating concentrations of the β-AR antagonist propranolol produced no significant changes in the PHE DMR concentration–response curve (Figure 2.3A), nor did the α2-AR antagonist rauwolscine (Figure 2.3B), suggesting that PHE DMR responses are not a result of β- or α2-AR receptor activation. In contrast, pretreating cells for 1 hour with 100 nM α1/α2-AR irreversible antagonist phenoxybenzamine abolished PHE DMR responses (Figure 2.2C). Likewise, the competitive α1/α2-AR antagonist phentolamine produced progressive rightward shifts in PHE concentration–response curve with successive half-log molar increments (Figure 2.2D). PHE potencies in the absence and presence of phentolamine were determined and used to calculate phentolamine affinity using Schild regression analysis (Arunlakshana et. al. 1959). Phentolamine inhibited PHE DMR responses with affinity constant (pA2) = −6.93, or 117 nM (Figure 2.2E; Table 2.2), which is within the range of previously reported values for binding the α_{1B}-AR subtype (Morrow et. al. 1986, Hong et. al. 2005, Bavadekar et. al. 2008).

We next assayed the affinity of the α1-AR–selective antagonist doxazosin (Figure 2.4, A and B), terazosin (Figure 2.4, C and D), and prazosin (Figure 2.4, E and F) for inhibiting PHE DMR responses. All three antagonists produced progressive rightward shifts in DMR concentration–

response curves facilitating Schild regression analysis to calculate antagonist pA2 values (listed in Table 2.2). The affinities for terazosin and doxazosin are consistent with previously reported affinity values for antagonizing α1-AR–stimulated contractions of the rabbit (Martin et. al. 1997) and human prostate (Kenny et. al. 1996, Muramatsu et. al. 1998). However, the observed prazosin DMR affinity is noticeably lower than what is reported in isolated tissue *in vitro* contraction assays examining the three α1-AR subtypes (Docherty, 2010). Instead, our observed prazosin affinity value is within the range of the elusive α1L-adrenoceptor, or low-affinity α1-AR prazosin binding site previously documented to be present in dog saphenous vein (Muramatsu et. al. 1990), rat small mesenteric artery (Stam et. al. 1999), rabbit urinary tract (Van der Graaf et. al. 1997), rat portal vein (Digges et. al. 1983), and rat vas deferens (Muramatsu et. al. 1996). Thus, the lack of effect of β- and α2-AR antagonists, and the pronounced inhibition of PHE DMR responses by mixed α1/α2-AR– and α1-AR–selective antagonists, indicate SW480 cells *do* express functional α1-ARs.

We next sought to identify the specific α1-AR subtype(s) expressed by comparing the ability of various α1-AR subtype-selective antagonists to inhibit PHE DMR responses. The antagonists tested included tamsulosin ($\alpha_{1A/D}$-AR selective), 5-methylurapidil and niguldipine (α_{1A}-AR selective), cyclazosin (α_{1B}-AR selective), and BMY7378 (α_{1D}-AR selective). All antagonist functional data are compiled in Table 2.2.

BMY7378 inhibited DMR responses with pA2 = −6.87, or 134 nM (Figure 2.5, A and B), which is significantly lower than previously reported BMY7378 functional affinities for inhibiting α_{1D}-AR –mediated contraction of rat (Goetz et. al. 1995, Kenny et. al. 1995, Indra et. al. 2002, Cleary et. al. 2005) or mouse thoracic aorta (Yamamoto et. al. 2001), and more indicative of an α_{1A}-AR or α_{1B}-AR affinity for this antagonist. Correspondingly, the $\alpha_{1A/D}$-AR antagonist tamsulosin blocked PHE-stimulated DMR (Figure 2.5C) with significantly lower apparent affinity (1 μM

tamsulosin pKB = −6.83 ± 0.08) than previously reported tamsulosin pA2 values for blocking the α_{1A}-AR or α_{1D}-AR subtypes (Noble et. al. 1997). The lack of α_{1A}-AR contribution to PHE responses was supported by the limited ability of α_{1A}-AR antagonists 5-methylurapidil (Figure 2.5D) and niguldipine (Figure 2.5E) to antagonize PHE-stimulated DMR responses.

Interestingly, maximum phenylephrine DMR values were significantly decreased with increasing concentrations of tamsulosin, 5-methylurapidil, and niguldpine. This observation demonstrates a potential limitation of using label-free DMR assays to calculate antagonist pA2 values. Label-free DMR assays are thought to measure the summation of all downstream signaling events following GPCR activation (Fang et. al. 2006, 2007, Schroder et. al. 2010). Thus, if an α1-AR antagonist binds and alters the activity of off-target proteins essential to the α1-AR signaling cascade, this may result in an alteration in the magnitude of the DMR output. For example, niguldipine inhibits both L-type Ca2+ channels (Boer et. al. 1989) and bTREK-1 K+ channels (Liu et. al. 2007), such that decreases in maximum PHE DMR responses observed at 10μM concentrations of niguldipine may be a result of disrupted electrochemical gradients. As such, the observed antagonist-dependent decreases in PHE maximal DMR responses preclude pA2 determination for tamsulosin, 5-methylurapidil, or niguldipine.

Regardless, the inability of BMY7378, tamsulosin, 5-methylurapidil, or niguldipine to antagonize PHE-stimulated DMR responses in SW480 with high affinity strongly suggests the α_{1A} and α_{1D} subtypes do not functionally contribute to phenylephrine responses. Conversely, the α_{1B}-AR–selective antagonist cyclazosin potently inhibited PHE responses with pA2 = −8.37, or 4.26 nM (Figure 2.5, F and G), consistent with reported affinities for blocking α_{1B}-AR–mediated contraction of rabbit thoracic aorta (Marucci et. al. 2005). Given the α_{1B}-AR antagonist cyclazosin produced the most potent inhibition of PHE DMR responses in SW480 cells, we hypothesize SW480 cells express predominantly the α_{1B}-AR subtype.

Label-free DMR pharmacological results were subsequently validated with quantitative reverse-transcriptase polymerase chain reaction (qRT-PCR) assays. Internal primers directed against individual α1-AR subtypes and the β2-AR were used to measure relative mRNA concentrations expressed as cycle threshold (CT) fold. All values were compared with APRT levels as a reference housekeeping gene. As shown in Figure 2.6A, α_{1B}AR mRNA levels were 2.53 ± 0.09-fold greater than APRT, whereas α_{1A}AR (0.02 ± 0.06) and α_{1D}-AR (6 × 10–4 ± 0.28) mRNA levels were barely detectable. β2-AR mRNA levels (0.09 ± 0.04) were greater than α_{1A}-AR and α_{1D}-AR, yet significantly lower than α_{1B}-AR.

In summation, SW480 cells produce relatively high levels of α_{1B}-AR mRNA and robust PHE-stimulated label-free DMR responses inhibited by the α_{1B}-AR–selective antagonist cyclazosin. Yet, α1-ARs are reported as minimally detectable in previous flow cytometry assays (Masur et. al. 2001). To clarify this discrepancy, we quantified endogenous α_{1B}-AR functional receptor density with [3H]-prazosin radioligand-binding and phosphoinositol hydrolysis assays. As a positive control, we included SW480 cells transfected with N-terminal SNAP-epitope–tagged α_{1B}-ARs. SNAP protein gels demonstrated 3 μg SNAP–α_{1B}-AR cDNA was optimal for ensuring SW480 cell viability and maximal SNAP–α_{1B}AR protein levels (Figure 2.6B, denoted with arrow at ~76.6 kDa). Remarkably, we did not detect significant levels of endogenous α_{1B}-AR binding sites (<10 fmol/mg protein) in SW480 cell lysates with [3H]-prazosin saturation radioligand-binding assays, whereas transfecting SNAP–α_{1B}-AR induced a robust increase in receptor density (Bmax to 59.3 ± 10.7 fmol/mg protein; Figure 2.6C).

Phosphoinositol hydrolysis assays produced equivalent results (Figure 2.6D). Specifically, application of 100 μM PHE did not generate significant increases in wild-type SW480 cellular inositol phosphate levels but did produce a 62.1% increase in inositol phosphate formation in

SW480 cells transfected with SNAP–α_{1B}-AR. Corresponding to this finding, maximal PHE-stimulated DMR responses were enhanced by 25.8% in SW480 cells when transfected with SNAP–α_{1B}-AR (Figure 2.6E). Taken together, these data demonstrate that SW480 cells express low levels of functional α_{1B}-AR that are undetectable with radioligand-binding and reductionist functional assays, but are robustly detectable with label-free DMR assays.

Although it has been shown that AR stimulation induces migration of cultured SW480 cells (Masur et. al. 2001), this study used NE as the adrenergic agonist, and thus the AR subtype(s) involved remains unclear. With the discovery that SW480 cells express low levels of functional α_{1B}-ARs, we sought to determine the effect of β- and α1-AR stimulation on SW480 cell viability and proliferation. β-AR stimulation with ISO produced a dose-dependent decrease in both cell viability and proliferation (Figure 2.7A). The antiproliferative effects of ISO were marginally greater than its anti-viability effects. Conversely, α1-AR stimulation with PHE produced a striking increase in cell viability, with no significant effects on cell proliferation (Figure 2.7B). The prosurvival effects of PHE were antagonized by the α1-AR antagonist terazosin, cyclazosin, phenoxybenzamine, and phentolamine (Figure 2.7C). These results show that SW480 cells express low densities of functional α_{1B}-ARs that, when activated, are prosurvival.

Because α_{1B}-ARs was previously undetected in SW480 cells, we sought to determine if this receptor has been overlooked in other cell types, and thus may be a new target for chemotherapy medications. Using MDAMB231 (metastatic breast cancer), HCT116 (colorectal cancer), and U251 (glioblastoma) cell lines, we performed DMR responses stimulated by AR subtype-selective agonists in real-time for 60 minutes. Agonist concentration curves are displayed in Figure 2.8 A-C which were determined at t=60 minutes to calculate agonist potencies. As shown in Figure 2.8A-C NE stimulated strong positive DMR responses in a concentration-dependent manor. The β-AR–selective agonist ISO and the α2-AR partial agonist CLN stimulated weaker

DMR responses than those observed with NE. 5-HT and histamine (data not shown) produced no significant DMR responses, suggesting members of these essential GPCR families are not endogenously expressed by MDAMB231, HCT116, and U251 cells. Interestingly, the α1-AR agonist PHE did also stimulate DMR responses in each of these cell lines and at a greater concentration than CLN and ISO (Figure 2A-C).

2.4 Discussion

With the ongoing and increasing usage of small molecules targeting adrenergic signaling mechanisms for the treatment of cardiovascular disease, central nervous system disorders, and numerous other diseases, understanding whether these medicines also influence tumor growth and/or metastasis is of *critical* importance. Accordingly, identifying subtypes of ARs expressed by specific cancer cells and characterizing the action of small molecules targeting this receptor family and their resulting effect on tumor cell fate will provide critical information that might drive patient-specific pharmacotherapy. In this study, we illustrate the inherent power of label-free DMR signaling technology to identify low-density, yet highly-functional ARs in SW480 colorectal cancer cells. Moreover, to the best of our knowledge, our study represents the first to combine label-free DMR assays with Schild regression analysis of antagonist affinities to facilitate pharmacological characterization of cancer cell–specific expression of endogenous GPCR subtypes. Based on these results, we provide evidence that antagonists targeting both α_{1B}-AR and β-AR may significantly affect cancer cell fate.

The effects of chronic AR stimulation on human health and disease have been extensively studied and documented. To date, the overwhelming majority of the data indicates chronic β-AR stimulation produces negative outcomes on cancer prognosis. Epidemiologic data compiled from breast cancer outcomes of patients on chronic β-blocker therapy had a 57% reduced risk of

metastasis and 71% reduction in mortality after 10 years (Powe et. al., 2010). A subsequent study discovered brain metastasis derived from breast cancer cells have increased β2-AR mRNA and protein expression levels and exhibit enhanced cell proliferation and migration (Choy et. al. 2016). Chronic β-AR activation induced by stress promotes colon cancer metastasis (Zhao et. al. 2015), potentially through transactivation of the epidermal growth factor receptor-Akt/extracellular signal-regulated kinase pathway (Chin et. al. 2016). Accordingly, β-AR blockade has been shown to be an effective treatment in experimental models of colon cancer (Barbieri et al., 2015; Sorski et al., 2016) and reduces the incidence of colon cancer in human populations (Chang et al., 2015).

Contrary to these findings, we found β-AR activation decreased SW480 cell viability and proliferation, similar to what has been reported in cardiomyocytes during heart failure, where prolonged β-AR stimulation leads cell death, fibrosis, and adverse remodeling (Lefkowitz et. al. 2000).

Significantly less information exists on the role of α1-AR activation in cancer outcomes. Studies investigating the effects of chronic α1-AR stimulation on cell survival from cardiovascular studies provide valuable insights (ALLHAT, 2002). A major revelation of the groundbreaking Antihypertensive and Lipid-Lowering Treatment to Prevent Heart Attack Trial (ALLHAT) was the increased incidence of deleterious cardiovascular events in the doxazosin-treatment arm, forcing an early termination of this portion of the study (Piller et al., 2002). This single observation has significantly diminished the use of α1-AR antagonists for hypertension, heart failure, and other cardiovascular diseases. Subsequent basic science studies showed that α1-AR stimulation inhibits apoptosis in *in vitro* and *in vivo* while enhancing ischemic preconditioning in human volunteers. It is believed to do so via activating prosurvival mechanisms such as induction of fetal gene transcription, increased protein synthesis, enhanced glycolysis, activation

of extracellular signal-regulated kinase, protein kinase C, and others (Jensen et. al., 2011). Additionally, a series of elegant knockout mice studies show that knocking the α_{1A}AR and α_{1B}AR subtypes induces maladaptive cardiac morphologic alterations, resulting in diminished cardiac output, impaired exercise tolerance, and enhanced mortality induced by transverse aortic constriction (TAC), suggesting α1-ARs are prosurvival in cardiomyocytes (O'Connell. et al. 2006). Despite these significant studies, the specific contributions of individual α1-AR subtypes to the prosurvival phenotype in various cancers remain unclear.

We found that α_{1B}-AR stimulation enhanced SW480 cell survival, despite their relatively low expression. Interestingly, mice overexpressing constitutively active α_{1B}-AR mutants display a host of maladaptive phenotypes, including cardiac hypertrophy post-TAC (Wang et. al. 2000), depression-like behavior (Doze et. al. 2009), age-related apoptotic neurodegeneration (Zuscik et. al. 2000, Papay et. al. 2002), and reduced life span (Collette et. al. 2014). Taken together, the effects of α_{1B}-AR stimulation on cell outcome may be directly correlated to their functional expression levels, with low to moderate expression of α_{1B}-ARs being prosurvival, whereas overexpression promotes morphologic changes leading to cell death. Further studies are needed to clarify the effect of chronic α_{1B}-AR stimulation on cancer cell fate, and whether these effects are specific to colon carcinoma cells.

In summary, we leveraged the power of label-free DMR signaling technology to identify and characterize low-density α_{1B}-ARs previously undetectable with traditional experimental approaches used to quantify GPCR functional expression levels in cell culture (i.e., as measured by flow cytometry, radioligand binding, or reductionist functional assays), which, when activated, increase the survival of human SW480 colorectal carcinoma cells. We also showed that other cell types, MDAMB231, HCT116, and U251 appear to show α1-AR activation as

well, highlighting a potentially previously unstudied receptor as a potential consideration for small molecule administration to patients with cancer.

To our knowledge, this study is the first to examine the effects of α_{1B}-AR stimulation on human colorectal carcinoma cell fate. Thus, label-free DMR should prove useful for characterizing membrane-signaling proteins functionally expressed on specific carcinoma cell types, thereby facilitating their investigation as potential antineoplastic targets using available therapeutic agents, or to predict the side effects of concurrently used medications on tumor cell outcome. As health-care systems move toward the era of precision medicine, the translational advantages of label-free technology provide a unique opportunity to drive patient-specific pharmacotherapy. Our discovery that α_{1B}-ARs are prosurvival in SW480 colorectal carcinoma cells may have relevance for the increasing number of patients taking α1-AR antagonists for benign prostatic hypertrophy, post-traumatic stress disorder, and/or cardiovascular disease. Thus, further investigation into the effects of α1-AR stimulation on numerous cancer cell fate is warranted.

Abbreviations: APRT, adenine phosphoribosyltransferase; AR, adrenergic receptor; DMEM, Dulbecco's modified Eagle's medium; DMR, dynamic mass redistribution; GPCR, G Protein–Coupled Receptor; HBSS, Hanks' balanced salt solution; NE, norepinephrine; pA2, affinity constant; pKB, apparent affinity; qRT-PCR, quantitative reverse-transcriptase polymerase chain reaction; TAC, transverse aortic constriction.

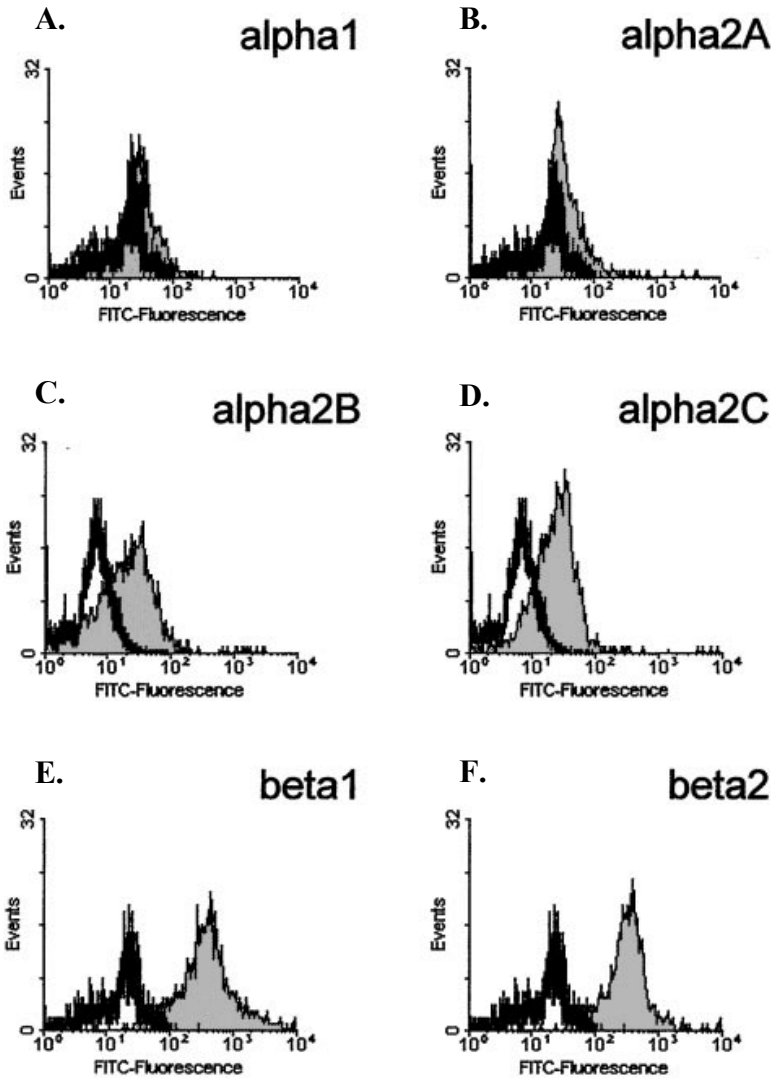

Figure 2.1. Adrenergic Receptors Present in SW480 Cells as Characterized by Masur et. al. The antibody bound FITC-fluorescence of specific antibodies (filled gray) was compared with an unspecific isotypic control (black line). A. α1-ARs compared to control. B. α_{2A}-ARs compared to control. C. α_{2B}-ARs compared to control. D. α_{2C}-ARs compared to control. E. β1-ARs compared to control. F. β2-ARs compared to control.

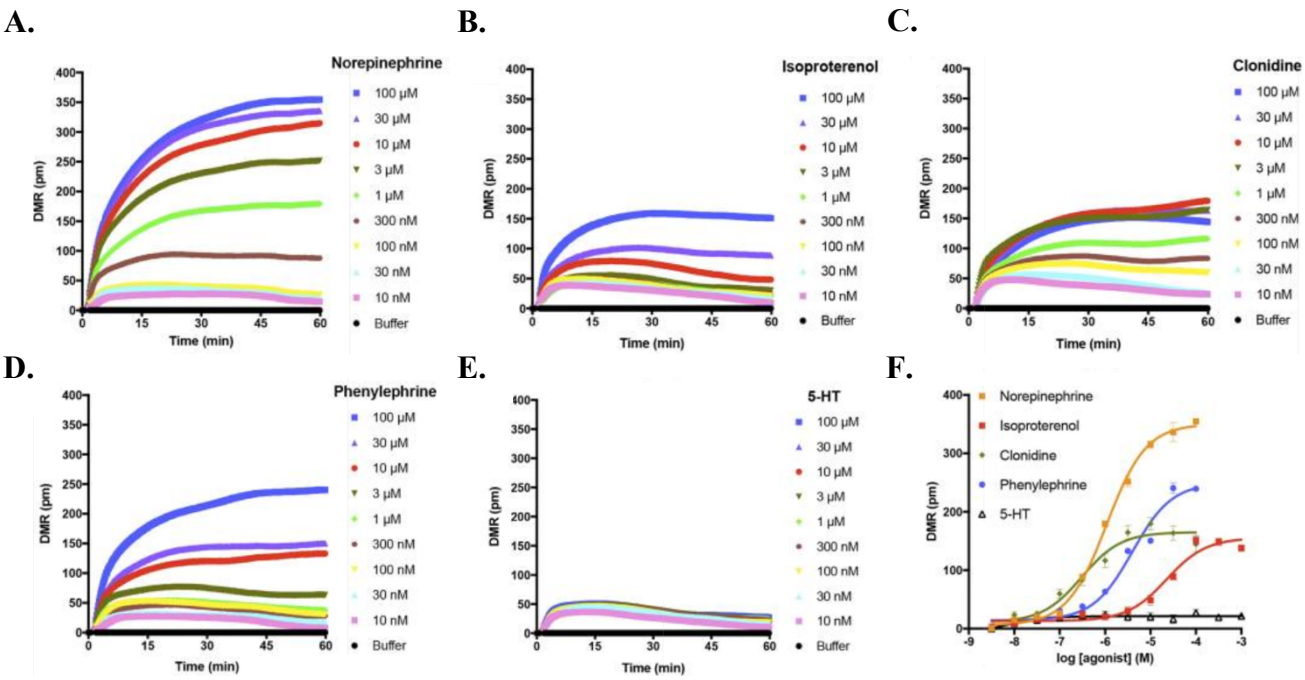

Figure 2.2. Agonist stimulated DMR responses in SW480 cells. Raw label-free DMR responses were measured for: A. The nonselective AR agonist Norepinephrine. B. The β-AR–selective agonist isoproterenol. C. The α2-AR–selective agonist clonidine. D. The α1-AR–selective agonist phenylephrine. E. 5-hydroxytryptamine/5-HT. F. Data were used to construct concentration–response curves to calculate agonist potencies and intrinsic activities for stimulating DMR responses at t = 60 minutes. Data are mean ± S.E.M. from three/four independent experiments performed with four replicates.

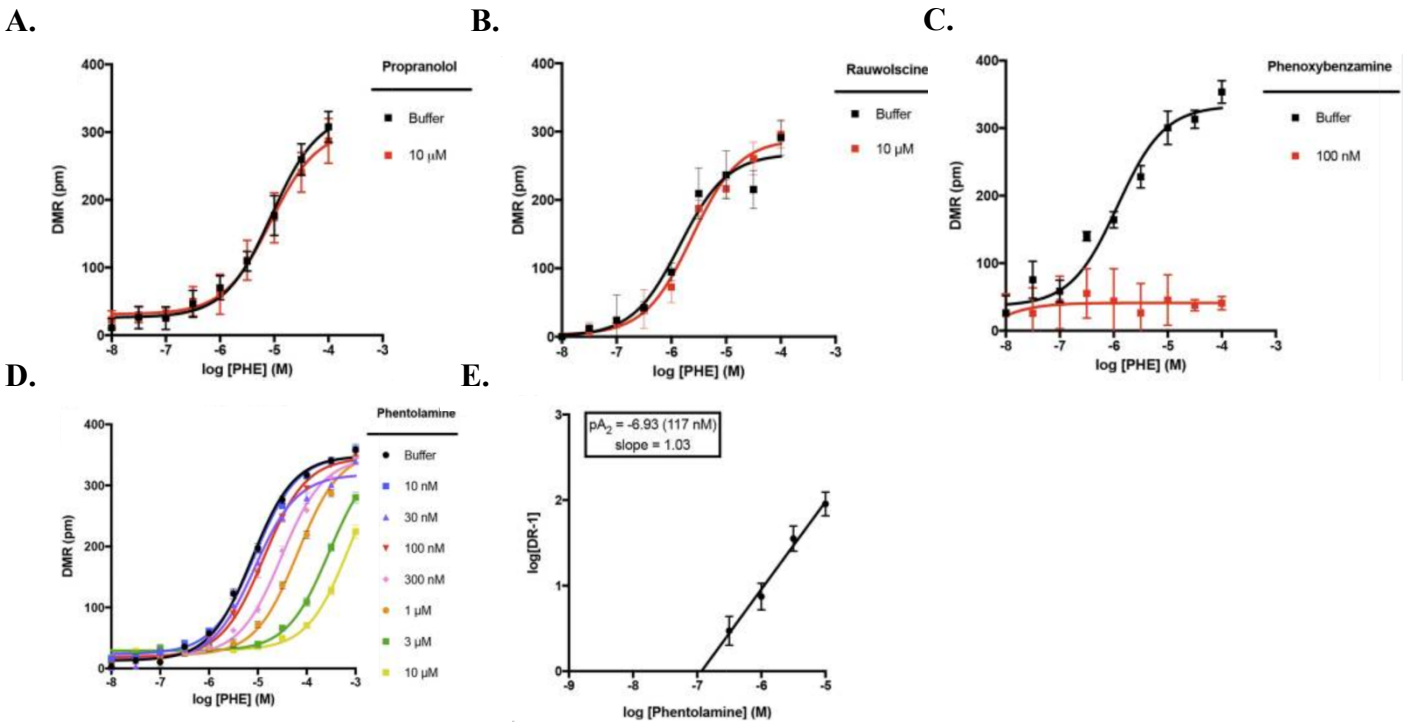

Figure 2.3. Phenylephrine-stimulated SW480 DMR responses are blocked by α-AR antagonists. Label-free DMR responses were measured for the α1-AR–selective agonist phenylephrine in the absence and presence of: A. The β-AR antagonist propranolol. B. The α2-AR antagonist rauwolscine. C. The irreversible α1/α2-AR antagonist phenoxybenzamine. D. The competitive α1/α2-AR antagonist phentolamine. For each condition, concentration–response curves were constructed using DMR values obtained at t = 60 minutes and used to calculate agonist potency. E. Schild regression analysis of phentolamine affinity. Data are mean ± S.E.M. from three independent experiments performed with four replicates.

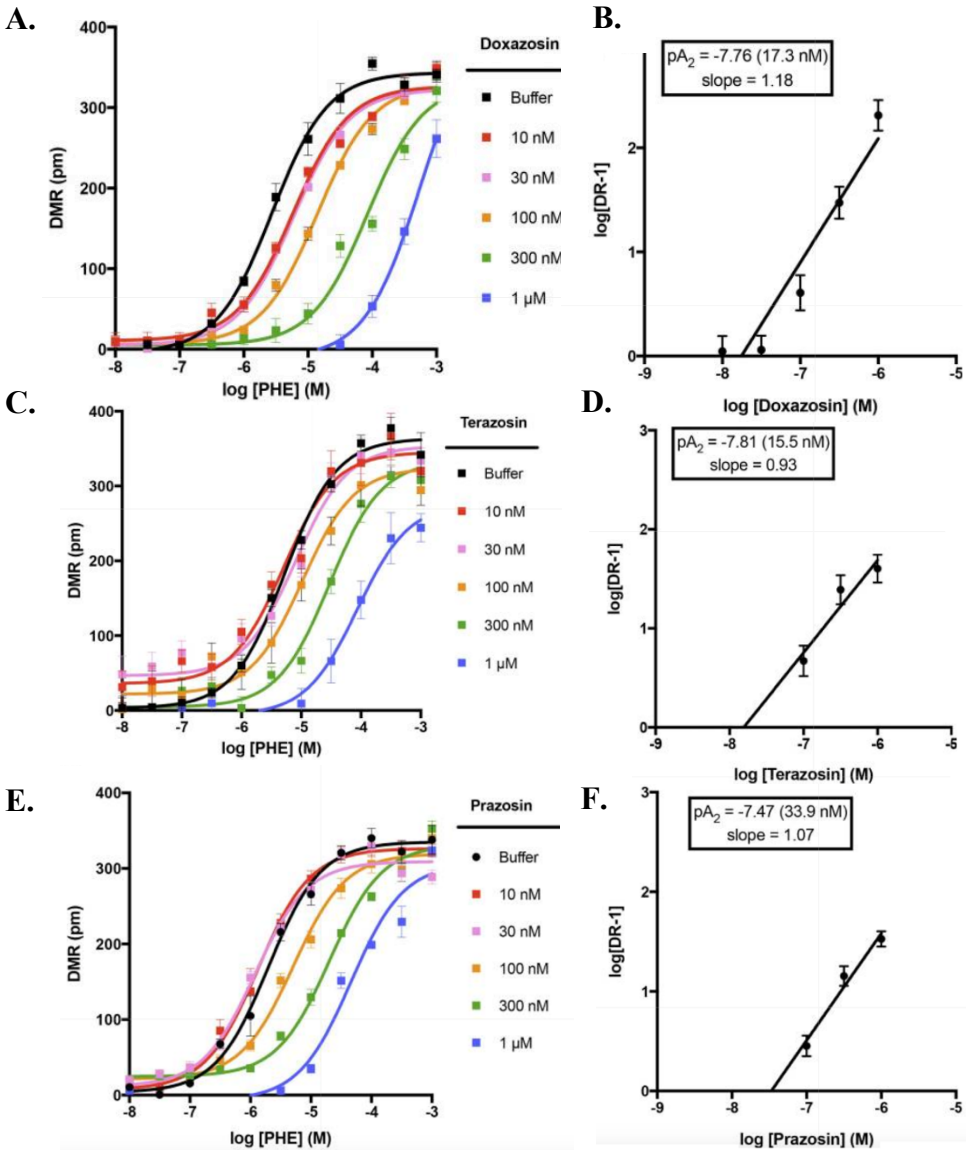

Figure 2.4. Phenylephrine-stimulated SW480 DMR responses are blocked with high affinity by α1-AR antagonists. Label-free DMR responses were measured for the α1-AR–selective agonist phenylephrine in the absence and presence of: A. The α1-AR–selective antagonists doxazosin C. Terazosin. E. Prazosin. For each condition, concentration–response curves were constructed using DMR values obtained at t = 60 minutes, from which agonist potencies were calculated for subsequent Schild regression analysis of affinity for: B. Doxazosin. D. Terazosin. F. Prazosin. Data are mean ± S.E.M. from three independent experiments performed with four replicates.

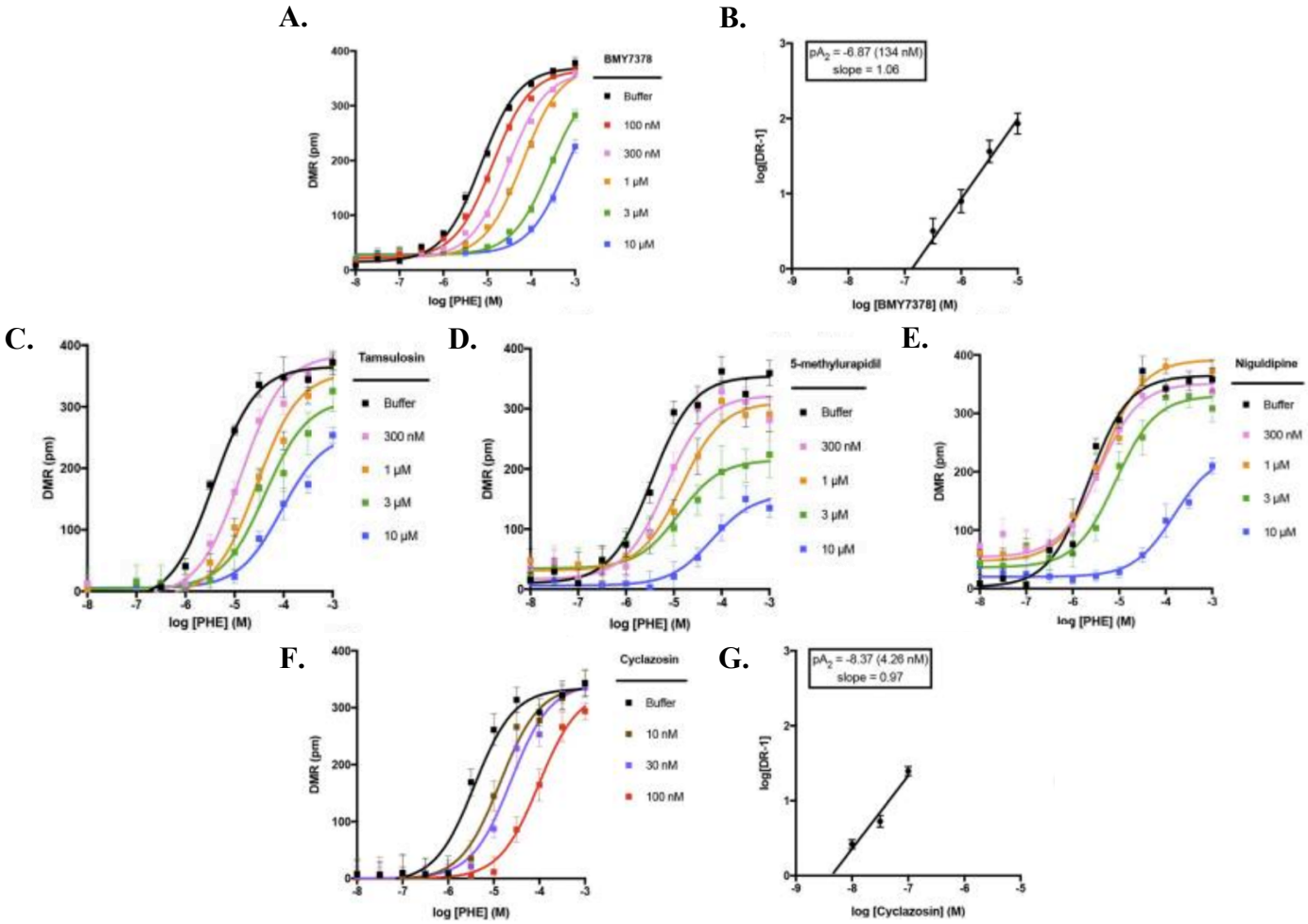

Figure 2.5. Phenylephrine-stimulated SW480 DMR responses are blocked with high affinity by the α_{1B}-AR–selective antagonist cyclazosin. Label-free DMR responses were measured for the α1-AR–selective agonist phenylephrine in the absence and presence of: A. The α_{1D}-AR subtype-selective antagonist BMY7378 (Schild regression analysis in B.). C. The $\alpha_{1A/D}$-AR subtype-selective antagonist Tamsulosin. D. The α_{1A}-AR subtype-selective antagonist 5-methylurapidil E. The α_{1A}-AR subtype-selective antagonist niguldipine. F. The α_{1B}-AR subtype-selective antagonist cyclazosin (Schild regression analysis in G.). For each condition, concentration–response curves were constructed using DMR values obtained at t = 60 minutes. When appropriate, agonist potencies were calculated for subsequent Schild regression analysis of affinity. Data are mean ± S.E.M. from three independent experiments performed with four replicates.

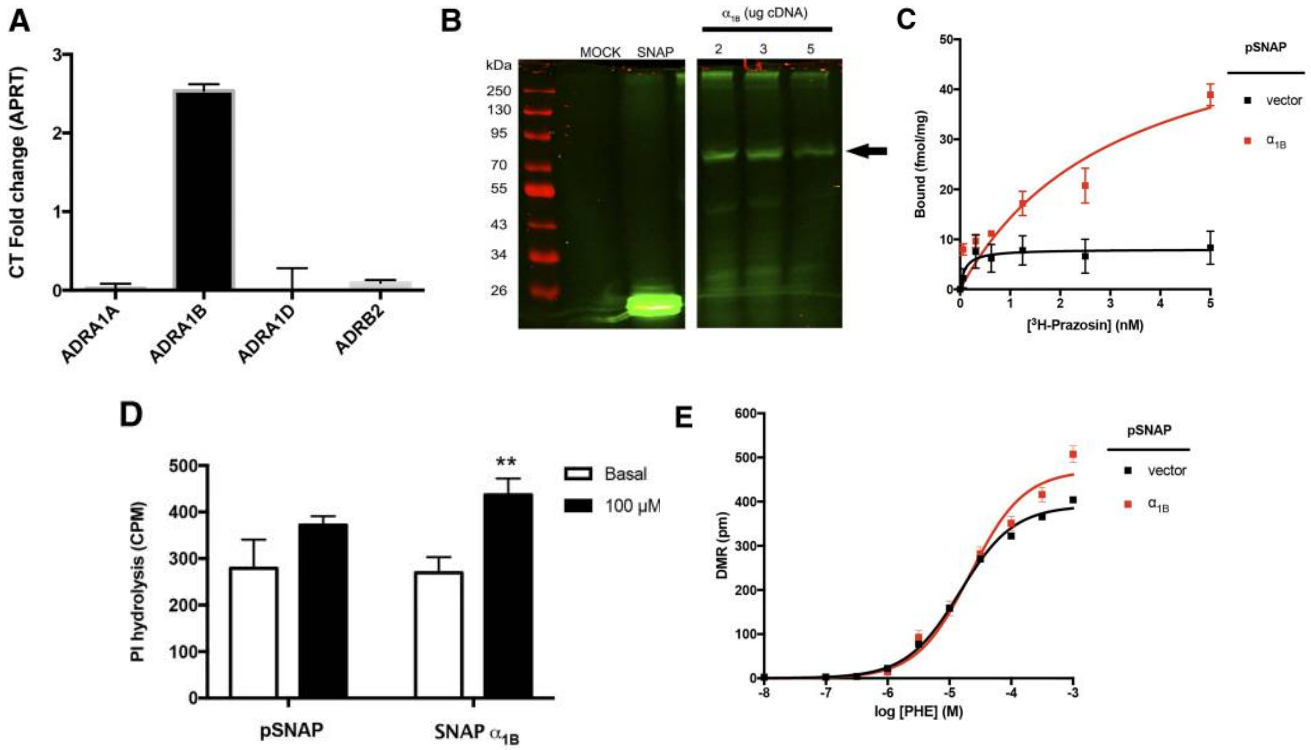

Figure 2.6. SW480 cells express high levels of α1B-AR mRNA and low densities of functional α_{1B}-ARs. A. Quantitative reverse-transcriptase polymerase chain reaction was performed on mRNA isolated from SW480 cell lysates using internal primers targeted to the α_{1A} (ADRA1A), α_{1B} (ADRA1B), α_{1D} (ADRA1D), and β2 (ADRB2)-AR subtypes. Data were normalized as cycle threshold (CT) fold change relative to APRT mRNA levels and are as expressed as mean ± S.E.M. (n = 2 with three replicates). B. Polyacrylamide gel electrophoresis of wild-type SW480 cell lysates (MOCK lane), or SW480 cell lysates following transfection with empty pSNAP vector (SNAP), and 2, 3, or 5 µg N-terminal SNAP-epitope–tagged α_{1B}-AR cDNA. SNAP–α_{1B}-AR protein bands are denoted with black arrow on right (76.6 kDa). C. Saturation [3H]-prazosin radioligand-binding assays were performed on SW480 cell lysates transfected with empty pSNAP vector (black ▪) or 3 µg SNAP-α_{1B}-AR cDNA (red ▪). Nonspecific binding was determined with 10 µM phentolamine. Data are the mean ± S.E.M. of three experiments with three replicates. D. Phosphoinositol hydrolysis assays were performed on SW480 cells transfected with empty pSNAP vector or 3 µg SNAP–α_{1B}-AR cDNA. Cells were preincubated with 1 µCi [3H]-myoinositol for 48 hours and treated with HBSS buffer or 100 µM phenylephrine for 1 hour. Data are expressed as the mean ± S.E.M. of three experiments performed in triplicate. **Student's t test, $P < 0.05$. E. Label-free DMR responses were measured for the α1-AR–selective agonist phenylephrine in SW480 cells transfected with empty pSNAP vector (black ▪) or 3 µg SNAP–α_{1B}-AR cDNA (red ▪). Data are the mean ± S.E.M. of two experiments with four replicates.

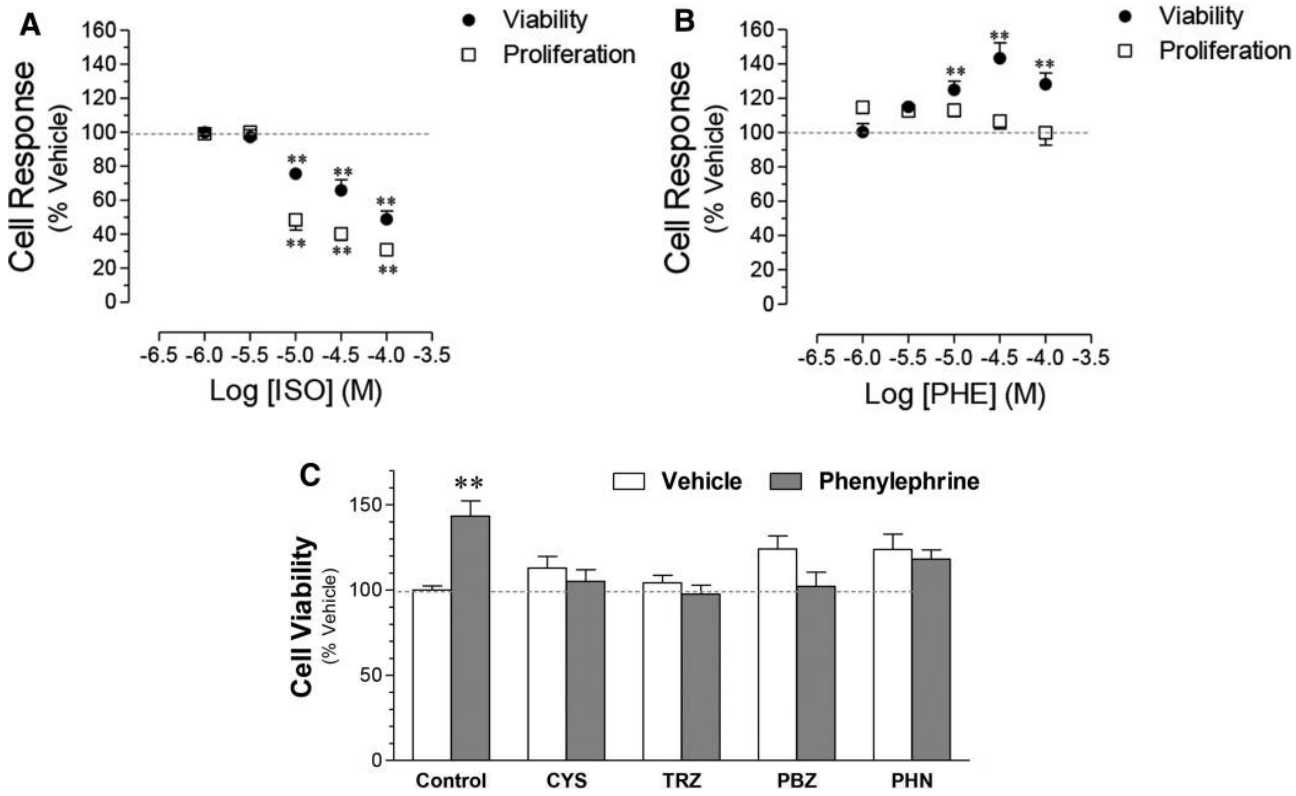

Figure 2.7. Stimulation of β-AR decreases cell proliferation and viability, and stimulation of α_{1B}-AR increases cell viability of water soluble tetrazolium salt (SW480) cells. Changes in SW480 cell proliferation and viability in response to drug treatment were measured using bromodeoxyuridine and WST-1 assays, respectively. A. The β-AR–selective agonist isoproterenol produces concentration-dependent decreases in both cell proliferation and viability. B. The α1-AR–selective agonist phenylephrine increases cell viability without affecting proliferation. C. Phenylephrine-stimulated increases in cell viability (100 μM) were antagonized by 10-minute pretreatment with cyclazosin (CYS, 100 nM) terazosin (TRZ, 1 μM), phenoxybenzamine (PBZ, 300 nM), or phentolamine (PHN, 10 μM). Data are the mean ± S.E.M. of three experiments with four replicates. **P < 0.01 compared with vehicle-treated cells (control) (one-way analysis of variance with Dunnett's post hoc test).

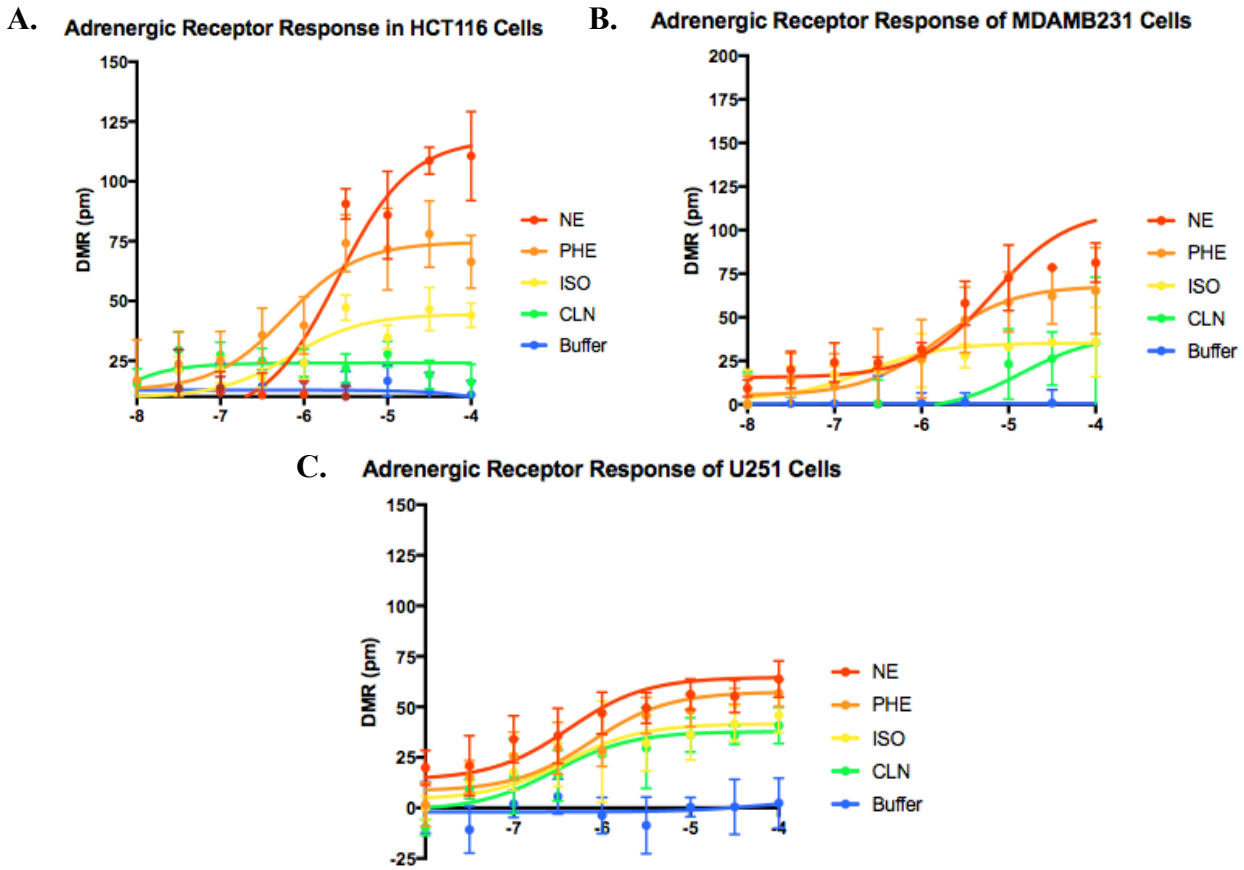

Figure 2.8. Agonist stimulation of HCT116, MDAMB231, and U251 cells *in vitro*. A. Dose response curve of Norepinephrine (NE), Phenylephrine (PHE), Isoproterenol (ISO), clonidine (CLN), and Buffer in HCT116 colorectal cancer cell lines. B. Dose response curve of Norepinephrine (NE), Phenylephrine (PHE), Isoproterenol (ISO), clonidine (CLN), and Buffer in MDAMB231 metastatic breast cancer cell lines. C. Dose response curve of Norepinephrine (NE), Phenylephrine (PHE), Isoproterenol (ISO), clonidine (CLN), and Buffer in U251 glioblastoma cell lines.

Agonist	pEC_{50}	EC50 (μM)	Max (pm)	IA
Norepinephrine	-5.96 +/- 0.04	1.08	354.74 +/- 4.72	1
Isoproterenol	-4.27 +/- 0.13	54.4	151.35 +/- 7.66	0.43
Clonidine	-6.52 +/- 0.12	0.3	144.47 +/- 13.2	0.41
Phenylephrine	-5.40 +/- 0.03	13.9	238.21 +/- 4.52	0.67
Serotonin	ND	ND	ND	ND

Table 2.1. Pharmacological properties of GPCR agonists in SW480 cells. Agonist-stimulated DMR concentration–response curves were constructed for responses measured at endogenous receptors expressed in SW480 cells. Log molar agonist potency (as stated prior to pEC50) were calculated using the time at which peak DMR response was observed. Intrinsic activities (IA) were calculated by setting norepinephrine maximal DMR responses equal to 1 and then normalizing other observed agonist maximal DMR values to this value. All data were analyzed with GraphPad Prism using nonlinear regression curve analysis and are expressed as mean ± S.E.M. of three to four independent experiments performed with four replicates. IA, intrinsic activity; Max, maximum response observed in pm; ND, not determined.

	Phenylephrine pEC_{50} +/- S.E.M.					Schild Analysis	
Agonist	Control	Dose 1	Dose 2	Dose 3	Dose 4	pA2	Slope
Phentolamine	-5.12 ± 0.03	-4.52 ± 0.03 (300nM)	-4.19 ± 0.04 (1M)	-3.54 ± 0.06 (3M)	-3.11 ± 0.10 (10M)	-6.93± 0.51	1.03 ± 0.08
Doxazosin	-5.56 ± 0.05	-5.24 ± 0.05 (10nM)	-5.23 ± 0.03 (30nM)	-4.86 ± 0.04 (100nM)	-4.07 ± 0.08 (300nM)	-7.76 ± 0.27	1.18 ± 0.34
Terazosin	-5.28 ± 0.05	-4.98 ± 0.11 (100nM)	-4.52 ± 0.11 (300nM)	-4.06 ± 0.14 (1M)	-	-7.81 ± 0.25	0.93 ± 0.29
Prazosin	-5.70 ± 0.06	-5.29 ± 0.05 (100nM)	-4.69 ± 0.05 (300nM)	-4.38 ± 0.07 (1M)	-	-7.47 ± 0.32	1.07 ± 0.21
Tamsulosin	-5.43 ± 0.06	-4.87 ± 0.07 (300nM)	-4.54 ± 0.07 (1M)	-4.38 ± 0.10 (3M)	-4.05 ± 0.10 (10M)	ND	ND
5-Methylurapidil	-5.45 ± 0.01	-4.84 ± 0.14 (300nM)	-4.84 ± 0.14 (1M)	-4.89 ± 0.25 (3M)	-4.21 ± 0.23 (10M)	ND	ND
Niguldipine	-5.65 ± 0.08	-5.08 ± 0.11 (3μM)	-3.82 ± 0.15 (10M)	-	-	ND	ND
Cyclazosin	-5.42 ± 0.11	-4.86 ± 0.12 (10 nM)	-4.86 ± 0.05 (30nM)	-4.62 ± 0.09 (100nM)	-	-8.37 ± 0.19	0.97 ± 0.21
BMY7378	-5.14 ± 0.03	-4.57 ± 0.05 (300 nM)	-4.57 ± 0.05 (1M)	-4.13 ± 0.03 (3M)	-3.57 ± 0.07 (10M)	-6.87 ± 0.47	1.06 ± 0.01

Table 2.2 . Pharmacological values used for α1-AR subtype–selective antagonist Schild regression analyses. Phenylephrine-stimulated concentration–response curves were calculated for stimulating DMR responses in SW480 cells. Log molar agonist potencies (pEC50) were calculated using the time at which peak DMR response was observed in the absence and presence of various α-AR antagonists (concentration of antagonist used shown in brackets for each phenylephrine pEC50 value). Agonist potencies were subsequently used to calculate antagonist affinity and slope via Schild regression analysis. All data were analyzed with GraphPad Prism and are expressed as mean ± S.E.M. of two to four independent experiments performed with four replicates.

CHAPTER III - Comparison of PDZ protein binding affinities to α_{1D}-CT PDZ Ligand

3.1 Introduction

G Protein-Coupled Receptors (GPCRs) account for ~4% of the human genome and are targets for ~30% of all FDA approved medications (Overington et. al. 2006). Typically, these medications compete with the endogenous ligand for the orthosteric binding site. However, there is a growing interest in identifying novel sites to modulate GPCR signaling, particularly in identifying GPCR interacting proteins. In the case of some GPCRs containing a C-terminal PDZ (PSD95/DLG/ZO-1) ligand, the PDZ domain containing proteins provide potential targets (Romero et. al. 2011, Ritter et. al. 2009) The structure-function analysis of GPCR:PDZ protein interfaces may lead to the development of novel small molecules used to selectively modulate GPCR function.

Only one adrenergic receptor, the α_{1D}-AR, contains a Type I PDZ ligand and has been implicated in many diseases (Olson et. al. 2011, Liu et. al 2015). However, deleterious side effects such as orthostatic hypotension and reflex tachycardia are often observed with chronic use of non-selective α1-AR antagonists. For example, the doxazosin arm of the ALLHAT anti-hypertensive study was prematurely halted due to increased morbidity (Miller et. al. 2000). Thus, these clinical findings highlight the need to develop novel approaches that selectively target α1-AR subtypes.

While the α_{1D}-AR has been historically difficult to study, we have made significant progress towards understanding how α_{1D}-ARs function in cells. We first discovered the α_{1D}-AR PDZ ligand interacts with syntrophins (Chen et. al. 2006), which recruits the Dystrophin Associated Protein Complex (DAPC) and signaling effectors, α-catulin, liprin and phospholipase-Cβ2 (Lyssand et. al. 2010, Lyssand et. al. 2011). Proteomic analyses subsequently revealed α_{1D}-ARs

also interact with the multi-PDZ domain containing protein, Scribble (SCRIB), and that α_{1D}-ARs can be expressed as modular homodimers containing both SCRIB and syntrophin. Moreover, α_{1D}-AR:PDZ protein interactions appear to be cell type specific – in SW480 colorectal carcinoma cells, α_{1D}-ARs interact with five PDZ proteins: SCRIB, syntrophin, hDLG1 (Human Disks Large), CASK (or LIN7C), and LIN7A (Camp et. al. 2015).

CASK and hDLG1 are both membrane-associated guanylate kinase proteins (MAGUK) that are characterized by the presence of at least one PDZ, SH3, and GuK domain (Nix et. al. 2000). The GuK domain is similar to guanylate kinase but is catalytically inactive (the P-loop that binds ATP is absent). It is thought that the Guk domain is used by MAGUK proteins as a binding domain for other proteins (Nix et. al. 2000; Lee et. al. 2002). The purpose of MAGUK proteins are for protein-protein interactions with cytoskeleton proteins, signal transduction, microtubule/actin machinery, synapse formation, and tight junction formation.

CASK is a MAGUK scaffolding protein that contains one PDZ domain. hDLG1 is also a MAGUK scaffolding protein with three PDZ domains. However, it is also known to transport NMDA and AMPA receptors from the endoplasmic reticulum (ER). One paper by Lin et. al. (2013) suggested that it is through the interaction with CASK that determines whether it is transporting AMPA or NMDA. LIN7A is not a MAGUK protein but is still responsible for scaffolding and contains one PDZ domain (Gruel et. al. 2016). These three proteins localize to the basolateral membrane.

hDLG1 is a promiscuous protein, interacting in several tripartite complexes. It is known to interact with MPP7 and LIN7A in the apical membrane of cells (Stucke et. al. 2007), but CASK and LIN7A in the basolateral membrane (Lozovatsky et. al. 2009). Several studies suggest that CASK and MPP7 compete for binding hDLG1, and one paper by Stucke et. al. (2007) suggested that MPP7 is in low concentrations in many different cell lines, which may explain why we did

not detect it in our proteomic screens. hDLG1 also has been shown to interact with SCRIB through LGL (Lethal Giant Larvae) in the leucine rich region (Su et. al. 2012; Zhu et. al. 2014) or, conflictingly, it has been shown that the GUK domain of hDLG1 interacts with GUKH, which is bound to SCRIB PDZ2 via its C-terminus PDZ ligand (Kallay et. al. 2006). However, despite our current knowledge, the precise architecture of the complex to the α_{1D}-AR remains unclear.

3.2 Materials and Methods

Plasmids and Chemicals. Molecular cloning was performed using inFusion HD cloning technology (Clontech/Takara Biotech, Mountain View, CA). Constructs used for bacterial expression were sub-cloned into pCOOL to add GST-tags. For mammalian expression, constructs were inserted into pGLUE to add streptavidin binding protein/TEV/calmodulin binding protein tags; or pSNAPf to add SNAP-epitope tags; or pcDNA3.1 to fuse MYC tags. BG-782 SNAP substrate was from New England Biolabs (Ipswich, MA).

Recombinant Protein Expression & Purification. Recombinant proteins were expressed in Rosetta™(DE3) competent cells (EMD Millipore, Burlington, MA) in Miller LB supplemented with 100 μg/mL Ampicillin and 34 μg/mL Chloramphenicol at 37°C until an OD_{600} = 0.6 – 1.0 was reached; followed by induction with 1 mM of IPTG at 18°C for 18 hours. Cells were harvested by centrifugation and lysed (20 mM Tris-HCl pH 8.0, 200 mM NaCl, 5 mM DTT). GST-tagged protein was immobilized on Pierce® glutathione agarose beads (Thermo Scientific, Waltham, MA) and washed (20 mM Tris-HCl pH 8.0 and 200 mM NaCl). Bound protein was eluted from the beads in wash buffer supplemented with 10 mM glutathione and concentration was determined using Bradford assay. Protein for crystallography was incubated with TEV at

4°C for 18 hours and subjected to size exclusion chromatography using a Superdex 75 Increase 10/300 GL (GE Healthcare, Chicago, IL) on an ATKA FPLC (Amersham Pharmacia Biotech, Little Chalfont, UK) in lysis buffer. The peak 215 nm fractions were collected. SDS-PAGE analysis was employed to determine purity, and protein was flash frozen and stored at -80°C until needed.

Affinity Purification/Co-immunoprecipitation. TAP purification was performed using the protocol as described previously (24). 5 μL of 25 μM BG-782 was included in the 1st overnight solubilization step with 0.5% digitonin to label SNAP-α_{1D}-ARs. SNAP-PAGE was used to observe SNAP-α_{1D}-AR protein levels. Gels were then transferred to nitrocellulose and blotted for anti-HA (#2367, Cell Signaling Technology, Danvers, MA) or anti-MYC (#9B11, Cell Signaling Technology, Danvers, MA), then anti-mouse Alexa-Fluor 2° antibodies in the 700-800 nm range (Invitrogen, Carlsbad, CA). Gels and blots were imaged with the LI-COR Odyssey CLx (LI-COR, Lincoln, NE).

Quantitative in vitro GST-pulldown Assay. SNAP-α_{1D}-C terminal (CT) was created by subcloning cDNA encoding the distal 16 amino acids of the human α_{1D}-CT domain into the 3' MCS of pSNAP. SNAP and SNAP-α_{1D}-CT were then subcloned into pCOOL to add N-terminal GST tags, expressed in, and purified from *E. coli* using the previously described method. Following TEV cleavage to remove GST, SNAP-α_{1D}-CT and SNAP were reacted with 1 μM BG-782 for 30 minutes at 37°C in the dark. Serial dilutions of BG-782:SNAP-α_{1D}-CT and SNAP were then subjected to SDS-PAGE and near infrared fluorescence (NIR: λ = 800 nm) was quantified with the LI-COR Odyssey CLx. Fluorescence intensity standard curves for SNAP and SNAP-α_{1D}-CT were generated to calculate protein concentrations. For GST-pulldown, 25 μL of

1 μM GST-tagged SCRIB proteins and 25 μL of BG-782:SNAP-α_{1D}-CT were incubated with 25 μL of packed Pierce® glutathione agarose beads and rotated in the dark for 1 hour at 4°C. Samples were centrifuged at 500 RPM at 4°C for 5 minutes. Supernatant was discarded and beads were washed 3x (20 mM Tris-HCl pH 8.0, 200 mM NaCl, and 0.05% NP-40). Samples were boiled in SDS-sample buffer, and 10 μL aliquots were subjected to PAGE, followed by LI-COR Odyssey CLx and GraphPad prism analysis.

Bio-layer Interferometry (BLI). BLI was performed using the Octet Red 96 system (Pall Forte Bio, Fremont, CA). All steps were performed in 20 mM Tris-HCl pH 8.0, 200 mM NaCl, and 0.1% bovine serum albumin. 50 nM of biotin labeled α_{1D}-CT (BioMatik, Cambridge, ON) was immobilized to streptavidin coated probes, followed by biocytin. The immobilized peptide was incubated in serial dilutions of target proteins until steady-state binding was reached. Biocytin was used to determine non-specific binding. For reverse BLI, GST-SCRIB was immobilized using anti-GST probes, and then incubated in serial dilutions of biotin labeled α_{1D}-CT.

3.3 Results

We previously discovered the α_{1D}-AR interacts with no less than 5 PDZ proteins (Scribble, syntrophin, CASK, DLG1, LIN7A) with cell-type specificity (Camp et. al. 2015). To attempt to elucidate the architecture of these interacting proteins as a single large macromolecular complex or as multiple complexes with the α_{1D}-AR, we employed multiple techniques. To first determine the potential binding of our receptors, we utilized SNAP-tag technology to quantify GST-SCRIB:α_{1D}-C-terminal (α_{1D}-CT) binding interactions using PAGE near infrared imaging (NIR). SNAP-epitope tags were fused to the N-terminus of α_{1D}-CT (SNAP-α_{1D}-CT). PDZ protein cDNAs were subcloned into pCOOL vector to add GST tags, expressed in *E. coli,* and purified.

The various proteins were then expressed with decreasing concentrations of α_{1D}-CT and run on a gel. SNAP NIR stain was used to detect the potential interaction of these proteins.

Interestingly, it appeared that all of our proteins interacted with the α_{1D}-AR – hDLG1 PDZ Domains 1-2, hDLG1 PDZ Domains 1-3, MPP7, and CASK, with CASK binding slightly better than MPP7 (Figure 3.1A). hDLG1 PDZ1-3 and hDLG1 PDZ1-2 did not bind to the α_{1D}-CT as well as CASK or MPP7. However, hDLG1 PDZ1-3 showing a higher affinity than hDLG1 PDZ1-2, possibly due to the increased number of potential binding sites for the α_{1D}-AR (Figure 3.1A). When isolating all the PDZ domains of hDLG1 and performing separate SNAP assays on the individual PDZ domains, it appeared that hDLG1 PDZ domain 3 had a significantly increased binding affinity than hDLG PDZ1-2 *or* 1-3 (Figure 3.1B). Also, of note, the binding of hDLG1 PDZ1 also had a higher affinity than either hDLG1 PDZ1-2 or 1-3 (Figure 3.1B). The individual hDLG2 bound with less affinity than hDLG1 or hDLG3, and with the same affinity of hDLG PDZ 1-3 (Figure 3.1B). These trends reached significance at high concentrations of the α_{1D}-AR (1μM) (Figure 3.1C, D). Taken together, these data suggest the potential for hDLG PDZ domain 2 as an inhibitor for binding of the α_{1D}-AR at a relatively high concentration of the agonist (1μM). Further research is needed to determine the role of this domain as an inhibitory domain.

From here, we took those hits and moved to OCTET Biolayer Interferometry (BLI) to more accurately quantify binding through equilibrium dissociation constants (K_D) for α_{1D}-AR PDZ ligand:PDZ-protein interactions. The previously purified PDZ proteins were incubated with Biotin labeled α_{1D}-CT then subjected to BLI analysis. We first compared α_{1D}-CT binding to Scribble (SCRIB) and syntrophin, as α_{1D}-ARs were found to interact with both PDZ proteins in all human cell lines examined (Camp et. al. 2015). Remarkably, α_{1D}-CT bound SCRIB (PDZ1234, K_D = 70 nM; Figure 3.2A) with ~8 higher affinity than syntrophin (K_D = 0.56 μM).

Subsequent BLI analysis revealed hDLG1 PDZ Domains 1-3 (K_D = 0.72 μM Figure 3.2B) and CASK (K_D = 2.13 μM, Figure 3.2C) bind the α_{1D}-CT with significantly lower affinity than SCRIB. MPP7 and LIN7A, known interactors of hDLG1 (Stucke et. al. 2007, Gruel et. al. 2016), displayed negligible BLI responses (Figure 3.2D).

As with hDLG1, a defining structural characteristic of SCRIB includes the presence of multiple (4) clustered PDZ domains. Thus, we questioned if α_{1D}-CT selectively associates with targeted PDZ domains on SCRIB or hDLG1 to validate our findings on the SNAP assays. To do so, we subcloned individual PDZ domains of SCRIB or hDLG1 into pCOOL for bacterial expression and purification. As shown, BLI analysis implies SCRIB PDZ1 (K_D = 0.78 μM; Figure 3.3A) and PDZ4 (K_D = 1.38 μM; Figure 3.3B) bind α_{1D}-CT with the highest affinity, followed by SCRIB PDZ2 (K_D = 13.04 μM; Figure 3.3C) and SCRIB PDZ3 (K_D = 86.09 μM; Figure 3.3D).

BLI analysis also implies that hDLG PDZ Domain 1 binds with greater affinity than SCRIB PDZ1 (K_D = 0.72 μM; Fig 3.3E), but not less than PDZ2-4 of SCRIB. hDLG PDZ Domain 2 binds between PDZ4 of SCRIB and PDZ2 of SCRIB (K_D = 5.75 μM; 3.3F). Lastly, hDLG PDZ3 did not indicate binding affinity. Comparative analyses of maximal BLI responses demonstrate α_{1D}-CT binds robustly to SCRIB containing all 4 PDZ domains (PDZ1234), followed by PDZ1 > PDZ4 >> PDZ1 = PDZ3 and α_{1D}-CT binds robustly to hDLG1 containing all 3 PDZ domains (PDZ123), followed by PDZ1>>PDZ2>>>PDZ3. These data show that hDLG PDZ 2 binds will less affinity than hDLG PDZ Domains 1-3, 1-2, or 1, which still may indicate the potential for it to play the role of an antagonist for the binding of the α_{1D}-AR to hDLG1 (Figure 3.3G).

3.4 Discussion

With the advent of new technologies that facilitate biochemical analysis of integral membrane proteins, interest has expanded in solving GPCR:PDZ-protein macromolecular complexes

(Tsunoda et. al. 1997, Cao et. al. 1999, Temkin et. al. 2011). Herein we extend previous findings (Chen et. al. 2006, Lyssand et. al. 2010, Lyssand et. al. 2011, Camp et. al. 2015) by providing novel insights into the biochemical architecture of the modular α_{1D}-AR:SCRIB:DAPC assembly. BLI and PAGE NIR pinpoint SCRIB PDZ domain 1/4 (PDZ1/4) as the primary interaction site for the α_{1D}-AR PDZ ligand; hDLG PDZ Domains 1-3, particularly PDZ Domain 1 as the primary interaction site for the α_{1D}-AR PDZ ligand, and that CASK and MPP7 are unlikely to bind except in high concentrations. This was to be expected as CASK has a type 2 PDZ binding domain and the α_{1D}-AR has a type 1 PDZ ligand (REDTI). The lack of binding with MPP7 was not surprising as this protein was not pulled down on our proteomics screen, and further supports the notion that the α_{1D}-AR accumulates at the basolateral membrane. All the proteins that are shown to interact with the α_{1D}-CT are localized to the basolateral membrane, while MPP7 is localized to the apical membrane. This was important to examine, as this protein has been shown to interact with hDLG1 and LIN7A as well.

However, the α_{1D}-AR PDZ ligand appears to be the only protein identified to interact with SCRIB PDZ1/4 to date. Thus, we proposed α_{1D}-AR:SCRIB PDZ1/4 as a potential target for drug discovery. Developing small molecules that can disrupt or enhance the α_{1D}-AR:SCRIB PDZ1/4 interaction may provide alternative strategies to selectively treat diseases associated with aberrant α_{1D}AR signaling, while not effecting the closely related α1-AR subtypes, or the α_2- or β-AR families of GPCRs. Additionally, hDLG1 PDZ Domain 1 may also provide a drug target for colorectal cancer due to the cell type specificity in SW480 cells. Again, targeting this protein rather than the α_{1D}-AR may decrease the incidence of binding to the closely related α_1-ARs.

A central goal of this study was to reconcile previous findings suggesting α_{1D}-ARs form cell type specific PDZ protein complexes. For example, syntrophin and SCRIB interact with α_{1D}-AR in all

human cell lines examined to date, whereas α_{1D}-AR interacts with PDZ proteins CASK, hDLG1 and LIN7A in SW480 colon carcinoma cells (Camp et. al. 2015). BLI analyses implicate SCRIB as the highest affinity PDZ protein interactor for α_{1D}-AR, suggesting SCRIB acts as the primary scaffolding protein in the α_{1D}-AR complex and anchors additional protein partners. In support of this hypothesis, yeast two-hybrid screening and confocal imaging identified the GUK domain of hDLG1 interacts with GUKH, which is bound to SCRIB PDZ2 via its C-terminus PDZ ligand in synaptic boutons of *Drosophila* (Matthew et. al. 2002). It has also been shown to bind to SCRIB through LGL (Lethal Giant Larvae) in the leucine rich region in Mardin Darby Canine Kindney (MDCK) cells (Su et. al. 2012, Zhu et. al. 2014). Additionally, extensive biochemical analyses uncovered a tripartite complex of hDLG1, CASK, and LIN7A via L27 domains in cell culture and brain (Butz et. al. 1998, Borg et. al. 1998, Lee et. al. 2002).

Based on current affinity data along with previous examples (Stucke et. al. 2007), it is possible that the CASK/LIN7A/hDLG complex is responsible for trafficking of the α_{1D}-AR from the ER to the scaffolding molecule SCRIB. After which, hDLG could bind SCRIB while CASK and LIN7A bind other proteins (as seen in Humbert et. al. 2003). Additionally, SCRIB is known to interact with numerous proteins in a PDZ dependent mechanism - e.g. β-PIX (Ivarsson et. al. 2014, Lim et. al. 2017) and thyrotropin receptor (Lahuna et. al. 2005) both interact with PDZ1 and PDZ3 – highlighting the dynamic nature of this "signalosome".

These data, taken together, paint a very intricate picture in the dynamic nature of the α_{1D}-AR signaling complex. By targeting any of these PDZ proteins directly with novel medications, we might abate some of the negative side effects of current medications on the market that are caused by the similarities in binding domains for the various α_1-ARs. These data could provide the foundation to develop new drugs that target such diseases as schizophrenia, PTSD, hypertension, and BPH.

Abbreviations: GPCR, G Protein-Coupled Receptors; PDZ, PSD95/DLG/ZO-1; DAPC, Dystrophin Associated Protein Complex; SCRIB, Scribble; hDLG1, Human Disks Large; MAGUK Proteins, Membrane-Associated Guanylate Kinase Proteins; ER, endoplasmic reticulum, CT, C-terminal; LGL, Lethal Giant Larvae; GST, glutathione S-transferase; *E. coli,* Escherichia coli; NIR, near infrared; BLI, Bio-layer interferometry.

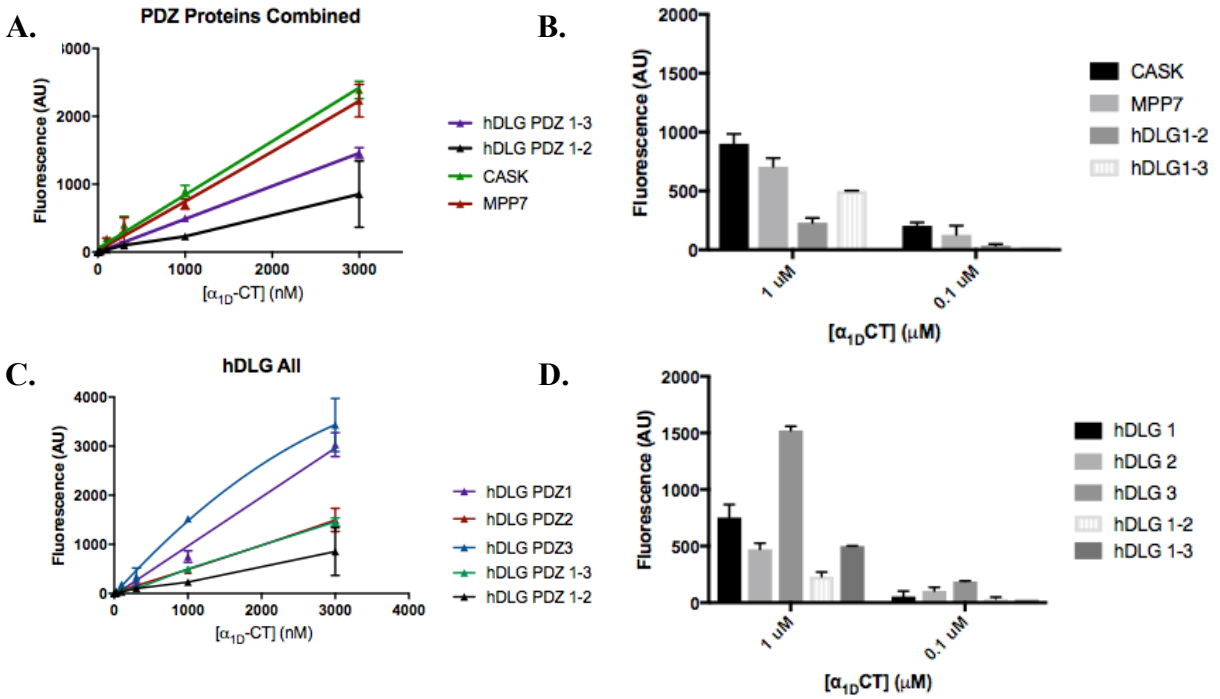

Figure 3.1. Modified GST Pull-down Assay showing the binding of the PDZ proteins to various concentrations of SNAP-α_{1D}-CT. A. Relative fluorescence of PDZ Proteins CASK, MPP7, and hDLG PDZ domains 1-2, 1-3. B. Analysis of PDZ proteins CASK, MPP7 and hDLG PDZ Domains 1-2, 1-3 at 1μM and 0.1μM. C. Relative fluorescence of all hDLG PDZ domains (1, 2, 3, 1-2, 1-3). D. Analysis of all hDLG PDZ domains (1, 2, 3, 1-2, 1-3) at 1μM and 0.1μM.

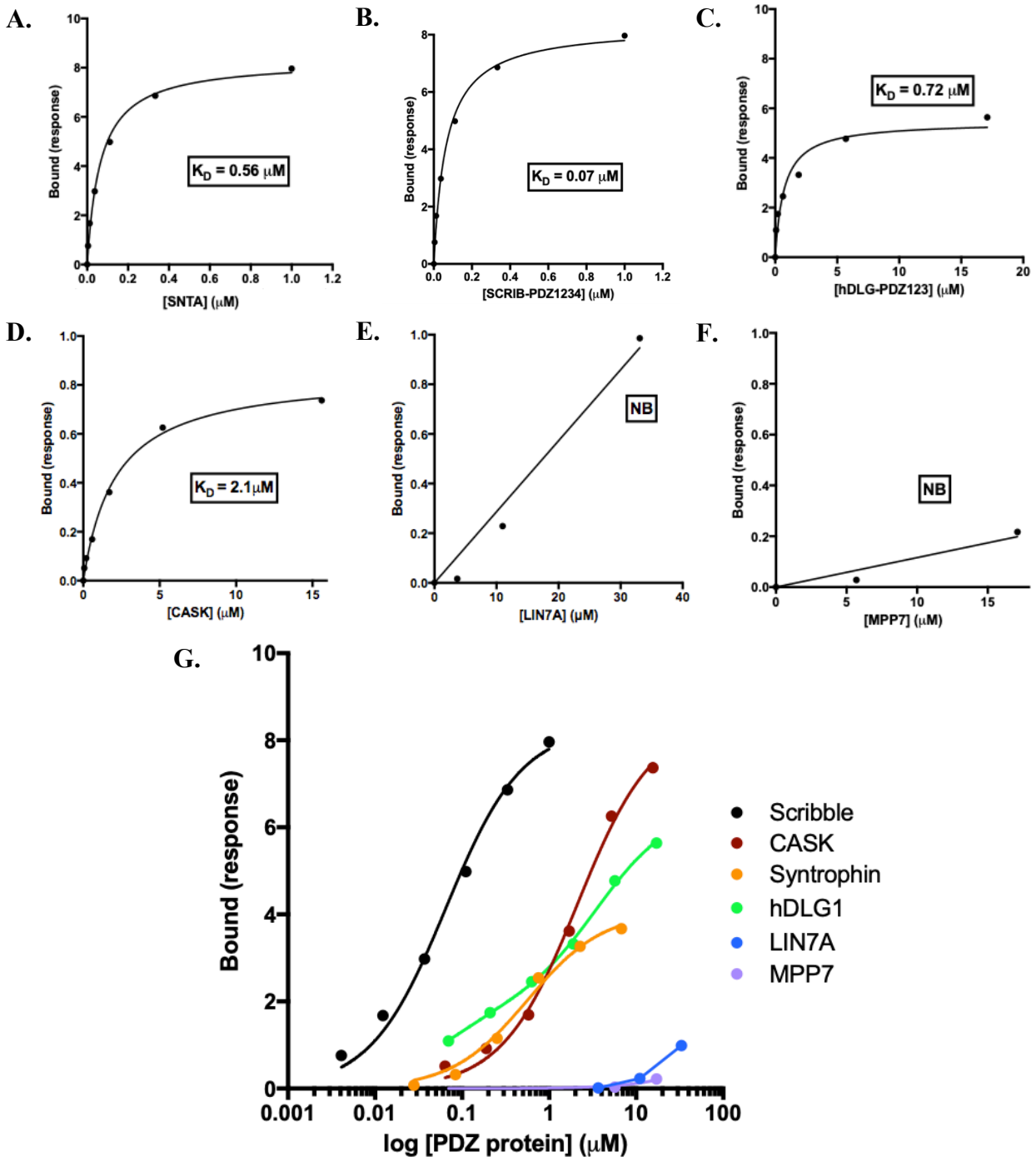

Figure 3.2. OCTET BLI on PDZ Proteins interacting with the α_{1D}-CT. A. Affinity of syntrophin binding to the α_{1D}-CT revealed to be 0.56μM. B. Affinity of SCRIB PDZ Domains 1-4 binding to the α_{1D}-CT revealed to be 0.56μM. C. Affinity of hDLG PDZ Domains 1-3 binding to the α_{1D}-CT revealed to be 0.72μM. D. Affinity of CASK binding to the α_{1D}-CT revealed to be 2.1μM. E. MPP7 showed no binding to the α_{1D}-CT. F. LIN7A showed no binding to the α_{1D}-CT. G. Summary of the binding affinity of various PDZ proteins to the α_{1D}-CT.

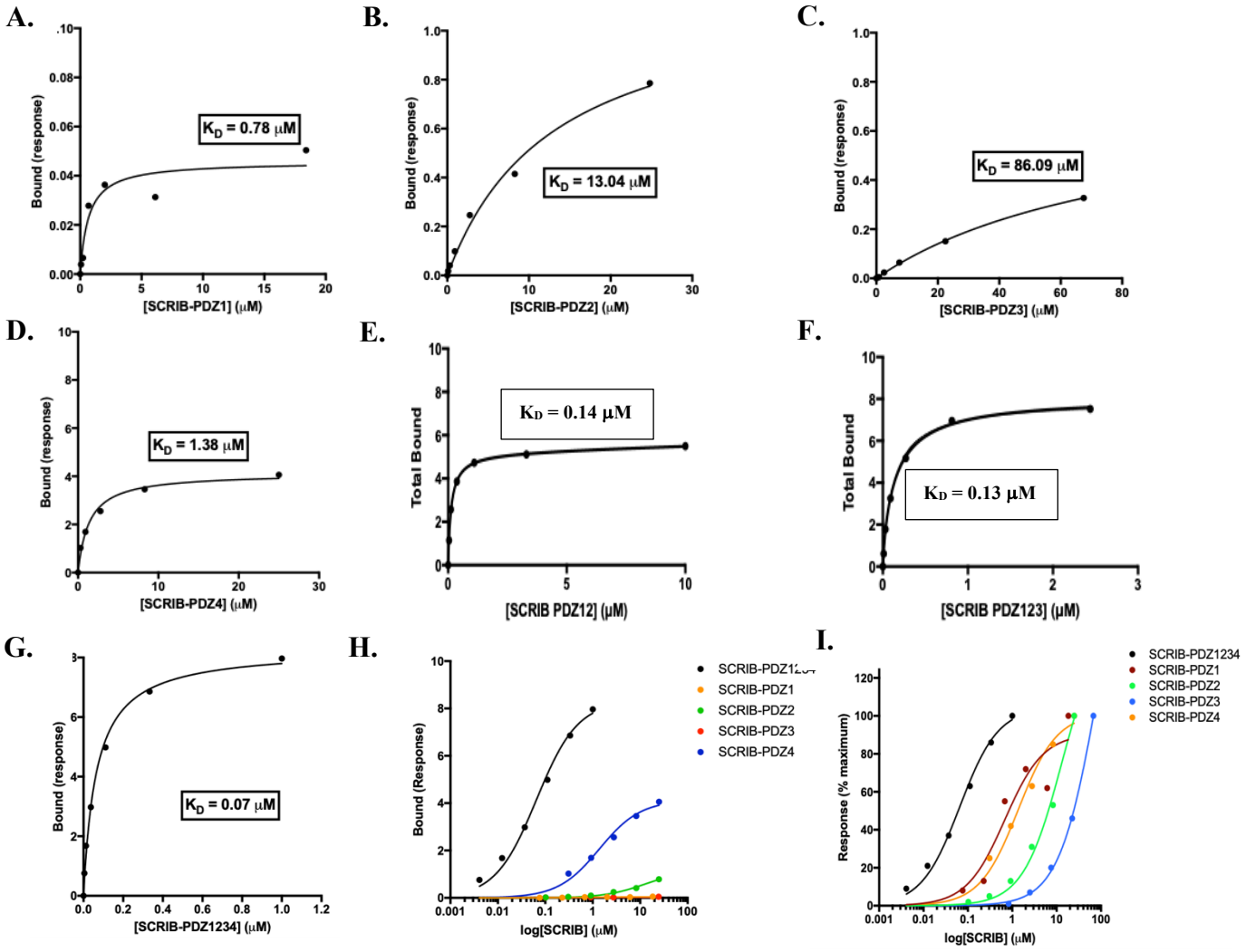

Figure 3.3. OCTET BLI on the various PDZ domains of SCRIB in binding the α_{1D}-CT. A. Affinity of SCRIB PDZ Domain 1 binding to the α_{1D}-CT revealed to be 0.78μM. B. Affinity of SCRIB PDZ Domain 2 binding to the α_{1D}-CT revealed to be 13.04μM. C. Affinity of SCRIB PDZ Domain 3 binding to the α_{1D}-CT revealed to be 86.09μM. D. Affinity of SCRIB PDZ Domain 4 binding to the α_{1D}-CT revealed to be 1.38μM. E. Affinity of SCRIB PDZ Domain 1-2 binding to the α_{1D}-CT revealed to be 0.14μM. F. Affinity of SCRIB PDZ Domain 1-3 binding to the α_{1D}-CT revealed to be 0.13μM. G. Affinity of SCRIB PDZ Domain 1-4 binding to the α_{1D}-CT revealed to be 0.07μM. H. Summary of the binding affinity of various individual SCRIB PDZ domains to the α_{1D}-CT. I. Summary of the binding affinity of various joint SCRIB PDZ domains to the α_{1D}-CT.

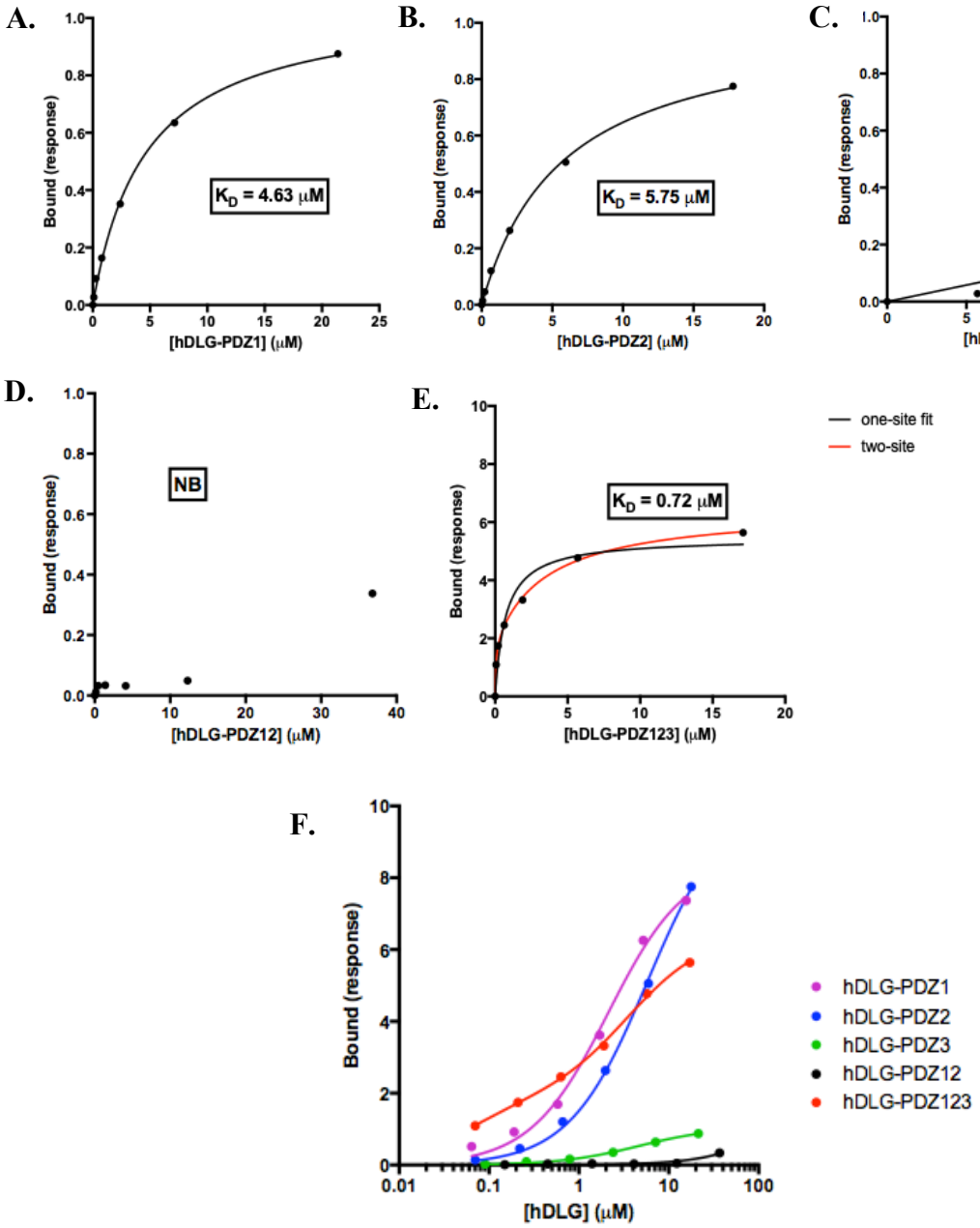

Figure 3.4. OCTET BLI on the various PDZ domains of hDLG1 in binding the α_{1D}-CT. A. Affinity of hDLG1 PDZ Domain 1 binding to the α_{1D}-CT revealed to be 0.78μM. B. Affinity of hDLG1 PDZ Domain 2 binding to the α_{1D}-CT revealed to be 13.04μM. C. Affinity of hDLG1 PDZ Domain 3 binding to the α_{1D}-CT revealed to be 86.09μM. D. Affinity of hDLG1 PDZ Domain 1-2 binding to the α_{1D}-CT revealed to be 0.14μM. E. Affinity of hDLG1 PDZ Domain 1-3 binding to the α_{1D}-CT revealed to be 0.13μM. F. Summary of the binding affinity of various individual hDLG1 PDZ domains to the α_{1D}-CT.

Protein Name	K_D (μM)
Syntrophin	0.56
Scribble PDZ Domains 1-4	0.07
Scribble PDZ Domains 1-3	0.13
Scribble PDZ Domains 1-2	0.14
Scribble PDZ Domain 1	0.78
Scribble PDZ Domain 2	13.04
Scribble PDZ Domain 3	86.09
Scribble PDZ Domain 4	1.38
hDLG1 PDZ Domains 1-3	0.72
hDLG1 PDZ Domains 1-2	NB
hDLG1 PDZ Domain 1	4.63
hDLG1 PDZ Domain 2	5.57
hDLG1 PDZ Domain 3	NB
CASK	2.13
LIN7A	NB
MPP7	NB

Table 3.1. Binding affinity of all PDZ Proteins to the α_{1D}-CT via OCTET BLI. Rank order of binding of all the PDZ proteins is as follows: SCRIB>SYNT>hDLG1>>CASK>>>LIN7A=MPP7. Rank order of the PDZ domains of SCRIB are as follows: SCRIB1-4>SCRIB1-3>SCRIB1-2>SCRIB 1>SCRIB4>>SCRIB2>>SCRIB3. Rank order of the PDZ domains of hDLG1 are as follows: hDLG1-3>>hDLG1>hDLG2>>>hDLG3=hDLG1-2.

Chapter IV - Comparison of 2D and 3D Cell Models for Studying α_{1D}-AR:PDZ Protein Complex Function

4.1 Introduction

Historically, two-dimensional (2D) models have been used to study disease and as an important tool for drug discovery due to the ease of use and broad applicability for high throughput screening. However, 2D models do not offer the opportunity to study cells in their native environment (Boussommier et. al. 2018). Additionally, there is a distinct lack of polarity with cells, whether that be apico-basolateral polarity or axonal-dendritic polarity. Thus, cells have limited communication and contact with other cells, thereby limiting their intracellular communication. Unfortunately, this leads to the critique that manipulating 2D cells can have limited physiological relevance.

Conversely, three-dimensional (3D) structures facilitating creation of both adherins and tight junctions, allowing for the directed transport of materials between cells (Ahlstrom et. al. 2014).

Recently, new methods for creating 3D cell cultures have been developed, including the intricate organ-on-a-chip method, to the affordable gel matrix approach (Larson et. al. 2015). These new methods represent important steps toward bridging studies between the historical 2D model and the more accurate 3D model. In providing a more organ-like environment for cells, the 3D culture models may more accurately reflect the architecture and biochemical characteristics of *in vitro* systems (Boussommier et. al. 2018).

Cell behaviors are influenced by cues in the microenvironment: cell morphology, polarity, proliferation, signal transduction, cellular cross-talk and biochemical activities (Rodriguez-Boulan et. al. 1989). Maintaining these systems are vital for the proper analysis and experimentation of cells. This becomes particularly important in epithelial and neuronal cell

systems, which have highly organized architecture and apicobasal or axonal-dendritic polarity *in vivo* (Figure 4.1, Bryant et. al. 2008).

Establishment of epithelial apico-basolateral polarity and neuronal axonal-dendritic polarity is vital for proper neuroendocrine and cardiovascular function. Polarity refers to the asymmetric distribution of proteins that allow the cells to form organized membrane subdomains for specialized functions including secretion, filtration, absorption, and sensory function (Rodriguez-Boulan et. al. 1989). The formation of polarity is established by an intricate network of protein-protein interactions (Ahlstrom et. al. 2014).

The kidney, like many organs, have polarized epithelia that form tubular structures with an apical membrane facing the lumen, and a basolateral membrane in which the lateral membrane forms cell-cell interactions and the basal membrane forms the cell-matrix basement membrane (Bryant et. al. 2008). Cell-cell interactions are mediated by transmembrane proteins such as cadherins and nectins. Tight junctions form the major barrier that separates the apical and basolateral membrane and allows for the transfer of molecules from one cell to another (Figure 4.2, Alhstrom et. al. 2014). Adherens junctions bind the actin filaments together between different cells. Desmosomes bind the intermediate filaments between cells, forming a tighter connection between cells and hemidesmosomes form a similar connection between a cell and the basement membrane (Ahlstrom et. al. 2014). All these proteins help to form a strong network of cells affixed to the basement membrane which prevents diseases such as organ fibrosis and carcinoma progression (Thiery et. al. 2009).

The basal membrane forms the cell-matrix interface. The extracellular matrix (ECM) consists of glycoproteins, collagens, and proteoglycans (Frantz et. al. 2010). The ECM is important for forming the structural framework that stabilizes tissues and provides support for cell attachment

(Frantz et. al. 2010, Yi et. al. 2017). It also plays an important role in cell functionality and differentiation with receptor-mediated signaling and regulation of gene expression.

The major protein complexes involved in polarity formation is the Par complex, Crumbs complex, the Scribble complex, and the hDLG1 complex (Pieczynski et. al. 2011). The Par and Crumbs complex are involved in formation of the apical membrane whereas the Scribble and hDLG1 complex is involved in the formation of the basolateral membrane (Pieczynski et. al. 2011). In general, the apical membrane forms first and antagonism to the apical membrane by the basolateral (BL) proteins leads to the switch that forms the BL membrane (Ahlstrom et. al. 2014). This antagonism is primarily mediated by protein-protein interactions at the tight junction that forms the boundary between the apical and BL membrane.

The conversion of epithelial cells to mesenchymal cells, known as epithelia-mesenchymal transition (EMT), is vital for embryonic morphogenesis, adult tissue repair, and is seen in disease states such as oncogenesis, chronic obstructive pulmonary disease (COPD), and organ fibrosis (Thiery et. al. 2009). This process occurs first by disrupting the cell-cell adhesion molecules such as E-Cadherins (adherens junctions) and occludins (tight junctions) in the lateral membrane (Ahlstrom et. al. 2014). Next, there is a disruption in the cell-ECM adhesion in which the interaction between integrins and fibronectin/laminin/collagen is severed (Ahlstrom et. al. 2014). Lastly, the polarity of the cell must be disrupted by inactivating the molecules that establish cell polarity (Ahlstrom et. al. 2014).

As mentioned, there are several new technologies when studying the polarization and 3D formation of cells. The most traditional method for studying 3D cell culture was to use Madin-Darby Canine Kidney (MDCK) cells. Balcarova-Stander et. al. (1984) discovered that cell polarity was formed using monoclonal antibodies for the BL membrane. More recent technologies include the organ on a chip, which is small and expensive to buy and can be linked

with other organs on a chip to study the effects on of a drug on human cell organ systems (Mauriac et. al. 2017). This is a great system for single organ systems, but further research needs to be conducted to increase the reliability of multiple organs on a chip.

Corning Life Sciences' Matrigel and ThermoFisher's Geltrex Matrices allow for basement-like-membranes that provide physical support for cultured cells in order to provide a more *in vivo*-like ECM (Giles et. al. 2014). These ECM-based growth substrates provide a physiological environment that supports and promotes cell functions. ECM molecules also interact with surface receptors and can play a key role in presenting the receptors at the surface of the cell (Larson et. al. 2015). Matrigel is made of about 60% laminin, 30% collagen, 8% entactin, and 2% growth factors, and metalloproteinases to create a reconstituted basement membrane by activation of Rac1, which induces the assembly of laminin networks (Huges et. al. 2010).

Another 3D modeling system is Corning Life Sciences' Spheroid Microplate. This is a 96 well plate that is coated with a covalent hydrogel layer to reduce cell attachment and aids in the promotion of multicellular spheroids (Bergeron et. al. 2017). The well geometry allows for the generation of a single, uniform, and reproducible 3D spheroid in all the wells.

In this study, we demonstrated the effectiveness of both Matrigel and the Spheroid Microplate for creating 3D environment. Our long-term goal is to use these approaches to examine the localization of the α_{1D}-AR to either the basolateral or apical membrane in polarized cell cultures. Additionally, we will determine if there are inherent differences in GPCR function between 2D and 3D cell cultures.

The loss of key polarization mechanisms and proteins may be a partial explanation as to why the α_{1D}-AR is localized to the ER in 2D cultured cells. It is known that α_{1D}-ARs are sequestered intracellularly in cultured cells, where they respond poorly to agonist stimulation (Hague et. al. 2004, Fan et. al. 2009, Kountz et. al. 2016). An important clue to solving this longstanding

mystery in the field was uncovered by Fan et. al. (2009), who elegantly demonstrated α_{1D}-ARs are functional in freshly dissociated vascular smooth muscle cells but are then lost 48 hours later. This loss of polarity involves remodeling of the ECM and this transition can lead to loss of cellular architecture and internalization of receptors, which may explain the internalization of the α_{1D}-ARs in cultured cells.

Additionally, the Hague lab determined that N-terminal (NT) truncation (either Δ1-79, Δ1-91) does allow for membrane expression of the α_{1D}-AR in 2D cells (Hague et. al. 2004, Kuntz et. al. 2016). Thus, we also wanted to compare Δ1-91 α_{1D}-ARs to full-length (FL) α_{1D}-ARs.

To date, we have discovered that Matrigel represents a rather difficult medium to work with and yields inconsistent results. In contrast, the Spheroid microplate has shown remarkable ease and consistency. This has allowed us to determine that in a 3D environment, the FL α_{1D}-AR expresses at the membrane of the cells as well as expressing normal pharmacodynamic properties when compared to the N-terminal truncation of the α_{1D}-AR.

4.2 Materials and Methods

Plasmids and Chemicals. Molecular cloning was performed using inFusion HD cloning technology (Clontech/Takara Biotech, Mountain View, CA). For mammalian expression, constructs were inserted into pSNAPf to add SNAP-epitope tags. BG-782 SNAP substrate was from New England Biolabs (Ipswich, MA). Matrigel and the 96 well spheroid microplate were obtained from Corning Life Sciences. Stains were purchased from commercial sources: Cell Surface SNAP 541, Hoechst 33342, Mouse anti-E-Cadherin primary antibody, Goat anti-Mouse secondary antibody, and Prolong Gold with DAPI.

Cell Culture and Transfection. HEK293 cells were propagated in Dulbecco's Modified Eagle's Medium containing 10% fetal bovine serum, 2% L-glutamine, and 100 units/mL penicillin at 37°C in 5% CO_2. The constructs were transfected using Polyethyleneimine transfection reagent (PEI, Sigma-Aldrich) when cells were ~80% confluent. Eight hours later, medium was aspirated from the plates and washed with Dulbecco's Phosphate-Buffered Saline at 37°C (PBS, Corning). Trypsin is added to each plate and placed back in the incubator until the cells detach. The cells were resuspended in 8mL of medium. Corning Cell Counter was used to count the cells and the cells were resuspended in the appropriate volume for cells/mL desired.

Matrigel. For each chamber of the plate, 100µL Matrigel was mixed with 100µL of cells and media in a 1.5mL microcentrifuge tube. All 200µL was immediately transferred to one of the chambers on the plate and the plate was placed back in the incubator until the mixture formed a gel-like consistency (15-20 minutes). Once solidified, 200µL medium was added to the top of the Matrigel in each chamber. The cells were placed back in the incubator and checked daily to monitory spheroid formation. Once spheroids form, the top medium layer was removed and the Matrigel was dissolved in 200µL PFA to each chamber. PFA was removed after 30-45 minutes and cells were washed three times with room temperature DPBS with calcium and magnesium (Sigma-Aldrich). Spheroids were permeabilized with PBS+ 0.02% Triton X-100 (Intgra) and incubated for 30 minutes at room temperature. 10µL DAPI stain was added overnight in 4°C fridge. Spheroids imaged 12-72 hours later.

Spheroid Microplate. Final volume of the cells was established at 100,000 cells/mL. 100µL cells and medium was plated into each of the 96 wells using a multichannel pipette. The cells were cultured in the incubator for 48 hours before harvesting and imaging.

Live cell Imaging: Cells were removed from incubator and placed in hood where SNAP stain was added (I:200 in DMSO, Sigma-Aldrich). Cells were placed back in incubator for 1 hour. Hoechst 33342 stain was added (1:1000, Sigma-Aldrich) 10 minutes before imaging.

Harvesting: Cells were removed from incubator and 100μL PFA was added to each well. PFA was removed after 30 minutes and cells were washed three times with room temperature DPBS. SNAP stain was prepared at 1:200 in DMSO and incubated for 1 hour at room temperature. SNAP stain was removed and spheroids were permeabilized with PBS+ 0.02% Triton X-100 (Intgra) and incubated for 30 minutes at room temperature. Permeabilization buffer was removed and 10μL DAPI stain was added overnight in 4°C fridge. Spheroids imaged 12-72 hours later.

Label-Free Dynamic Mass Redistribution (DMR) Assays. HEK293 cells containing both FL and Δ1-91 α_{1D}-ARs (passage number 3–10) were plated in a 96 well Corning Spheroid Microplate at 10,000 cells/well and cultured for 48 hours in DMEM plus fetal bovine serum. Label-free DMR assays were performed using a method derived from previously documented studies (Fang et. al. 2006, 2007). HEK293 cells containing both FL and Δ1-91 α_{1D}-ARs (passage number 3–10) were seeded at 10,000 cells/well in in Corning Epic sensor microplates and cultured for 48 hours in DMEM plus fetal bovine serum. On the day of the experiment, the spheroids were transferred into the Corning EPIC sensor microplate using wide bore tips (Corning). The cells were spun down at 500rpm for 5 minutes. The cells were transferred to the Corning Epic BT reader, which was permanently housed in a Thermo cell culture incubator at 37°C as this magnified the amplitude of recorded DMR responses. Cells were incubated, during which baseline DMR measurements were recorded. All compounds were added using a Sorenson Biosciences 96-well Benchtop Pipettor. Agonist DMR responses were recorded for 1 hour. Raw data were exported to Microsoft Excel using Epic Analyzer Software and then imported into GraphPad Prism software

to calculate agonist (potency, intrinsic activity) and antagonist (affinity) properties. Agonist concentration–response curves were fit using variable slope nonlinear regression to determine potency (EC50). The y-axis values on raw DMR data and agonist DMR concentration–response curves represent the shift in light wavelength in picometers (pm) as a result of DMR.

EMT Studies. Cells were plated in 96 well spheroid microplate and harvested as described above. After fixing the cells, they were incubated in blocking buffer for 45 minutes at RT. Anti-E-Cadherin primary antibody (1:250) was added and incubated for 3 hours at RT. Secondary antibody (1:1000) was added and incubated for 1 hour at RT. SNAP stain (1:200) was added for 1 hour at RT. DAPI was added to each well and placed in 4°C fridge overnight before imaging.

4.3 Results

To determine the localization of the α_{1D}-ARs to the apical or basolateral membrane, we must first determine an effective 3D modeling system. Thus, we first pursue the Corning Gel Matrix (Matrigel) by comparing the use of this technology with HEK293 cells as well as SW480 cells (Figure 4.3). Our interest in using these cell types was due to previous research (Camp et. al. 2015) indicating the additional PDZ proteins interacting with the α_{1D}-ARs with cell-type specificity. By examining these cell types with the Matrigel, we noted the formation of the spheroids were complete with HEK293 cells (at around 88% completed spheroids) rather than the SW480 cells (at around 21% completed spheroids). This informed our future studies as we decided to use Matrigel with HEK293 cells.

Now that we had decided on a cell type with which to perform the experiments, we then conducted a time course of spheroid formation (Figure 4.4) via methods described in Giles et. al. (2014). This was necessary to determine the proper length of time needed for the spheroids and

lumen to adequately form. However, the formation of the lumen, which is a quintessential element of the formation of the 3D spheroid (Martin-Belmonte et. al. 2008), was inconsistent over the number of days the time course. In addition, many of the spheroids on the same day did not appear to be at the same stage of formation.

This was not uncommon to see as mentioned in Debanth et. al. (2003). In cases where the lumen tends to take some additional time to form, this tends to be due to a hollowing event rather than cavitation; in which cells die by apoptosis rather than migrate out of the center of the spheroid (Martin-Belmonte et. al. 2008). So, following the methodology in Debanth et. al. (2003), we hoped to determine if it might be a more successful protocol for formation of the lumen. Unfortunately, this protocol did not even form the spheroid (Figure 4.5, C). We continued working with Matrigel while searching for an alternative method of 3D spheroid formation. Despite our numerous attempts, we were not able to successfully replicate the Matrigel protocol described in the literature with HEK293 cells (Figure 4.5, A-B).

We then obtained Corning Spheroid Microplates and used the protocol described in Corning Life Sciences (2018) to form the spheroids. As seen in Figure 4.6, we successfully formed the spheroids in HEK293 cells and image the results using the SNAP-tag.

We next set out to determine if the presence of stably transfected adrenergic receptors would alter the formation of the spheroid and the length of time it took for form the spheroid. With the exception of a slight difference of spheroid shape in the N-terminal truncation of the α_{1D}AR, the receptors did not alter the length of time to form a spheroid or the shape of the spheroids as seen with the addition of the SNAP-tagged α_{1D}-ARs receptors, both full length (FL) and the NT truncation (Δ1-91, Figure 4.7, 4.8).

To compare expression levels of the α_{1D} adrenergic receptor in 2D vs 3D cell modeling, the Hague laboratory had determined that the FL receptor does not express well at the membrane,

but with the NT truncation, the adrenergic receptor was able to express at the membrane. This contests with what we then saw in our 3D modeling systems. When plated on a spheroid microplate, the full-length α_{1D}-AR expresses at the membrane of the cells (Figure 4.9).

Based on difference of expression level in the 2D vs. 3D cell culture of the α_{1D}-AR, we determined if this indicated a difference in the pharmacodynamics in 2D vs 3D cell modeling using the EPIC Dynamic Mass Redistribution (DMR) protocol. This protocol was not determined for the spheroids, but with literature review (Corning Life Sciences, 2017) and the addition of wide bore tips I was able to transfer the spheroid from the 96 well spheroid microplate into the EPIC sensor microplate. Once the spheroids were transferred, we used the established protocol to determine pharmacodynamics (Fang et. al. 2006, 2007).

Excitingly, we do see a significant difference in the 2D vs 3D cell modeling systems with the addition of the drug to our receptors. First, we performed EPIC DMR assays on both 2D and 3D cells containing the NT truncation of the α_{1D}-AR. Based on the imaging studies, we expected the pharmacodynamics to be similar in this case as the amount of expression is similar. Indeed, we see that there seems to be no significant difference between the two expect perhaps a slight shift in the Emax (Figure 4.10 A).

More interestingly was the addition of PHE to the FL α_{1D}-AR. In 2D cells, stimulation leads to very low response (as expected due to low receptor presence at the membrane). However, when the cells are in spheroidal form, there is a large increase in both the EC_{50} and E_{max} as shown in Figure 4.10 B. This increase is likely due to the higher concentration of receptors at the surface of the cells.

Additionally, we noticed an anomaly when comparing the spheroid shape of 3D full length α_{1D}-AR and the NT truncation of the α_{1D}-AR via live cell imaging. This was seen in the hundreds of spheroids screened. Once this was determined to be consistent and not a product of an individual

experiment, the shape of the spheroids was determined by comparing circularity (Figure 4.11). We examined this due to the perfect spheroidal shape of HEK293 cells, HEK293 cells with the SNAP-α_{1A}-AR receptor (data not shown), and HEK293 cells with the FL SNAP-α_{1D}-AR.

Note that the cells seemed to be migrating out of the spheroid shape. To determine if this was a migratory event, I tested if the cells were undergoing an epithelial to mesenchymal transition (EMT), and explain the lack of shape in the 3D N-terminal truncation of the SNAP-α_{1D}AR, and stained for the presence of E-Cadherin, which is known to decrease in expression during the transition of cells to an epithelial state. As shown, the level of E-Cadherin was greatly decreased in cells expressing SNAP-Δ1-91 α_{1D}-AR in comparison to cells expressing SNAP-FL α_{1D}-AR (Figure 4.12), suggesting that the spheroids containing the Δ1-91 α_{1D}-AR may be undergoing a spontaneous EMT event.

4.4 Discussion

Recent years has seen a marked increase in three-dimensional (3D) methods and tools to study disease and promote novel drug findings. This is due to the concern over the physiological relevance of traditional two-dimensional (2D) methods (Boussommier et. al. 2018). In addition, these new 3D methodologies provide relatively quick, inexpensive, and, perhaps most importantly, human cells with which to study. In contrast, animal models are time consuming, expensive, and do not have the added benefit of human physiology (Hoarau-Vechot et. al. 2018). However, most 3D modeling systems are relatively new and can provide some difficulties with variations in cell culture, batch differences, and even the cell types themselves. Thus, they must all be optimized to the research being performed. We started with the Corning Matrigel technology, which is similar to Thermo-Fisher's Geltrex and Sigma Alsrich's MaxGel and creates a 3D environment by providing a reconstituted basement membrane through the presence

of laminin (Huges et. al. 2010). Unfortunately, SW480 cells did not form an adequate spheroid, let alone lumen, by 5 days post plating in the Matrigel. However, HEK293 cells did appear to form a spheroid and the start of the lumen. The lumen formation is necessary to determine apico-basolateral formation as the apical membrane faces the lumen. It is common for some cell types to take longer to form the lumen, so a time course was conducted to determine the optimal time for the formation of these polarized spheroids.

Once the time course was completed, several concerns became immediately apparent. Despite following the same protocol, the formation of the spheroid (and consequently the lumen), would not consistently form on the same day. It would seem that the formation of the lumen would almost be complete on day 5, however, it would not be as far along on day 10. Due to complications following the first protocol, we decided to follow a protocol by Debath et. al. (2003) which was optimized for cells that took longer to form the lumen. When we tried this new protocol, we noticed that the cells failed to form spheroids. It was then we took to seeking another 3D modeling type due to lack of reliability and consistency.

These issues could have been due to Matrigel batch-to-batch inconstancies as this was a reportedly common problem (Fang et. al. 2017). Additionally, it is not typically recommended to use a gel matrix for cells that take longer to form the polarized spheroid as the longer it takes, the greater the likelihood for failure (Giles et. al. 2014). It is also likely that the reason the second protocol did not form the spheroid is due to the thickness of the gel. It is recommended that the gel layer be thin for cell attachment and proliferation to study cell-cell and polarized cell interactions (Corning Matrigel, 2013).

The next 3D methodology we tried was the Corning Spheroid Microplate. This is a unique plate with rounded bottoms and an Ultra-Low Attachment (ULA) coating that allows for the formation of a single spheroid in every well within 48 hours of plating (Bergeron et. al. 2017). With this

new protocol, we set out to determine if the spheroid formation is reliable and consistent. With the first experiment plating SNAP-HEK293 cells and HEK293 cells containing SNAP -FL and -Δ1-91 α_{1D}-AR, we saw that the cells were, indeed able to form spheroids.

Next, we wanted to determine the differences between 2D and 3D localization of the receptor as well as the pharmacodynamics. There seemed to be not much difference between the SNAP-Δ1-91 α_{1D}-AR in either expression or pharmacodynamics. Interestingly, we did notice a significant difference in the localization of the FL α_{1D}-AR to the membrane. This then correlated to an increase of receptor response in the presence of PHE.

These results raise new questions. Previous research showed the sequestration of the α_{1D}AR in the ER in cultured cells or cells cultured within 48 hours of removal from the rat aorta (Hague et. al. 2004, Fan et. al. 2009). However, once the cells become polarized, the receptor is once again found on the surface membrane. This seems to indicate the necessity for polarizing proteins to traffic α_{1D}-AR to the proper membrane. Since hDLG1 is a protein localized primarily to the basolateral membrane (Lozovatsky et. al. 2009) and since it is known to traffic proteins to the membrane (Lin et. al. 2013) this key protein may play a large part in assisting α_{1D}-AR to the proper membrane as well.

The Hague lab has discovered that an NT truncation of the receptor can allow for membrane expression in 2D cells (Hague et. al. 2004, Kuntz et. al. 2017). This begs the question as to whether this is because the receptor undergoes an endogenous NT cleavage event, or if there is another reason the receptor can reach the membrane in 2D cells culture. Interestingly, a clue to answering this question may have been found in the imaging of the 3D spheroids.

In examining several hundred spheroids, it became quickly evident that HEK293 cells as well as the cells containing the FL α_{1D}-AR formed almost perfect spheroids every time. When

examining the Δ1-91 α_{1D}-AR, the cells did not seem to form a solid, consistent spheroidal shape. In fact, some of the spheroids seemed to have cells that were breaking off from the spheroid itself. Upon literature review, we wondered if this was an EMT event occurring in these cells. Preliminary data using an E-Cadherin antibody was able to confirm the potential for an EMT. E-Cadherin levels are known to decrease significantly when undergoing an EMT (Lamouille et. al. 2014). This loss of the E-Cadherin is part of what allows for the separation of the junctions between the cells so that they may begin to move apart (Ahlstrom, 2014). From our data, we did see a significant decrease in E-Cadherin levels in cells containing the Δ1-91 α_{1D}-AR. Further work will need to be performed to determine if this is, in fact, an EMT, but our preliminary results sets the stage for this research.

Abbreviations: GPCR, G Protein-Coupled Receptors; PDZ, PSD95/DLG/ZO-1; DAPC, Dystrophin Associated Protein Complex; SCRIB, Scribble; hDLG1, Human Disks Large; ER, endoplasmic reticulum, GST, glutathione S-transferase; *E. coli,* Escherichia coli; NIR, near infrared; AR, Adrenergic Receptor; FL, full length; EMT, epithelial to mesenchymal transition; 3D, three dimensional; 2D, two dimensional; ECM, extracellular matrix; COPD, chronic obstructive pulmonary disease; PHE, phenylephrine; MDCK, Madin-Darby Canine Kidney cells; HEK293, Human Embryonic Kidney Cells; ULA, Ultra Low Attachment.

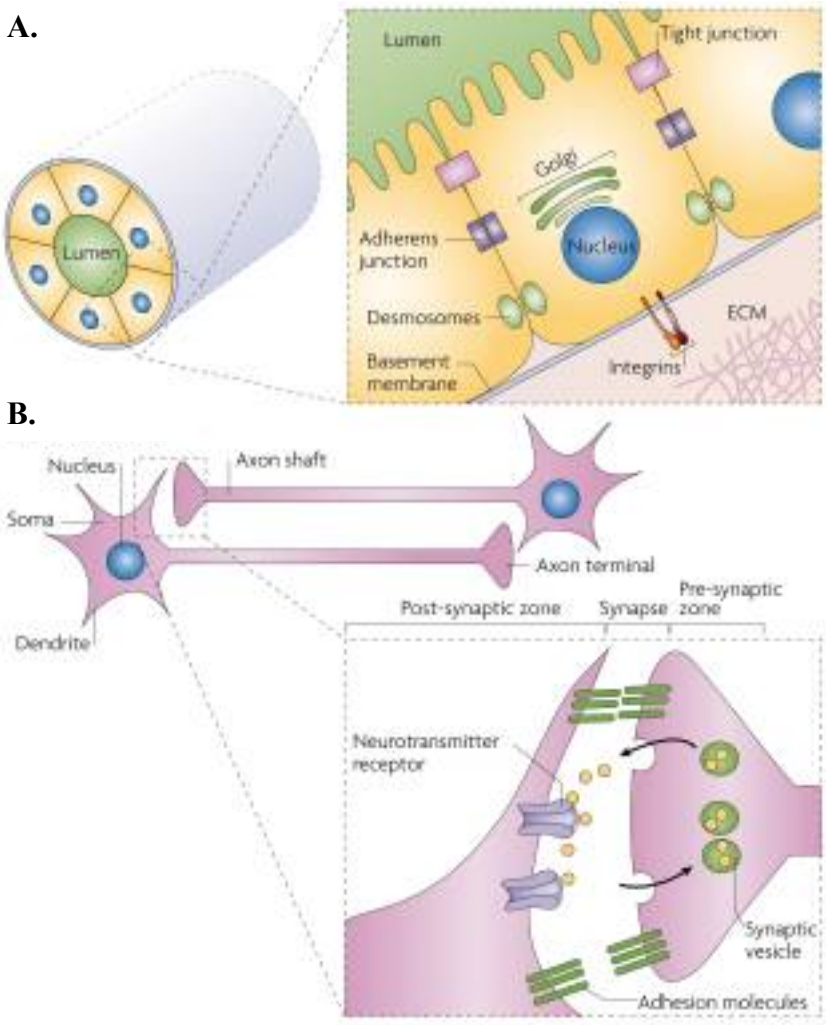

Figure 4.1. Polarity of epithelial and neuronal cell lines. A. Architecture and polarity of epithelial cells. Epithelial cells are comprised of an apical membrane that faces the lumen, a basal membrane that faces the ECM, and a lateral membrane that consists of adherins junctions, tight junctions, and desmosomes. B. Architecture and polarity of neuronal cells. Neuronal cells have an axonal and dendritic polarity that are highly organized.

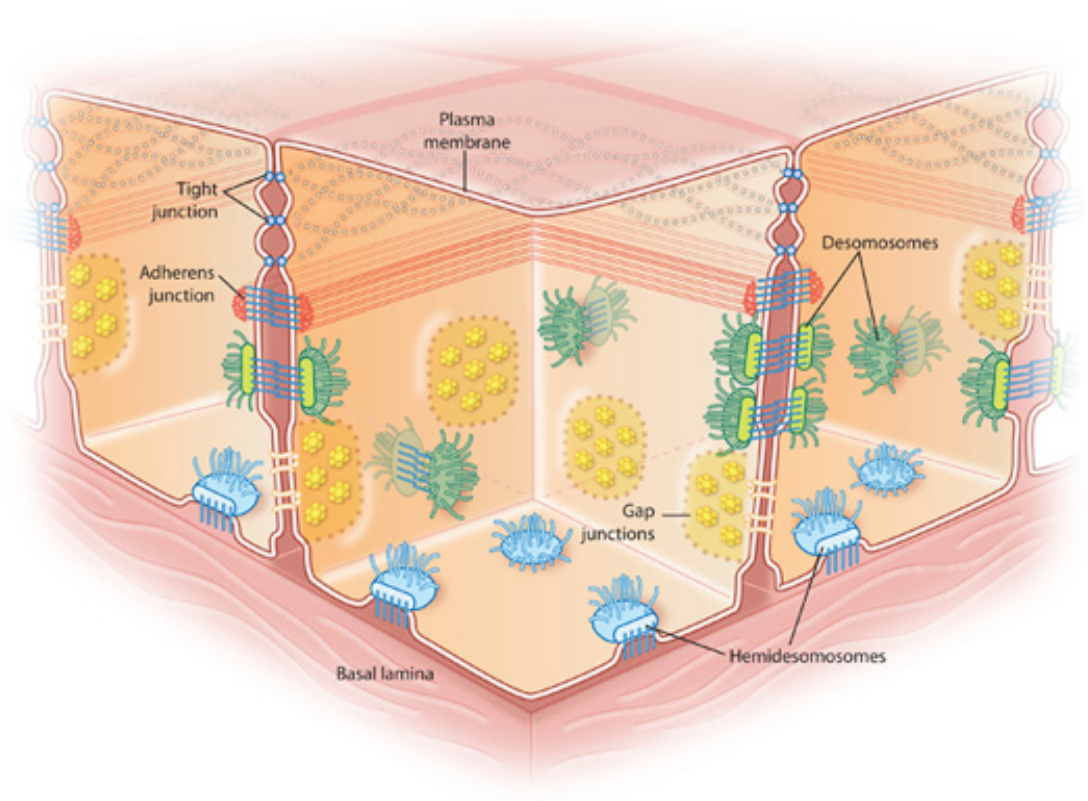

Figure 4.2. Different types of cell junctions. Tight junctions (blue dots) between cells are connected areas of the plasma membrane that stitch cells together. Adherens junctions (red dots) join the actin filaments of neighboring cells together. Desmosomes are even stronger connections that join the intermediate filaments of neighboring cells. Hemidesmosomes (light blue) connect intermediate filaments of a cell to the basal lamina, a combination of extracellular molecules on other cell surfaces. Gap junctions (yellow) are clusters of channels that form tunnels of aqueous connectivity between cells.

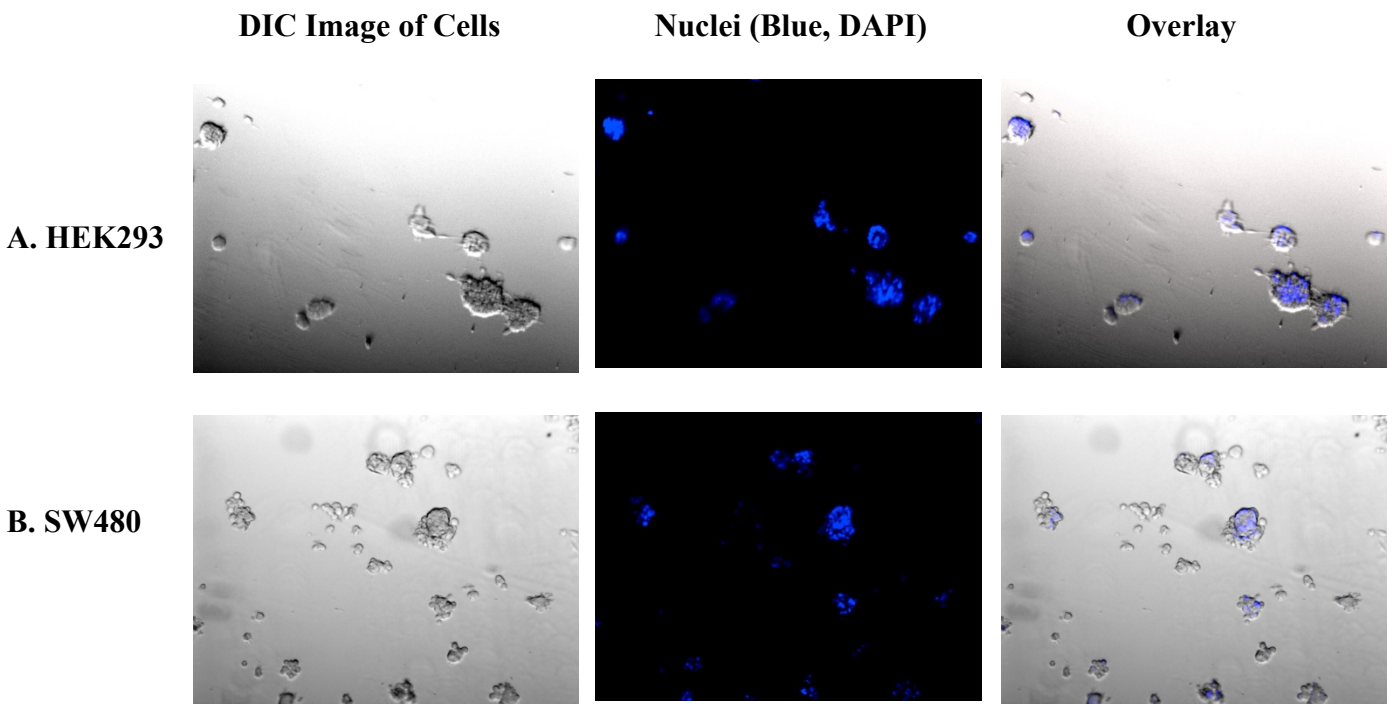

Figure 4.3. Comparison of the formation of spheroids in HEK293 and SW480 cells after 5 days incubating in Matrigel. HEK293 cells formed spheroids and start of lumen. SW480 cells did not form the tight spheroid by 5 days. Cells were stained with DAPI (blue, nuclear stain) and imaged.

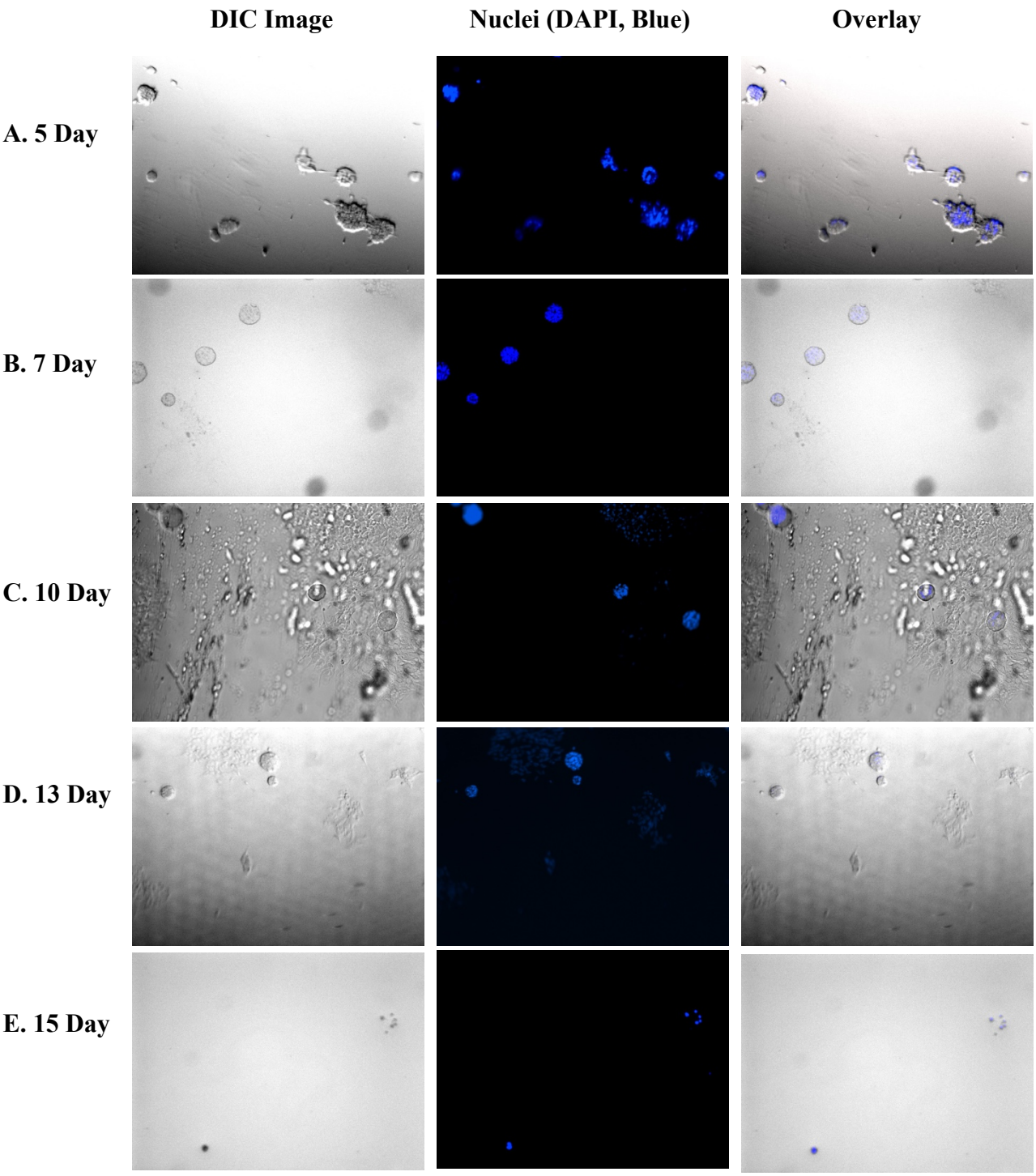

Figure 4.4. Time course of Matrigel spheroid formation in HEK293 cells. Time course of 5 (A), 7 (B), 10 (C), 13 (D), and 15 (E) days post plating with Matrigel. Formation of lumen was almost completed by 13 days post plating with Matrigel but cells began apoptosing at day 15 post plating with Matrigel.

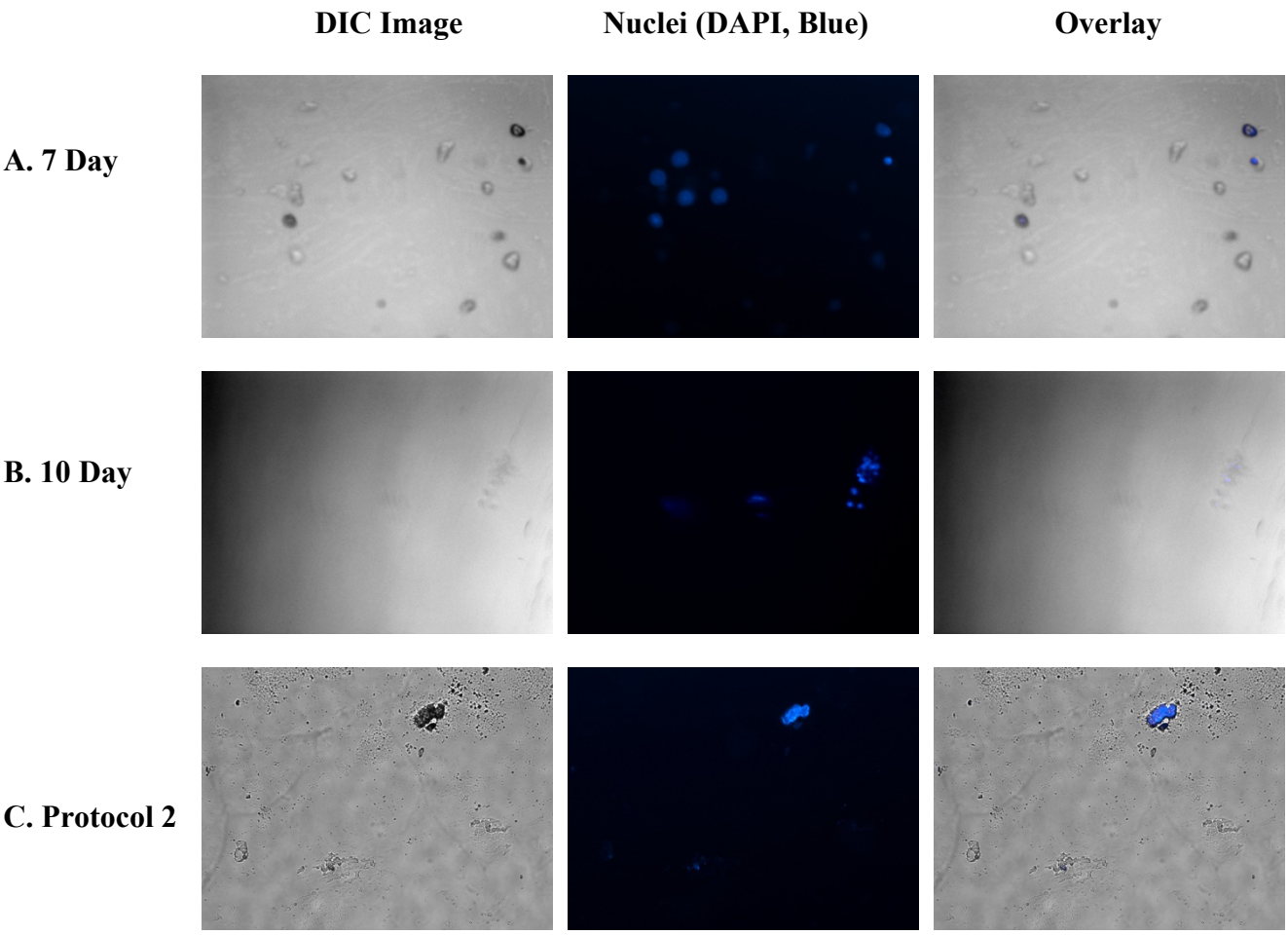

Figure 4.5. Inconsistencies of Matrigel spheroid formation. A sample of additional experiments indicating a difference between the spheroid formation itself at 7 days (A), 10 Days (B), and using an additional protocol (C). Results also indicate a difference when comparing days of the same time length.

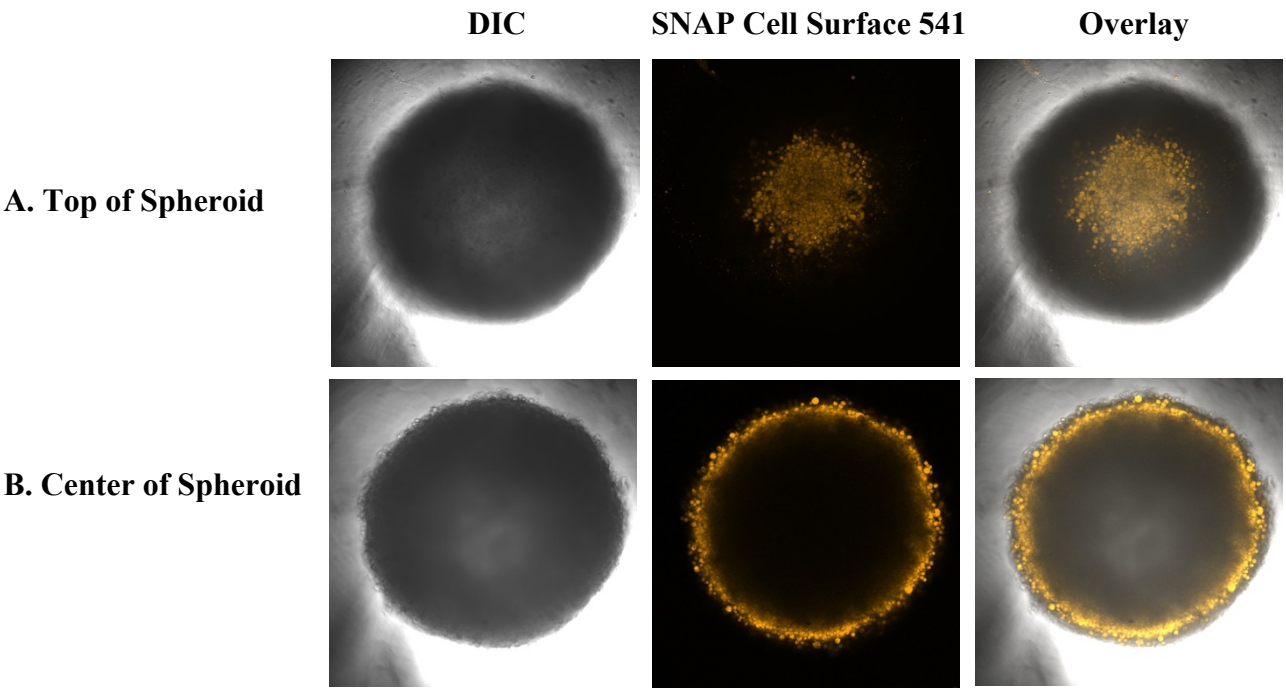

Figure 4.6. Spheroid formation of HEK293 Cells. Spheroid formation using the Corning Ultra Low Adherence Spheroid Microplate with the addition of SNAP. Cells were stained with SNAP surface Alexa Fluor 541 and images were taken at the top (A) and at the center (B) of the spheroid at 10x zoom.

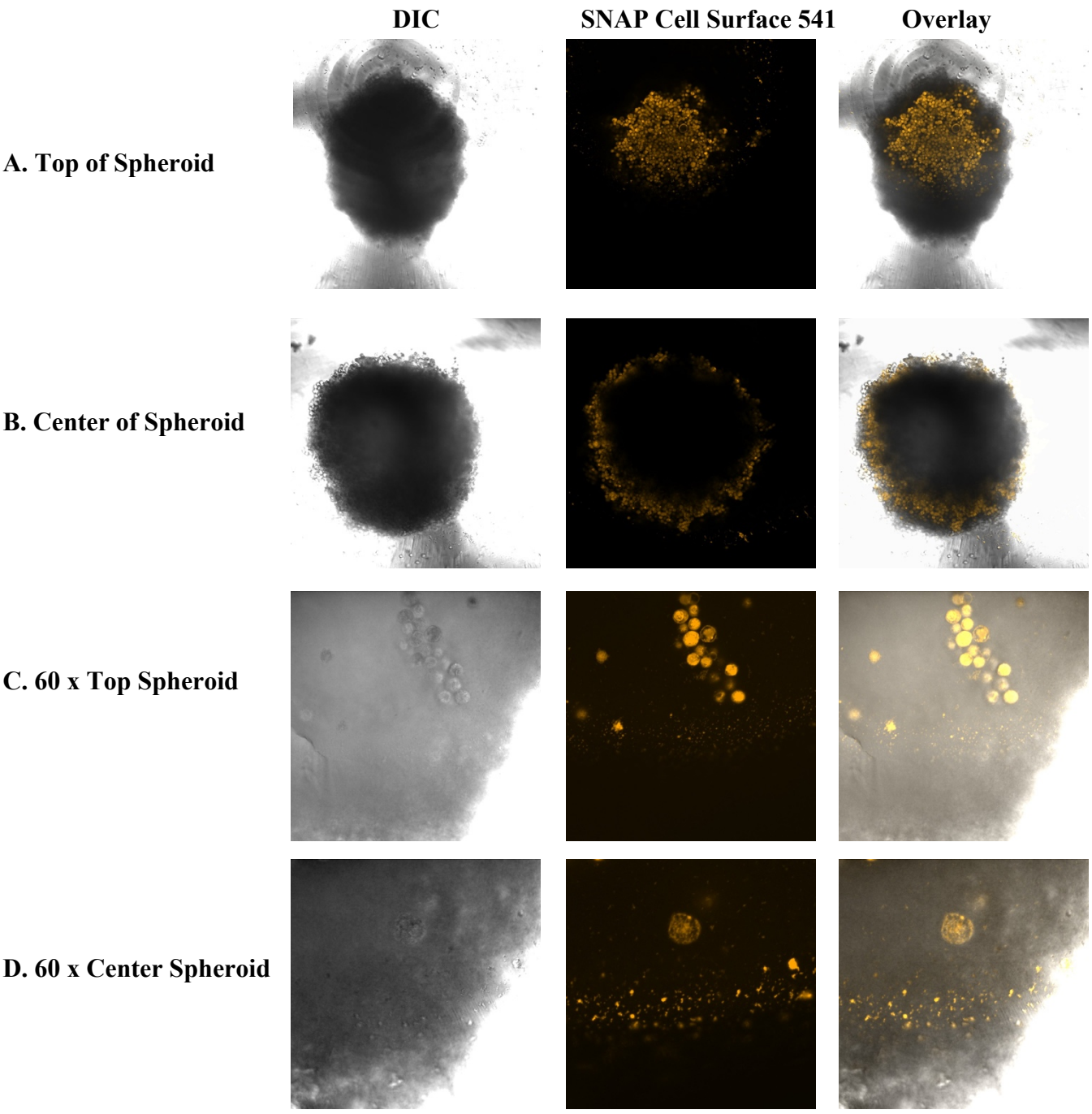

Figure 4.7. Spheroid formation with the addition of SNAP-Δ1-91 α_{1D}-AR. Spheroid formation using the Corning Ultra Low Adherence Spheroid Microplate with the addition of SNAP-Δ1-91 α_{1D}-AR. Cells were stained with SNAP surface Alexa Fluor 541 and images were taken at the top (A, C) and at the center (B, D) of the spheroid, both at 10x (A, B) and 60x (C, D) zoom.

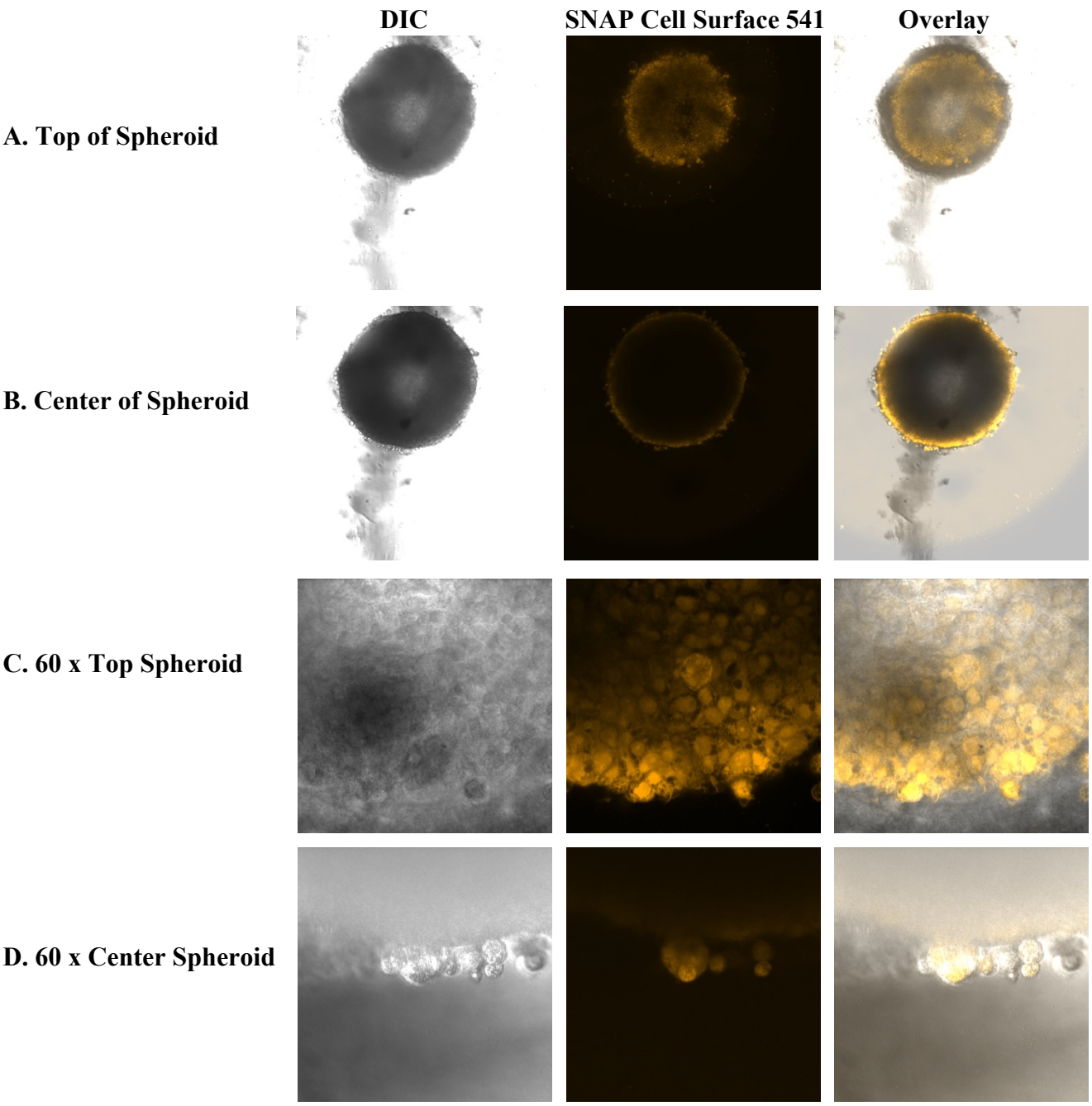

Figure 4.8. Spheroid formation with the addition of FL SNAP-α_{1D}-AR. Spheroid formation using the Corning Ultra Low Adherence Spheroid Microplate with the addition of SNAP-FL α_{1D}-AR. Cells were stained with SNAP surface Alexa Fluor 541 and images were taken at the top (A, C) and at the center (B, D) of the spheroid, both at 10x (A, B) and 60x (C, D) zoom.

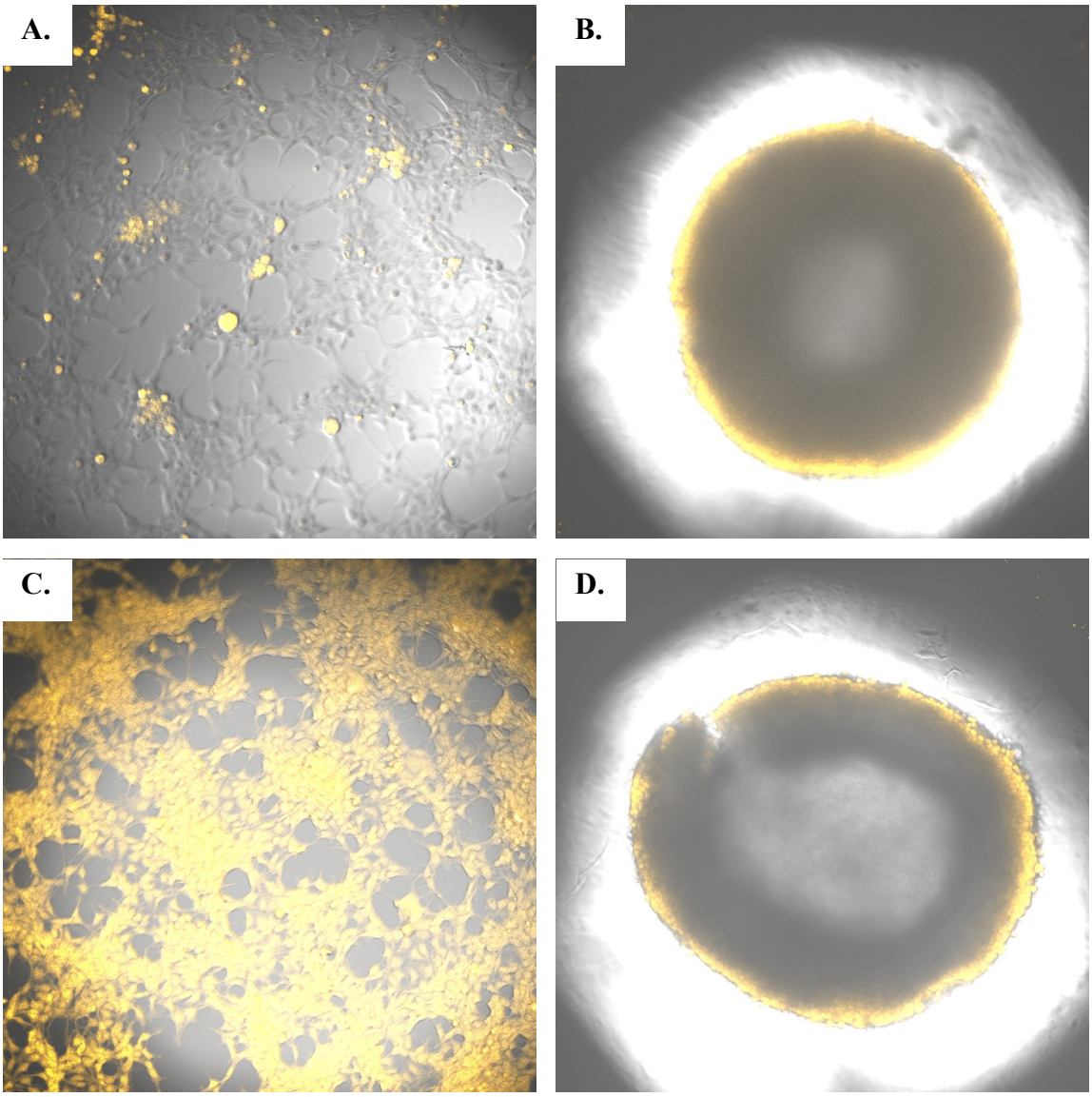

Figure 4.9. Comparison of differences in localization of 2D and 3D methods. A. 2D expression of SNAPFL α_{1D}-AR at the surface of the cell membrane. B. 3D expression of the SNAP FL α_{1D}-AR at the surface of the cell membrane. C. 2D expression of SNAP-Δ1-91 α_{1D}-AR at the surface of the cell membrane. D. 3D expression of SNAP-Δ1-91 α_{1D}-AR at the surface of the cell membrane.

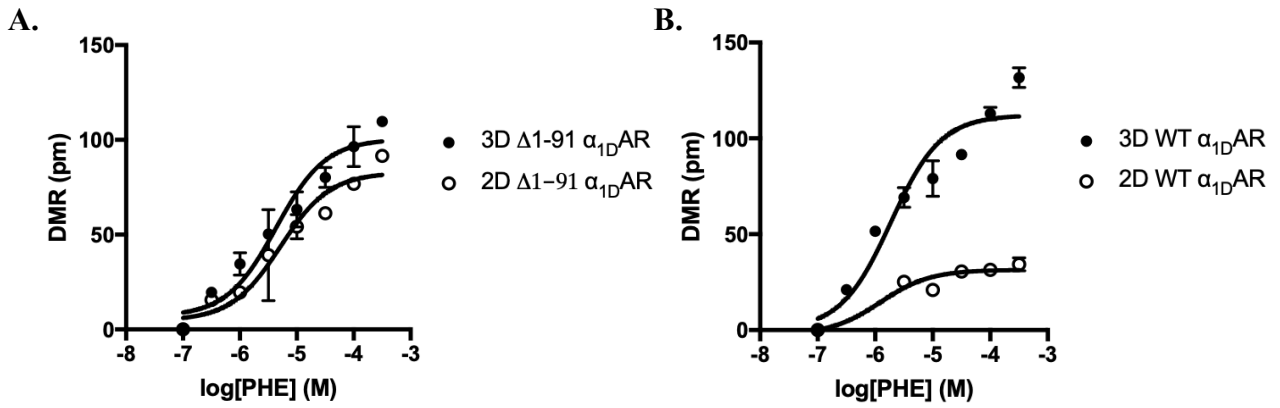

Figure 4.10. EPIC DMR comparison between 2D and 3D modeling systems. A. Comparison of 2D and 3D Phenylephrine response on HEK293 Δ1−91 α_{1D}-AR cells. B. Comparison of 2D and 3D Phenylephrine response on HEK293 FL α_{1D}-AR cells.

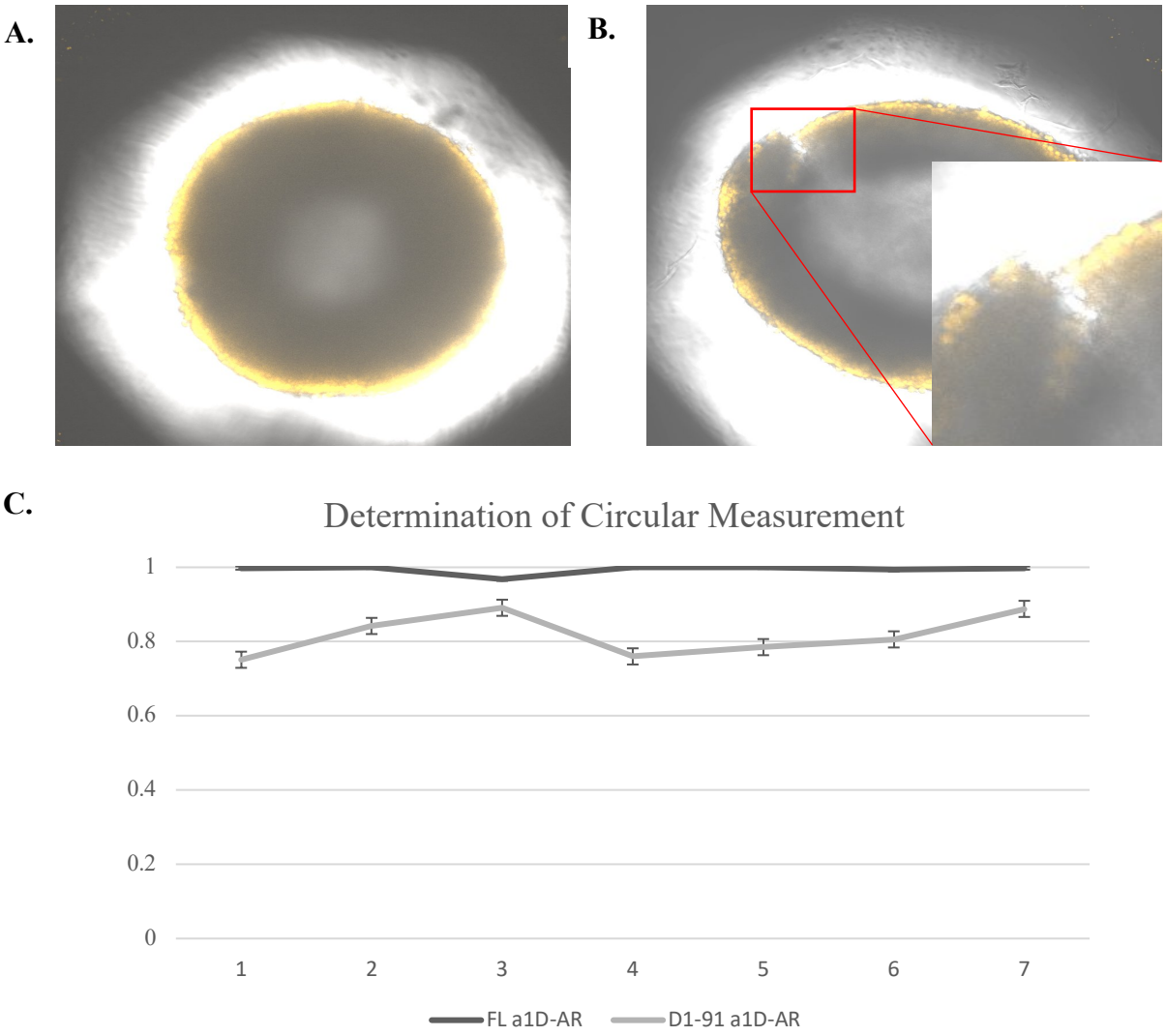

Figure 4.11. Circularity differences in FL and Δ1-91 α_{1D}-AR spheroids. A. FL α_{1D}-AR spheroid. B. Δ1–91 α_{1D}-AR spheroid with an inset showing the marked difference in circularity. C. Graph showing the comparisons of FL and Δ1–91 α_{1D}-AR in circularity. A value of 1 shows perfect circularity and less than 1 shows deviation from that. FL α_{1D}-AR had a deviation of 0.0101. Δ1–91 α_{1D}-AR had a deviation of 0.0499.

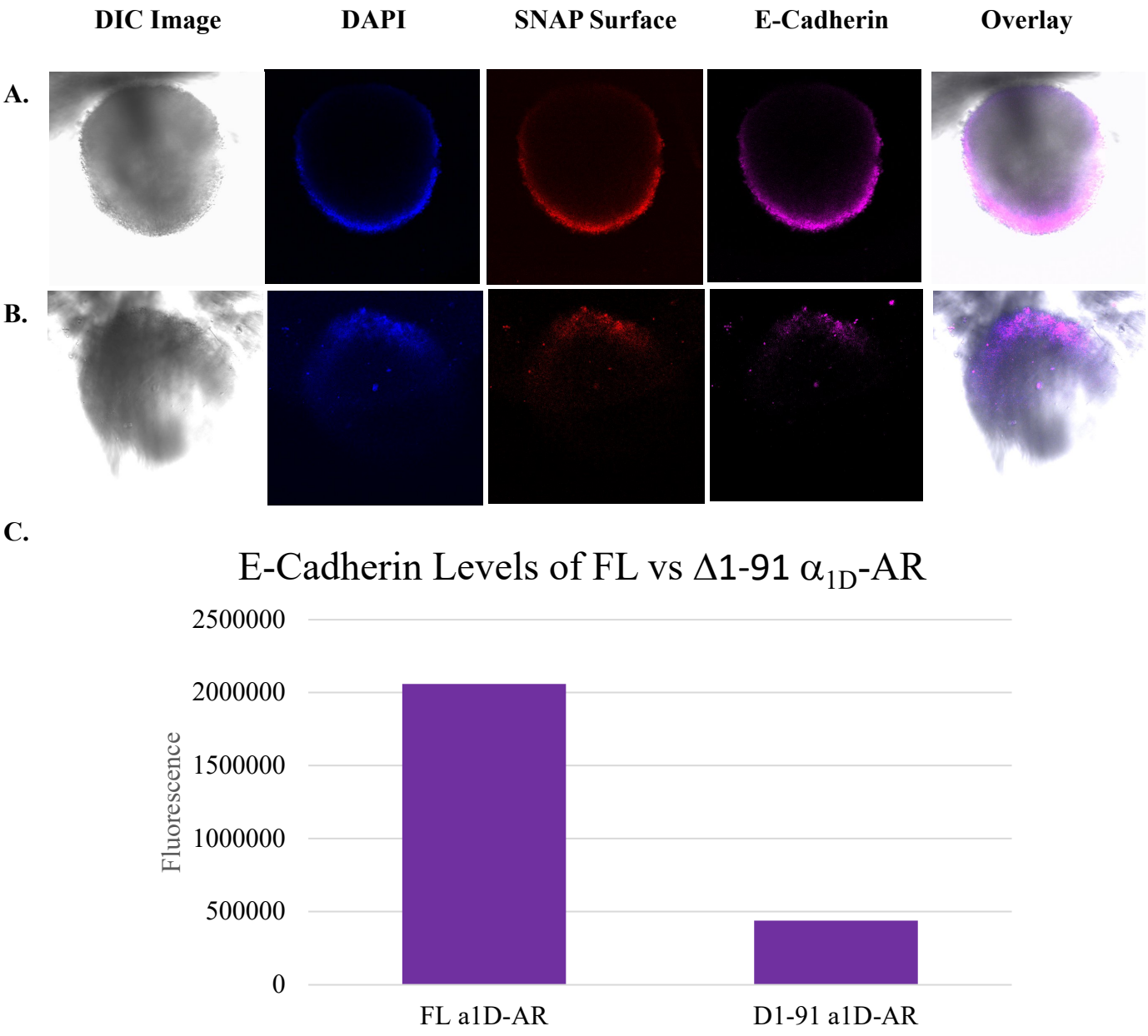

Figure 4.12. Comparison of E-Cadherin levels in FL and Δ1–91 α_{1D}-AR spheroids. A. HEK293 cells contain SNAP-FL α_{1D}-AR. DIC (grey) shows cells, DAPI (blue) shows nucleus, SNAP Surface Alexa Fluor 647 (red) shows receptor, Goat α–Mouse secondary antibody (purple) shows the presence of E-Cadherin. B. HEK293 cells contain SNAP-Δ1–91 α_{1D}-AR. DIC (grey) shows cells, DAPI (blue) shows nucleus, SNAP Surface Alexa Fluor 647 (red) shows receptor, Goat α–Mouse secondary antibody (purple) shows the presence of E-Cadherin. C. Quantification of the E-Cadherin fluorescence levels with SNAP -FL and -Δ1–91 α_{1D}-AR.

Chapter V - Conclusions

The G Protein-Coupled Receptor (GPCR) family represents a large part of the human genome at around 4% and is the target for about 30% of all FDA approved medications (Sriram et. al. 2018). While these receptors were once thought to be simple seven-transmembrane spanning proteins coupled to heterotrimeric G proteins, it has since been discovered that many of these GPCRs are, in fact, quite intricate (Jastrzebska 2014). From the way these proteins are trafficked to the membrane to the complex architecture to the multiple downstream signaling events, these receptors require careful consideration and study (Pavlos et. al. 2018).

In particular, the α_{1D}-AR is a highly dynamic, fascinating receptor to study. The adrenergic receptors (ARs) are a class of GPCR that respond to the endogenous catecholamines epinephrine and norepinephrine. When stimulated, the receptor activates the $G\alpha_{q/11}$ heterotrimeric G proteins which then stimulates phospholipase C (PLC). PLC activation then leads to the increase in diacyl glycerol (DAG), inositol triphosphate (IP3), and calcium.

The Hague lab has made fantastic strides in attempting to decipher this receptor. In 2004, it was discovered that, while notoriously difficult to study due to its intracellular localization, truncating the N-terminus (NT) of the α_{1D}-AR could increase membrane expression. In the following decade, it was discovered that the α_{1D}-AR could homodimerize to bind a myriad of PDZ interacting proteins such as α– or β– syntrophin (and by extension the Dystrophin Associated Protein Complex – DAPC) and Scribble (Chen et. al. 2006, Lyssand et. al. 2008, Camp et. al. 2015). Though a proteomic screen it was discovered the presence of three additional PDZ protein in one cell type – SW480 colorectal cancer (CRC) cells (Camp et. al. 2015).

It was this research that then informed my dissertation work. I have attempted to determine if it was, in fact, the α_{1D}-AR present in SW480 CRC cells (which could present the first cell line to

endogenously express α_{1D}-ARs), determine the architecture of theα_{1D}-AR signaling complex with the additional PDZ proteins discovered, and determine a protocol for 3D modeling to determine localization and functionality of the receptors.

SW480 Colorectal Cancer Cells express the α_{1B} Adrenergic Receptor Subtype

Research conducted previously in which Masur et al (2001) attempted to characterize the adrenergic receptors present in SW480 cells with the presence of antibodies determined that there were no α1-ARs, little to no α_{2A}-ARs, some α_{2B}- and α_{2C}-ARs, but primary β1- and β2-ARs. However, while the antibodies were specific for each of the α2-ARs and β–ARs, a nonspecific antibody for all α1-ARs was used.

Through EPIC DMR, radioligand binding, and qRT-PCR, we were able to determine which of the adrenergic receptors were expressed in SW480 cells. Both EPIC DMR and qRT-PCR revealed the presence of the α_{1B}-ARs in these cells. Interestingly, using radioligand binding assays, we were unable to detect any endogenous α_{1B}-ARs in SW480 cells. This indicates that perhaps traditional methods are not as sensitive as the EPIC DMR can be used to identify previously undetectable, low-density receptors in various cell types.

Additionally, we determined that the presence of the α_{1B}-AR increases the viability but has no effect on the proliferation of cancer cells. This indicates that the receptors are prosurvival in SW480 cells, but these effects could be antagonized with the addition of cyclasosin, terazosin, phenoxybenzamine, and phentolamine. Remarkably, when other cancer cell lines were screened (HCT116, a melanoma cancer cell line; MDAMB231, a metastatic breast cancer cell line; and U251, a glioblastoma cell line) using EPIC DMR, we see that the primary adrenergic receptor in

these cell types is likely α1-ARs. These data combined could indicate a novel, and previously overlooked, drug target in the treatment of cancer.

The Primary Interacting Protein to the α_{1D}-AR is Scribble

With the discovery of these three additional PDZ proteins: CASK, LIN7A, and hDLG1, we wanted to determine the new architecture of the α_{1D}-AR with its interacting proteins. To do this, we employed SNAP-gel assays as well as OCTET Bio-Layer Interferometry (BLI). These methods would allow us to determine the affinity of the various PDZ proteins to the α_{1D}-CT (the last 4-8 amino acids containing the PDZ ligand).

The SNAP-gel assay provided a clue as to the likelihood of the interacting proteins and provides a launching point for other research methods. First, we examined hDLG1, which had three separate PDZ domains. Full length hDLG1 showed binding activity, so we attempted to elucidate which PDZ domain had the highest affinity. Rank order of binding affinity was as follows: FL hDLG1>hDLG1 PDZ1>>hDLG1 PDZ1-2=hDLG1 PDZ 3>>hDLG1 PDZ 2. This seems to imply there might be some negative inhibition by PDZ domain 2 of hDLG1, but further work needs to be conducted to confirm these results. Additionally, I discovered that both MPP7 and CASK appeared able to bind the α_{1D}-CT.

Next, we performed OCTET BLI experiments to obtain the binding affinity values of the various PDZ proteins to the α_{1D}-CT. Eric Janezic studied the Scribble PDZ protein, a protein that contains four PDZ domains. He discovered that Scribble PDZ domains 1 and 4 bind with the highest affinity of all the individual domains (at 0.78 and 1.38 μM respectively). It was also discovered that hDLG1 PDZ domain 1 bound with the highest affinity of the individual PDZ domains (at 4.63 μM). Rank order for the affinity of all PDZ proteins to the α_{1D}-CT are as follows: SCRIB>Synt>hDLG1>>Cask>>>LIN7A = MPP7.

These data combined lead us to conclude that the α_{1D}-AR homodimerizes, with one PDZ ligand binding SCRIB PDZ domain 1, and the other binding syntrophin and the DAPC. Additionally, another homodimerized α_{1D}-AR PDZ ligand could bind SCRIB PDZ domain 4. Of the tripartite complex hDLG1, CASK, and LIN7A, it is hDLG1 that binds the α_{1D}-AR. Their role in the architecture is still a bit unclear as hDLG1 has been shown to be important in transportation of receptors (Lin et. al. 2013) as well as can bind SCRIB (Kallay et. al. 2006, Su et. al. 2012, Zhu et. al. 2014). Further research needs to be conducted to conclusively determine the presence in the α_{1D}-AR:PDZ Protein architecture.

3D Cell Modeling Can Alter Receptor Expression and Pharmacodynamics

Three dimensional (3D) methods of research have been increasing in popularity in recent years. 3D methods provide physiologic cell-to-cell contact and allows for the diffusion gradient of drugs, oxygen, and nutrients. These 3D models form polarized cells in which there are spatial differences in shape, structure, and function within a cell (Rodriguez-Boulan et. al. 1989). In epithelial cells, the two spatial membranes are the apical membrane (which faces the lumen), and the basolateral membrane (which is affixed by basement membrane). Interestingly, CASK, hDLG1, and LIN7A are all basolateral proteins and may play a role in the localization of the α_{1D}-AR to the basolateral membrane.

However, to determine which membrane the α_{1D}-AR is localized to, we must first find a reliable 3D modeling system. I started with Corning Matrigel, which is a reconstituted basement membrane that allows for the formation of the lumen. Upon further examination with HEK293 cells, the lumen never seemed to form. Through a time-course as well as through several methodologies, I discovered that the formation of the spheroid and the beginning of the formation of the lumen was not a reliable technique to use.

Another 3D methodology that I decided to try was the Corning Spheroid Microplate. This is a plate that contains a hydrophobic, ULA coating that allows for a single spheroid to form in each well. I plated SNAP-HEK293 cells, HEK293 cells with SNAP-FL α_{1D}-AR, and HEK293 cells with SNAP-Δ1-91 α_{1D}-AR. Imaging analysis revealed consistent and reliable spheroid formation.

I examined the differences in 2D and 3D expression levels and pharmacodynamics. The SNAP-Δ1-91 α_{1D}-AR 2D and 3D expression levels remained largely the same, both showing a high expression at the surface of the cell. SNAP-FL α_{1D}-AR 2D cells showed the same internalization and low expression levels at the cell membrane as previous research (Hague et. al. 2004, Fan et. al. 2009) but the 3D spheroids showed an increase in the surface expression of the SNAP-FL α_{1D}-AR. Previously, there was no established protocol for determining pharmacodynamics with the EPIC DMR on spheroids. Using this protocol, I discovered that the increase of receptor expression correlated with an increase in pharmacodynamic responses to PHE.

This provides an interesting advantage to 3D cell culture. Previously low expression of the α_{1D}-AR localizes to the surface of the spheroid, which increases the activity of the receptor. These findings could yield novel exploration into previously undetectable receptors at the membrane of cells.

The N-Terminal Truncation of the α_{1D}-AR May Lead to a Type II EMT

While examining the differences between 2D and 3D expression of SNAP-Δ1-91 α_{1D}-AR and SNAP-FL α_{1D}-AR, I noticed a unique trait in the SNAP-Δ1-91 α_{1D}-AR spheroids. Of the hundreds of spheroids examined, only this type of spheroid showed a migration of cells outside of the normal, circular shape. This appeared to potentially be an epithelial to mesenchymal

transition (EMT), of which there are three different types. Type I is seen in development, Type II is seen in wound repair and fibrosis, and Type III is seen in cancer (Kalluri et. al. 2009, Heerboth et. al. 2015, Stone et. al. 2016, Kim et. al. 2018). To determine if this *was* an EMT event, and I decided to conduct preliminary data.

In addition to tracking the shape changes in the spheroidal shape, I also stained both SNAP-FL α_{1D}-AR and SNAP-Δ1-91 α_{1D}-AR for the presence of E-Cadherin. During an EMT, E-Cadherin levels decrease, and N-Cadherin levels increase (Wells et. al. 2008). Both blank HEK293 cells and HEK293 containing the SNAP-FL α_{1D}-AR had an almost perfect circular shape. In contrast, HEK293 cells with SNAP-Δ1-91 α_{1D}-AR had variable shape that was decidedly not circular. The staining of E-Cadherin indicated significantly decreased levels in SNAP-Δ1-91 α_{1D}-AR over SNAP-FL α_{1D}-AR.

This EMT with the NT truncation of the α_{1D}-AR could indicate a wound repair event or disease state. Previous research has indicated the α_{1D}-AR is upregulated in diabetic kidneys (Zhao et. al. 2014) and antagonists of the α_{1D}-AR are treatments for post-traumatic stress disorder (PTSD) (Raskind et. al. 2018), benign prostatic hypertrophy (BPH, Schwinn et. al. 2004) and cardiovascular disease (Lyssand et. al. 2008). This could lead to novel therapeutics targeting either the FL or the NT truncation of the α_{1D}-AR.

Final Conclusions

Our current working model of the α_{1D}-AR signalosome has the α_{1D}-AR scaffolded to the membrane as a homodimer, binding SCRIB on one PDZ ligand and the syntrophin/DAPC complex on the other PDZ Ligand (Figure 5.1). Due to the localization of the PDZ interacting proteins CASK, LIN7A, hDLG1, and SCRIB, we think that the α_{1D}AR localizes to the

basolateral membrane (Figure 5.2). The heterotrimeric complex of hDLG1, CASK, and LIN7A may be responsible for transport to the basolateral membrane, where it may interact with SCRIB through LGL, or may bind the other side of the homodimerized α_{1D}-AR PDZ ligand.

This receptor is highly complex, tightly regulated, and more research needs to be conducted to determine the exact role in disease. Research conducted using 3D modeling indicates the NT truncation of the α_{1D}-AR may indicate a wound repair or disease form. All of this could lead to the development of novel drugs for better treatment of hypertension, PTSD, schizophrenia, PBH, or any number of other α_{1D}-AR related diseases.

Abbreviations: GPCR, G Protein-Coupled Receptors; ARs, Adrenergic Receptors; PLC, phospholipase C; DAG, diacyl glycerol; IP3, inositol triphosphate; PDZ, PSD95/DLG/ZO-1; DAPC, Dystrophin Associated Protein Complex; SCRIB, Scribble; hDLG1, Human Disks Large; ER, endoplasmic reticulum, AR, Adrenergic Receptor; FL, full length; SW480, colorectal cancer cell line; MDAMB231, metastatic breast cancer cell line; U251, glioblastoma cell line; MDCK, Madin-Darby Canine Kidney cells; HEK293, Human Embryonic Kidney Cells; CT, C-tail; NT- N-terminal; BLI, Bio-Layer Interferometry; 3D, three dimensional; ULA, Ultra Low Attachment; PHE, phenylephrine; EMT, epithelial to mesenchymal transition; PTSD, Post Traumatic Stress Disorder; BPH, Benign Prostatic Hypertrophy.

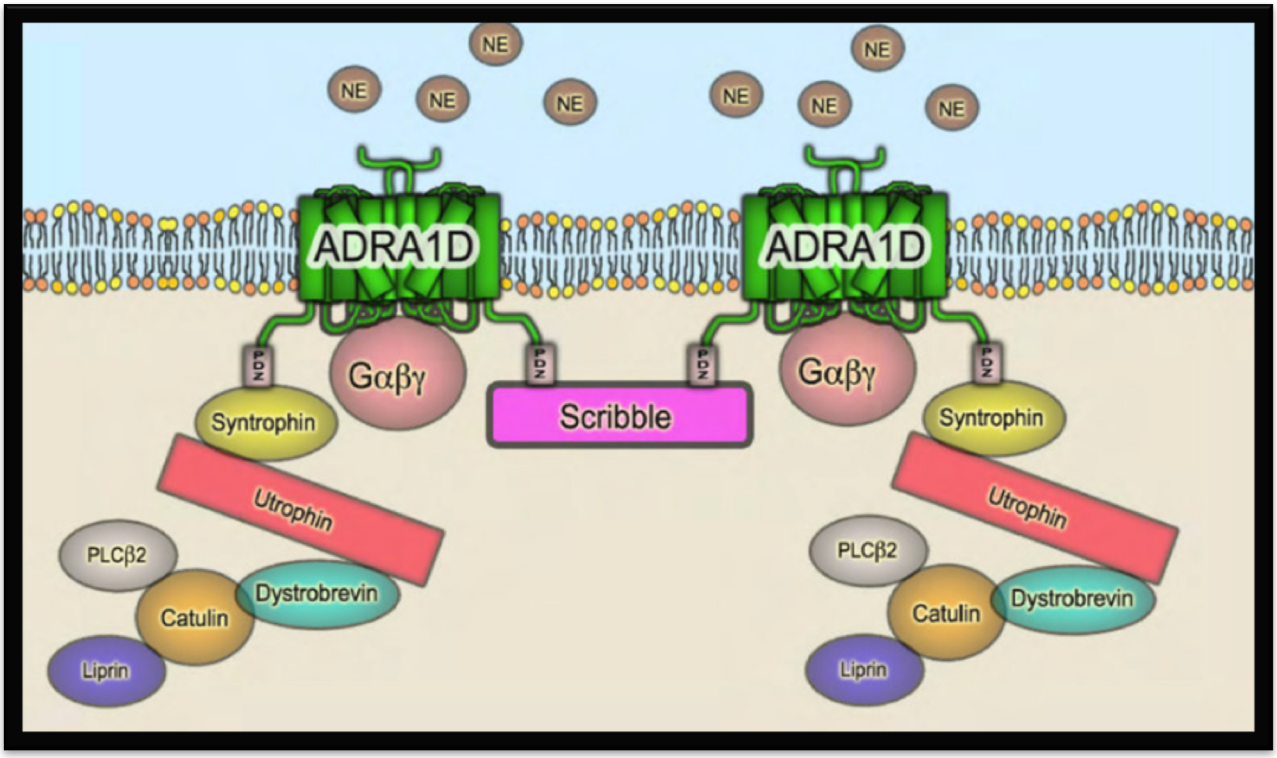

Figure 5.1. Architecture of the α_{1D}-AR and its Interacting Proteins.

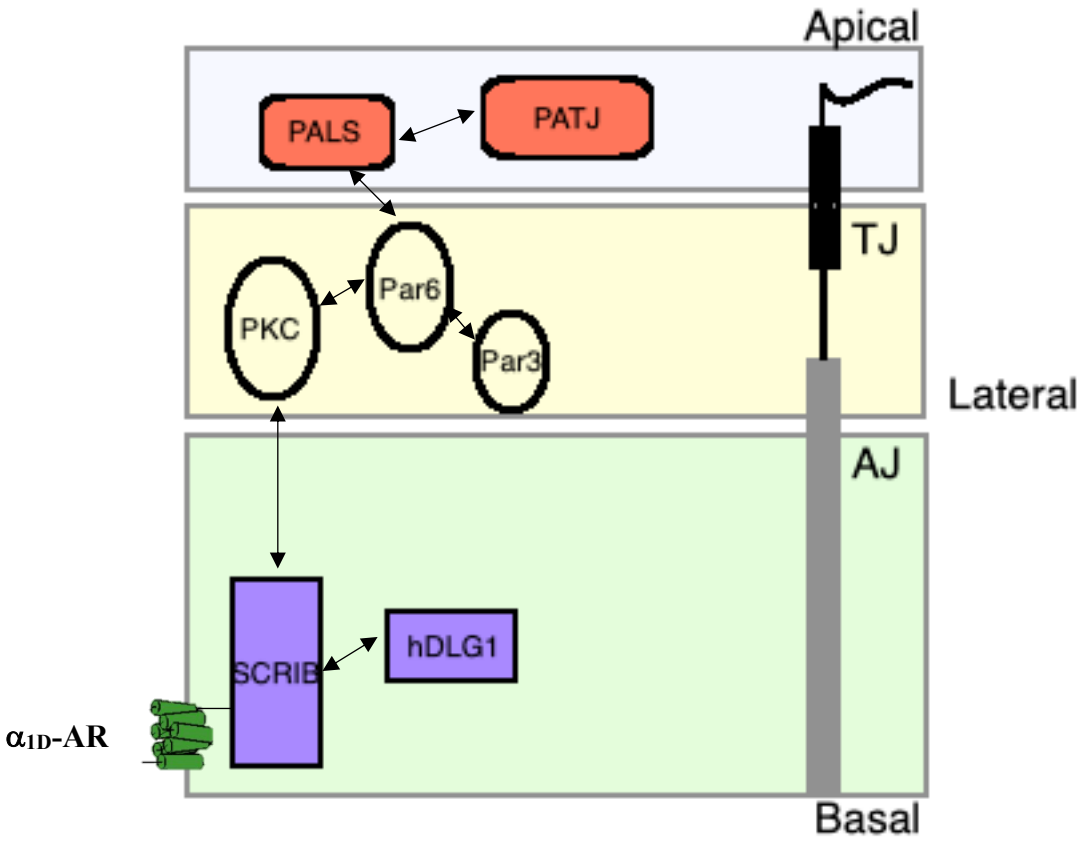

Figure 5.2. Localization of the α_{1D}-AR to the Basolateral membrane and interaction with PDZ proteins.

References

Adams ME, Dwyer TM, Dowler LL, White RA, Froehner SC (1995) Mouse alpha 1-and beta 2-syntrophin gene structure, chromosome localization, and homology with a disks large domain. *J Biol Chem.* 270(43):25859-25865.

Ahlstrom JD (2014) Molecular Organization of Cells. *Chapter 8 of Principles of Tissue Engineering, Elsevier Inc.* 4:147-160.

Anglin IE, Glassman DT, and Kyprianou N (2002) Induction of prostate apoptosis by a1-adrenoceptor antagonists: mechanistic significance of the quinazoline component. *Prostate Cancer Prostatic Dis* 5:88–95.

Arunlakshana O and Schild HO (1959) Some quantitative uses of drug antagonists. *Br Pharmacol Chemother* 14:48–58.

Balcarova-Stander J, Pfeiffer SE, Fuller SD, Simons K (1984) Development of cell surface polarity in the epithelial Madin-Darby canine kidney (MDCK) cell line. *The EMBO Journal.* 3(11):2687-2694.

Barbieri A, Bimonte S, Palma G, Luciano A, Rea D, Giudice A, Scognamiglio G, La Mantia E, Franco R, Perdonà S, et al. (2015) The stress hormone norepinephrine increases migration of prostate cancer cells in vitro and in vivo. *Int J Oncol* 47:527–534.

Bavadekar SA, Hong S-S, Lee S-I, Miller DD, and Feller DR (2008) Bioisosteric phentolamine analogs as selective human a(2)- versus a(1)-adrenoceptor ligands. *Eur J Pharmacol* 590:53–60.

Bergeron A and Gitschier H (2017) Co-Culturing and Assaying Spheroids in the Corning Spheroid Microplate. *Corning Life Sciences.*

Bezprozvanny I and Maximov A (2001) Classification of PDZ Domains. *Elsevier Science Direct*. 3(14):457-462.

Blake DJ, Tinsley JM, Davies KE. Utrophin: a structural and functional comparison to dystrophin. *Brain Pathol.* 6(1)37-47.

Boer R, Grassegger A, Schudt C, and Glossmann H (1989) (1)-Niguldipine binds with very high affinity to Ca21 channels and to a subtype of a1-adrenoceptors. *Eur J Pharmacol* 172:131–145.

Bohl J, Brimer N, Lyons C, Vande-Pol SB (2007) The Stardust Family Protein MPP7 forms a Tripartite Complex with LIN7A and DLG1 That Regulates the Stability and Localization of DLG1 to Cell Junctions. *J Biol Chem* 13:9392-9400.

Borg JP, Straight SW, Kaech SM, de Taddeo-Borg M, Kroon DE, Karnak D, Turner RS, Kim SK, Margolis B (1998) Identification of an evolutionarily conserved heterotrimeric protein complex involved in protein targeting. *J. Biol Chem* 273(48):3163-31636.

Brady AE and Limbird LE (2002) G Protein-Coupled receptor interacting proteins: Emerging roles in localization and signal transduction. *Cellular Signaling.* 14(4)297-309.

Bryant DM and Mostov KE (2008) From Cells to Organs: Building Polarized Tissue. *Nat Rev Mol Cell Biol* 9(11):887-901.

Butz S, Okamoto M, Südhof TC (1998) A tripartite protein complex with the potential to couple synaptic vesicle exocytosis to cell adhesion in brain. *Cell* 94:773-782.

Camp ND, Lee KS, Cherry A, Wacker-Mhyre JL, Kountz TS, Park JM, Harris DA, Estrada M, Stewart A, Stella N, et al. (2016) Dynamic mass redistribution reveals diverging importance of PDZ-ligands for G protein-coupled receptor pharmacodynamics. *Pharmacol Res* 105:13–21.

Camp ND, Lee K-S, Wacker-Mhyre JL, Kountz TS, Park JM, Harris DA, Estrada M, Stewart A, Wolf-Yadlin A, and Hague C (2015) Individual protomers of a G proteincoupled receptor dimer integrate distinct functional modules. *Cell Discov* 1:15011. 10.1038/celldisc.2015.11.

Cao F, Miao Y, Xu K, Liu P. Lethal (2) Giant Larvae: An Indispensable Regulator of Cell Polarity and Cancer Development. *Int J Biol Sciences.* 11(4):380-389.

Cao TT, Deacon HW, Reczek D, Bretscher A, von Zastrow M (1999). A kinase-regulated PDZ-domain interaction controls endocytic sorting of the β2-adrenergic receptor. *Nature* 401(6750):286.

Catapano LA and Manji HK (2007) G protein-coupled receptors in major psychiatric disorders. *Biochim Biophys Acta* 1768:976–993.

Chang PY, Huang WY, Lin CL, Huang TC, Wu YY, Chen JH, and Kao CH (2015). Propranolol reduces cancer risk: a population-based cohort study. *Medicine* 94:e1097.

Chen Z, Hague C, Hall RA, Minneman KP (2006). Syntrophins regulate α_{1D}-adrenergic receptors through a PDZ domain-mediated interaction. *J Biol Chem* 281(18):12414-12420.

Cherry AE, Haas BR, Naydenov AV, Fung S, Xu C, Swinney K, Wagenbach M, Freeling J, Canton DA, Coy J, et al. (2016) ST-11: a new brain-penetrant microtubule-destabilizing agent with therapeutic potential for glioblastoma multiforme. *Mol Cancer Ther* 15:2018–2029.

Chess-Williams RG, Williamson KL, and Broadley KJ (1990) Whether phenylephrine exerts inotropic effects through a- or b-adrenoceptors depends upon the relative receptor populations. *Fundam Clin Pharmacol* 4:25–37.

Chin CC, Li JM, Lee KF, Huang YC, Wang KC, Lai HC, Cheng CC, Kuo YH, and Shi CS (2016) Selective b2-AR blockage suppresses colorectal cancer growth through regulation of EGFR-Akt/ERK1/2 signaling, G1-phase arrest, and apoptosis. *J Cell Physiol* 231:459–472.

Chou EC, Capello SA, Levin RM, Longhurst PA (2003) Excitatory α1-adrenergic receptors predominate over inhibitory β-receptors in rabbit dorsal detrusor. *J. Urol*. 170 (6): 2503–2507.

Choy C, Raytis JL, Smith DD, Duenas M, Neman J, Jandial R, and Lew MW (2016) Inhibition of b2-adrenergic receptor reduces triple-negative breast cancer brain metastases: the potential benefit of perioperative b-blockade. *Oncol Rep* 35:3135–3142.

Clark DA Mancama D, Kerwin RW, Arranz MJ (2006) Expression of the alpha1-adrenergic receptor in schizophrenia. *Neurosci Lett*. 401(3)248-251.
Cleary L, Murad K, Bexis S, and Docherty JR (2005) The a(1D)-adrenoceptor antagonist BMY 7378 is also an a(2C)-adrenoceptor antagonist. *Auton Autacoid Pharmacol* 25:135–141.

Cole SW and Sood AK (2012) Molecular pathways: b-adrenergic signaling in cancer. *Clin Cancer Res* 18:1201–1206.

Collette KM, Zhou XD, Amoth HM, Lyons MJ, Papay RS, Sens DA, Perez DM, and Doze VA (2014) Long-term a1B-adrenergic receptor activation shortens lifespan, while a1A-adrenergic receptor stimulation prolongs lifespan in association with decreased cancer incidence. *Age (Dordr)* 36:9675.

Corning Life Sciences (2012) Corning Matrigel Matrix: Frequently Asked Questions. *Corning Life Sciences.* 1-8.

Dev KK (2004) Making Protein Interactions Druggable: Targeting PDZ Domains. *Nature Reviews.* 3:1047-1056.

Digges KG and Summers RJ (1983) Characterization of postsynaptic a-adrenoceptors in rat aortic strips and portal veins. Br J Pharmacol 79:655–665. Docherty JR (2010) Subtypes of functional a1-adrenoceptor. *Cell Mol Life Sci* 67:405–417.

Docherty JR (2010) Subtypes of functional α1-adrenoceptor. *Cellular Molecular Life Science*. 65(3):405-417.

Doze VA, Handel EM, Jensen KA, Darsie B, Luger EJ, Haselton JR, Talbot JN, and Rorabaugh BR (2009) a(1A)- and a(1B)-adrenergic receptors differentially modulate antidepressant-like behavior in the mouse. *Brain Res* 1285:148–157.

Drews J (2004) Paul Ehrlich: Magister mundi. *Nat. Rev. Drug Disc*. 3:797–801.

Duval K, Grover H, Han LH, Mou Y, Pegoraro AF, Fredberg J, Chen Z (2017) Modeling Physiological Events in 2D vs. 3D Cell Culture. *APS Physiology.* 32(4):266-277.

Ehmsen J, Poon E, Davies K (2002) The dystrophin-associated protein complex. *J Cell Scien.* 115:2801-2803.

Evans RM (1988). The steroid and thyroid hormone receptor superfamily. *Science.* 240 (4854): 889–95.

Fan LL, Ren S, Zhou H, Wang Y, Xu PX, He JQ, Luo DL (2009) α1D-Adrenergic receptor insensitivity is associated with alterations in its expression and distribution in cultured vascular myocytes. *Acta Pharmacologica Sinica.* 30:1585-1593.

Fang Y and Eglen R, (2017) Three-Dimensional Cell Cultures in Drug Discovery and Development. *SLAS Disc.* 22(5)456-472.

Fang Y, Ferrie AM, Fontaine NH, Mauro J, and Balakrishnan J (2006) Resonant waveguide grating biosensor for living cell sensing. *Biophys J* 91:1925–1940.

Fang Y, Li G, and Ferrie AM (2007) Non-invasive optical biosensor for assaying endogenous G protein-coupled receptors in adherent cells. *J Pharmacol Toxicol Methods* 55:314–322.

Frantz C, Stewart KM, Weaver VM (2010) The Extracellular Matrix at a Glance *J Cell Sci* 123:4195-4200.

Fuentes AV, Pineda MD, Venkata KCN (2018) Comprehension of Top 200 Prescribed Drugs in the US as a Resource for Pharmacy Teaching, Training, and Practice. *Pharmacy Basel.* 6(2):43.

Fuh G, Pisabarro MT, Li Y, Quan C, Lasky LA, Sidhu SS (2000) Analysis of PDZ Domain-Ligand Interactions using Carboxyl-terminal Phage Display. *Jour Bio Chem.* 275:21486-21491.

Gardoni F (2008) MAGUK Proteins: new targets for pharmacological intervention in the glutamatergic synapse. *Eur J Pharmacol.* 585(1):147-152.

Giles RH, Ajzenberg H, Jackson PK (2014) 3D spheroid model of mIMCD3 cells for studying ciliopathies and renal epithelial disorders. *Nature Protocols.* 9(12):2725-2731.

Goetz AS, King HK, Ward SD, True TA, Rimele TJ, and Saussy, Jr DL (1995) BMY 7378 is a selective antagonist of the D subtype of a1-adrenoceptors. *Eur J. Pharmacol* 272:R5–R6.

Gordon M (2018) Chapter 5: Autonomic Pharmacology and Adrenergic Drugs. *Medical Pharmacology.*

Greengrass P and Bremmer R (1979) Binding Characteristics of 3H-Prazosin to Rat Brain α-Adrenergic Receptors. *European Journal of Pharmacology.* 55(3):323-326.

Hague C, Chen Z, Pupo AS Schelte NA, Toews ML, Minneman KP (2004) The N-terminus of the human alpha1D-adrenergic receptor prevents cell surface expression. *J Pharmacol Exp Ther* 309(1): 388-397.

Harris BZ and Lim WA (2001) Mechanism and role of PDZ domains in signaling complex assembly. *Sign Trans and Cell Organization.* 114:3219-3228.

Hartung T (2008) Thoughts on limitations of animal models. *Science Direct Elsevier.* 14(2):S81-S83.

Haruki H, Gonzalez, MR, Johnsson K (2012) Exploiting Ligand-Protein Conjugates to Monitor Ligand-Receptor Interactions. *Public Library of Science.* 7(5): e37598.

Hauser AS, Attwood MM, Rask-Andersen M, Schioth HB, Gloriam DE (2017), Trends in GPCR drug discovery: new agents, targets and indications. *Nat Rev Drug Disc.* 16:829-842.

Heerboth S, Housman G, Leary M, Longacre M, Byler S, Lapinska K, Willbanks A, Sakar S (2015) EMT and Tumor Metastasis. *Clin Transl Med.* 4:6.

Hille, B (1984). Ionic Channels of Excitable Membranes. *Trends in Neurosciences.* 8:226.

Hong S-S, Bavadekar SA, Lee S-I, Patil PN, Lalchandani SG, Feller DR, and Miller. DD (2005) Bioisosteric phentolamine analogs as potent a-adrenergic antagonists. *Bioorg Med Chem Lett* 15:4691–4695.

Hoarau-Vechot J, Rafii A, Touboul C, Pasquier J (2018) Halfway between 2D and Animal Models: Are 3D Cultures the Ideal Tool to Study Cancer-Microenvironment Interactions? *Int J Mol Sci.* 19(1):181.

Hsueh YP (2006) The role of the MAGUK protein CASK in neural development and synaptic function. *Curr Med Chem.* 13(16)1915-1927.

Hubbard SR (1999) Structural analysis of receptor tyrosine kinases. *Progress in Biophysics and Molecular Biology.* 71 (3–4): 343–58.

Huges CS, Postovit LM, Lajoie GA (2010) Matrigel: a complex protein mixture required for optimal growth of cell culture. *Proteomics.* 10 (9):1886-1890.

Indra B, Matsunaga K, Hoshino O, Suzuki M, Ogasawara H, Muramatsu I, Taniguchi T, and Ohizumi Y (2002) (1/-)-Domesticine, a novel and selective a1D-adrenoceptor antagonist in animal tissues and human a1-adrenoceptors. *Eur J Pharmacol* 445:21–29.

Ivanova S, Gregorc U, Vidergar N, Javier R, Bredt DS, Vanderbeele P, Pardo J, Simon MM, Turk V, Banks L, Turk B (2011) MAGUKS, scaffolding proteins at cell junctions, are substrates of different proteases during apoptosis. *Cell Death and Disease*. 2:e116.

Ivarsson Y, Arnold R, McLaughlin M, Nim S, Joshi R, Ray D, Liu B, Teyra J, Pawson T, Moffat J, Li SSC, Kim PM (2014). Large-scale interaction profiling of PDZ domains through proteomic peptide-phage display using human and viral phage peptidomes. *Proc Natl Acad Sci USA* 111(7):2542-2547.

Ivarsson Y, Wawrzyniak AM, Kashyap R, Polanowska J, Betzi S, Lembo F, Vermeiren E, Chiheb D, Lenfant N, Morelli X, Borg JP, Reboul J, Zimmermann P (2013). Prevalence, Specificity, and Determinants of Lipid-Interacting PDZ Domains from an In-Cell Screen and *in vitro* Binding Experiments. *PLOS One.* 8(2):e54581.

Jastrzebska B (2014). GPCR – G protein complexes – the fundamental signaling assembly. *Amino Acids.* 45(6).

Jemal A, Siegel R, Xu J, Ward E (2010) Cancer Statistics 2010. *CA Cancer J Clin.* 60:277-300.

Jensen BC, O'Connell TD, and Simpson PC (2011) a-1-adrenergic receptors: targets for agonist drugs to treat heart failure. *J Mol Cell Cardiol* 51:518–528.

Jensen BC, Swigart PM, Simpson PC (2009) Ten commercial antibodies for alpha-1-adrenergic receptor subtypes are nonspecific. *Naunyn-Schmiedeberg's Archives of Pharmacology.* 379 (4):409-412.

Jung D, Yang B, Meyer J, Chamberlain JS, Campbell KP (1995) Identification and characterization of the dystrophin anchoring site on beta-dystroglycan. *J Biol Chem.* 270(45)27305-27310.

Kallay LM, McNickle A, Brennwald PJ, Hubbard AL, Braiterman LT (2006). Scribble associates with two polarity proteins, Lgl2 and Vangl2, via distinct molecular domains. *J Cell Biochem* 99(2):647-664.

Kenny BA, Chalmers DH, Philpott PC, and Naylor AM (1995) Characterization of an a1D-adrenoceptor mediating the contractile response of rat aorta to noradrenaline. *Br J Pharmacol* 115:981–986.

Kenny BA, Miller AM, Williamson IJ, O'Connell J, Chalmers DH, and Naylor AM (1996) Evaluation of the pharmacological selectivity profile of a1 adrenoceptor antagonists at prostatic a1 adrenoceptors: binding, functional and in vivo studies. *Br J Pharmacol* 118:871–878.

Kim DH, Xing T, Yang Z, Dudek R, Lu Q, Chen YH (2017) Epithelial Mesenchymal Transition in Embryonic Development, Tissue Repair, and Cancer: A Comprehensive Overvew. *J Clin Med.* 7(1):1.

Kountz TS, Lee KS, Aggarwal-Howarth S, Curran E, Park JM, Harris DA, Stewart A, Hendrickson J, Camp ND, Wolf-Yadlin A, et al. (2016) Endogenous N-terminal domain cleavage modulates a1D-adrenergic receptor pharmacodynamics. *J Biol Chem* 291:18210–18221.

Kyprianou N, Vaughan TB, and Michel MC (2009) Apoptosis induction by doxazosin and other quinazoline a1-adrenoceptor antagonists: a new mechanism for cancer treatment? *Naunyn Schmiedebergs Arch Pharmacol* 380:473–477.

Lagerstrom MC and Schioth HB (2008) Structural diversity of G protein-coupled receptors and significance for drug discovery. *Nat Rev Drug Disc.* 7:339-357.

Lahuna O, Quellari M, Achard C, Nola S, Méduri G, Navarro C, Vitale N, Borg JP, Misrahi M (2005). Thyrotropin receptor trafficking relies on the hScrib–βPIX–GIT1–ARF6 pathway. *EMBO J* 24(7):1364-1374.

Lamkin DM, Sung HY, Yang GS, David JM, Ma JCY, Cole SW, Sloan EK (2016) α2-adrenergic blockade mimics the enhancing effect of chronic stress on breast cancer progression. *Phsychoneuroendocrinology.* 51:262-270.

Lamouille S, Xu J, Derynck R (2014) Molecular mechanisms of epithelial-mesenchymal transition. *Nat Rev Mol Cell Biol.* 15(3):178-196.

Larson B (2015) 3D Cell Culture: A Review of Current Techniques. *Biotek*.

Lee HJ and Zheng JJ (2010) PDZ Domains and their binding partners: structure, specificity, and modification. *Cell Com and Sign.* 8:8.

Lee S, Fa S, Makarova O, Straight S, Margolis, B (2002) A novel and conserved protein-protein interaction domain of mammalian Lin-2/CASK binds and recruits SAP97 to the lateral surface of epithelia. *Mole Cell Biol* 22(6):1778-1791.

Lefkowitz RJ, Rockman HA, and Koch WJ (2000) Catecholamines, cardiac β-adrenergic receptors, and heart failure. *Circulation* 101:1634–1637.

Lepor, H (2007) Alpha Blockers for the Treatment of Benign Prostatic Hyperplasia. *Rev Urol.* 9(4):181-190.

Lin EL, Jeyifous O, Green WN (2013) CASK Regulates SAP97 Conformation and Its Interactions with AMPA and NMDA Receptors. *Journal of Neuroscience.* 33:12067-12076.

Liu H, Enyeart JA, and Enyeart JJ (2007) Potent inhibition of native TREK-1 K1 channels by selected dihydropyridine Ca21 channel antagonists. *J Pharmacol Exp Ther* 323:39–48.

Liu J, Julnes PS, Chen J, Ehrlich S, Walton E, Calhoun VD (2015). The association of DNA methylation and brain volume in healthy individuals and schizophrenia patients. *Schizophr Res* 169:447-452.

Lozovatsky L, Abayasekara N, Piawah S, Walther Z (2009) CASK Deletion in Intestinal Epithelia Causes Mislocalization of LIN7 and hDLG1/SCRIB Polarity Complex without Affecting Cell Polarity. *Molecular Biology of the Cell.* 20:4489-4499.

Lu'o'ng KVQ and Nguyen LTH (2012). The roles of beta-adrenergic receptors in tumorigenesis and the possible use of beta-adrenergic blockers for cancer treatment: possible genetic and cell-signaling mechanisms. *Cancer Manag Res.* 4:431-445.

Lyssand JS, DeFino MC, Tang XB, Hertz AL, Feller DB, Wacker JL, Adams ME, and Hague C (2008) Blood pressure is regulated by an a1D-adrenergic receptor/dystrophin signalosome. *J Biol Chem* 283:18792–18800.

Lyssand JS, Whiting JL, Lee KS, Kastl R, Wacker JL, Bruchas MR, Miyatake M, Langeberg LK, Chavkin C, Scott JD, et al. (2010) Alpha-dystrobrevin-1 recruits alpha-catulin to the alpha1D-adrenergic receptor/dystrophin-associated protein complex signalosome. *Proc Natl Acad Sci USA* 107:21854–21859.

Martin DJ, Lluel P, Guillot E, Coste A, Jammes D, and Angel I (1997) Comparative a-1 adrenoceptor subtype selectivity and functional uroselectivity of a-1 adrenoceptor antagonists. J *Pharmacol Exp Ther* 282:228–235.

Marucci G, Angeli P, Buccioni M, Gulini U, Melchiorre C, Sagratini G, Testa R, and Giardinà D (2005) (1)-Cyclazosin, a selective a1B-adrenoceptor antagonist: functional evaluation in rat and rabbit tissues. *Eur J Pharmacol* 522:100–107.

Masur K, Niggemann B, Zanker KS, and Entschladen F (2001) Norepinephrineinduced migration of SW 480 colon carcinoma cells is inhibited by b-blockers. *Cancer Res* 61:2866–2869.

Mauriac H, Casquillias GV, Pannetier C (2017) Introducing Organs on a Chip. *Elveflow.*

Michel MC, Hanft G, Brob G (1994) Radioligand binding studies of a1 adrenoceptor subtypes in rat heart. *British Journal of Pharmacology.* 111:533-538.

Miller JL (2000) Doxazosin dropped from ALLHAT study. *Am J Health Syst Pharm* 57 8:718.

Molinoff PB (1984) Alpha- and beta-adrenergic receptor subtypes, properties, distribution, and regulation. *Drugs.* 28(2):1-15.

Moniotte S Vaerman JL, Knockx MM, Larrouy D, Langin D, Noirhomme P, Balligand JL (2001) Real-time RT-PCR for the detection of b-adrenoceptor messenger RNAs in small human endomyocardial biopsies. *Journal of Molecular Cellular Cardiology.*33:2121-2133.

Morrow AL and Creese I (1986) Characterization of a1-adrenergic receptor subtypes in rat brain: a reevaluation of [3H]WB4104 and [3H]prazosin binding. *Mol Pharmacol* 29:321–330.

Muller CE, Schiedel AC, Baqi Y (2012) Allosteric modulators of rhodopsin-like G protein-coupled receptors: Opportunities in drug development. *Elsevier.* 135:292-315.

Muramatsu I, Ohmura T, Kigoshi S, Hashimoto S, and Oshita M (1990) Pharmacological subclassification of a1-adrenoceptors in vascular smooth muscle. *Br J Pharmacol* 99:197–201.

Muramatsu I, Takita M, Suzuki F, Miyamoto S, Sakamoto S, and Ohmura T (1996) Subtype selectivity of a new a1-adrenoceptor antagonist, JTH-601: comparison with prazosin. *Eur J Pharmacol* 300:155–157.

Muramatsu I, Taniguchi T, and Okada K (1998) Tamsulosin: a1-adrenoceptor subtype-selectivity and comparison with terazosin. *Jpn J Pharmacol* 78:331–335.

Noble AJ, Chess-Williams R, Couldwell C, Furukawa K, Uchyiuma T, Korstanje C, and Chapple CR (1997) The effects of tamsulosin, a high affinity antagonist at functional a1A- and a1D-adrenoceptor subtypes. *Br J Pharmacol* 120:231–238.

Nix SL, Chishti, AH, Anderson JM, Walther Z (2000) hCASK and hDlg Associate in Epithelia and Their Src Homology 3 (SH3) and Guanylate Kinase (GuK) Domains Participate in Both Intramolecular and Intermolecular Interactions. *Journal of Biological Chemistry.* 275, 41192-41200.

O'Brien LE, Zegers MMP, Mostov KE (2002) Building epithelial architecture: insights from three-dimensional culture models. *Nat Rev Mol Cell Biol*. 3:531-537.

O'Connell TD, Swigart PM, Rodrigo MC, Ishizaka S, Joho S, Turnbull L, Tecott LH, Baker AJ, Foster E, Grossman W (2006) a1-adrenergic receptors prevent a maladaptive cardiac response to pressure overload. *J Clin Invest* 116:1005–1015.

Olefsky JM (2001). Nuclear receptor minireview series. *The Journal of Biological Chemistry.* 276 (40): 36863–4.

Olson VG, Rockett HR, Reh RK, Redila VA, Tran PM, Venkov HA, DeFino MC, Hague C, Peskind ER, Szot P, Raskind MA (2011). The role of norepinephrine in differential response to stress in an animal model of posttraumatic stress disorder. *Biol Psychiatry* 70(5):441-448.

Overington JP, Al-Lazikani B, Hopkins AL (2006). How many drug targets are there? *Nat Rev Drug Discov* 5(12):993.

Papay R, Zuscik MJ, Ross SA, Yun J, McCune DF, Gonzalez-Cabrera P, Gaivin R, Drazba J, and Perez DM (2002) Mice expressing the a(1B)-adrenergic receptor induces a synucleinopathy with excessive tyrosine nitration but decreased phosphorylation. *J Neurochem* 83:623–634.

Parkin DM, Bray F, Ferlay J, Piuni P (2005) Gloal cancer statistics, 2002. *CA Cancer J Clin.* 55:74-108.

Partin JV, Anglin IE, and Kyprianou N (2003) Quinazoline-based a1-adrenoceptor antagonists induce prostate cancer cell apoptosis via TGF-b signalling and IkBa induction. *Br J Cancer* 88:1615–1621.

Pavlos NJ and Friedman PA (2018) GPCR Singaling and Trafficking: The Long and Short of It. *Trends Endocrinol Metab.* 28(3):213-226.

Pérez-Sayáns M, Somoza-Martín JM, Barros-Angueira F, Diz PG, Gándara Rey JM, and García-García A (2010) b-adrenergic receptors in cancer: therapeutic implications. *Oncol Res* 19:45–54.

Perez DM (2006). The adrenergic receptors in the 21st century. *Humana Press.* 54: 129–134

Perez DM and Doze VA (2011) Cardiac and neuroprotection regulated by α1-adrenergic receptor subtypes. *Journal of Receptor Signaling and Transduction Research.* 31(2):98-110.

Petersen RL (2017) Strategies Using Bio-Layer Interferometry Biosensor Technology for Vaccine Research and Development. *Biosensors.* 7(4):49.

Piascik MT and Peres DM (2001) α_1-Adrenergic Receptors: New Insights and Directions. *Hourn of Pharm and Exp Ther.* 298(2):403-410.

Pieczynski J, Margolis B (2011) Protein Complexes that control renal epithelial polarity. *American Journal of Physiological Renal Physiology.* 300(3):F589-601.

Piller LB, Davis BR, Cutler JA, Cushman WC, Wright, Jr JT, Williamson JD, Leenen FH, Einhorn PT, Randall OS, Golden JS, et al. The ALLHAT Collaborative Research Group (2002) Validation of heart failure events in the antihypertensive and lipid lowering treatment to prevent heart attack trial (ALLHAT) participants assigned to doxazosin and chlorthalidone. *Curr Control Trials Cardiovasc Med* 3:10.

Powe DG, Voss MJ, Zänker KS, Habashy HO, Green AR, Ellis IO, and Entschladen F (2010) b-blocker drug therapy reduces secondary cancer formation in breast cancer and improves cancer specific survival. *Oncotarget* 1:628–638.

Rains SL, Amaya CN, Bryan BA (2017) Beta-adrenergic receptors are expressed across diverse cancers. *Onvoscience.* 4(7-8):95-105.

Raskind MA, Peskind ER, Chow B, Harris C, Davis-Karim A, Holmes HA, Hart KL, McFall M, Mellman TA, Reist C, Romesser J, Rosenheck R, Shih MC, Stein MB, Swift R, Gleason T, Lu Y, Huang GD (2018) Atrial of Prazosin for Post-Traumatic Stress Disorder in Military Veterans. *N Engl J Med.* 378(6):507-517.

Ring AM, Manglik A, Kruse AC, Enos MD, Weis WI, Garcia KC, Kobilka BK (2014) Adrenaline-activated structure of the β2-adrenoceptor stabilized by an engineered nanobody. *Nature.* 502(7472):575-579.

Rodriguez-Boulan E, Nelson WJ (1989) Morphogenesis of the polarized epithelial phenotype. *Science.* 245(4919):718-725.

Romero G, von Zastrow M, Friedman PA (2011). Role of PDZ proteins in regulating trafficking, signaling, and function of GPCRs: means, motif, and opportunity. *Adv Pharmacol* 62:279-314.

Rosenbaum DM, Rasmussen SGF, Koblika BK (2009) The structure and function of G-protein-coupled receptors. *Nature.* 459(7245):356-363.

Ritter SL, Hall RA (2009). Fine-tuning of GPCR activity by receptor-interacting proteins. *Nat Rev Mol Cell Biol* 10(12):819.

Schröder R, Janssen N, Schmidt J, Kebig A, Merten N, Hennen S, Müller A, Blättermann S, Mohr-Andrä M, Zahn S, et al. (2010) Deconvolution of complex G protein-coupled receptor signaling in live cells using dynamic mass redistribution measurements. *Nat Biotechnol* 28:943–949.

Schmitz JM, Graham RM, Sagalowsky A, Pettinger WA (1981) Renal alpha-1 and alpha-2 adrenergic receptors: biochemical and pharmacological correlations. *The Journal of Pharmacology and Experimental Therapeutics.* 219 (2): 400–6.

Schwinn DA, Price DT, Narayan P (2009) α1-Adrenoceptor Subtype Selectivity and Lower Urinary Tract Symptoms. *Mayo Clinic Proceedings.* 79(11):1423-1434.

Simon PY and Rousseau PF (2017) Treatment of Post-Traumatic Stress Disorders with the Alpha-1 Adrenergic Receptor Antagonist Prazosin. *Can J Psychiatry* 62(3)186-198.

Small KM, McGraw DW, Liggett SB (2003) Pharmacology and Physiology of Human Adrenergic Receptor Polymorphisms. *Annual Review of Pharmacology Toxicology.* 43:381-411.

Smet FD, Christopoilos A, Carmeliet P (2014). Allosteric Targeting of receptor tyrosine kinases. *Nature Biotech.* 32:1113-1120.

Sorski L, Melamed R, Matzner P, Lavon H, Shaashua L, Rosenne E, and Ben-Eliyahu S (2016) Reducing liver metastases of colon cancer in the context of extensive and minor surgeries through b-adrenoceptors blockade and COX2 inhibition. *Brain Behav Immun* 58:91–98.

Sriram K and Insel P (2018). GPCRs as targets for approved drugs: How many targets and how many drugs? *Mol Phar Fast For.* 1-23.

Stam WB, Van der Graaf PH, and Saxena PR (1999) Analysis of a1L-adrenoceptor pharmacology in rat small mesenteric artery. *Br J Pharmacol* 127:661–670.

Stone RC, Pastar I, Ojeh N, Liu S, Garzon KI, Tomic-Canic M (2016) Epithelial-mesenchymal transition in tissue repair and fibrosis. *Cell Tissue Res.* 365(3):495-506.

Strosberg AD (1993) Structure, function, and regulation of adrenergic receptors. *Protein Science.* 2:1198-1209.

Tallarida RJ and Murray RB (1987) pA2 Analysis 1: Schild Plot. *Manual of Pharmacologic Calculations.* 53-56.

Thiery JP, Acloque H, Haung RYJ, Nieto MA (2009). Epithelial-Mesenchymal Tranisitions in Development and Disease. *Cell* 139(6):871-890.

Torp KD, Tschakovsky ME, Halliwill JR, Minson CT, and Joyner MJ (2001) b-Receptor agonist activity of phenylephrine in the human forearm. *J Appl Physiol* (1985) 90:1855–1859.

Tsunoda S, Sierralta J, Sun Y, Bodner R, Suzuki E, Becker A, Socolich M, Zuker CS (1997). A multivalent PDZ-domain protein assembles signaling complexes in a G-protein-coupled cascade. *Nature* 388(6639):243.

Ustyugov AA, Chicheva MM, Lysikova EA, Vikhareva EA, Sipyagina NA, Malkova AN, Straumal EA, Bovina EV Senatov FS, Salimon AI, Maksimkin AV, Lermontov SA (2010) Development of 3D Cell Culture on Ultra High Molecular Weight Polyethylene (UHMWPE) as the Basis of Cellular Matrix. *Biom Chem Res Meth.* 1(3):e00048.

Van der Graaf PH, Deplanne V, Duquenne C, and Angel I (1997) Analysis of a1-adrenoceptors in rabbit lower urinary tract and mesenteric artery. *Eur J Pharmacol* 327:25–32.
Venkatakrishnan AJ, Deupi X, Lebon G, ate CG, Schertler GF, Babu MM (2013) Molecular signatures of G Protein-Coupled Receptors. *Nature.* 494:185-194

Wagner J, Endoh M, and Reinhardt D (1974) Stimulation by phenylephrine of adrenergic a- and b-receptors in the isolated perfused rabbit heart. *Naunyn Schmiedebergs Arch Pharmacol* 282:307–310.

Wang BH, Du XJ, Autelitano DJ, Milano CA, and Woodcock EA (2000) Adverse effects of constitutively active a(1B)-adrenergic receptors after pressure overload in mouse hearts. *Am J Physiol Heart Circ Physiol* 279:H1079–H1086.

Weis WI and Kobilka BK (2018) The Molecular Basis of G Protein–Coupled Receptor Activation. *Annual Review of Biochemistry.* 87:897-919.

Wells A, Yates C, Shepard CR (2013) E-Cadherin as an indicator of mesenchymal to epithelial recerting transitions during the metastatic seeding of disseminated carcinomas. *Clin Exp Metastasis.* 25(6):621-628.

Wheatley M, Wootten D, Conner MT, Simms J, Kendrick R, Logan RT, Poyner DR, Barwell J (2011) Lifting the lid on GPCRs: the role of extracellular loops. *British Jour of Pharm.* 165:1688-1703.

Yamamoto Y and Koike K (2001) Characterization of a1-adrenoceptor-mediated contraction in the mouse thoracic aorta. *Eur J Pharmacol* 424:131–140.

Yi S, Ding F, Gong L, Gu X (2017) Extracellular matrix scaffolds for Tissue Engineering and Regenerative Medicine. *Curr Stem Cel Res Ther* 12(3):233-246.

Zhang B, Korolj A, Lai BFLL, Radisic M (2018) Advances in organ-on-a-chip engineering. *Nature Reviews Materials.* 3:257-278.

Zhao L, Xu J, Liang F, Li A, Zhang Y, and Sun J (2015) Effect of chronic psychological stress on liver metastasis of colon cancer in mice. *PLoS One* 10:e0139978.

Zhao X, Zhang Y, Leander M, Li L, Wang G, Emmett N (2014) Altered Expression Profile of Renal a1D-Adrenergic Receptors in Diabetes and Its Modulation by PPAR Agonists. *J Diabetes Res* 725634.

Zhu J, Shang Y, Wan Q, Xia Y, Chen J, Du Q, Zhang M (2014). Phosphorylation-dependent interaction between tumor suppressors Dlg and Lgl. *Cell Res* 24(4):451-463.

Zuscik MJ, Sands S, Ross SA, Waugh DJ, Gaivin RJ, Morilak D, and Perez DM (2000) Overexpression of the a1B-adrenergic receptor causes apoptotic neurodegeneration: multiple system atrophy. *Nat Med* 6:1388–1394.

Zwick E, Bange J, Ullrich A (2001). Receptor tyrosine kinase signaling as a target for cancer intervention strategies. *Endocrine-Related Cancer.* 8 (3): 161–73.

Curriculum Vitae

Education

September 2015 - Present	University of Washington, Seattle, WA Ph.D. Pharmacology (Expected June 2019)
September 2011 - June 2015	University of Washington, Seattle, WA B.S. Neurobiology

Research Experience

September 2015-Present	Department of Pharmacology. Dr. Chris Hague. Focus in Neuroendocrine and Cardiovascular Pharmacology. Previously undiscovered α_{1B}ARs are present in SW480 colorectal cancer cell lines and lead to increased survivability of the cells. Elucidating the architecture of the α_{1D}AR interacting proteins yields the hDLG1 complex as a potential transport protein complex and SCRIBBLE as a scaffolding protein. Differences between 2D and 3D cell culture modeling shows altered receptor localization as well as pharmacodynamics.
September 2012-June 2015	Department of Pharmacology. Dr. Chris Hague. Focus in Neuroendocrine and Cardiovascular Pharmacology. Lymphocytes can be used as a diagnostic for Pregnancy Induced Hypertension using the Label-Free EPIC Dynamic Mass Redistribution. Determining the importance of the PDZ ligand on the 5HT2A and 5HT2C serotonin receptors in signaling. Determining the importance of the PDZ ligand on the α_{1D}AR adrenergic receptor in signaling.
Summer 2012	Department of Bioengineering. Dr. Richard To. Using siRNA to counteract antibiotic resistance in prokaryotic cells.

Conferences

November 2018	Graduate Program for Leaders in Life Innovation, Joint Conference with University of Tokyo and University of Washington. "Label Free Dynamic Mass Redistribution Identifies Low Density Adrenergic Receptors in Cancer Cells." (Oral).
October 2014	23rd Annual McNair Scholars Research Conference Milwaukee, WI. "Characterizing the Role of the PDZ-Binding Motif of Serotonin Receptors in vitro." (Oral).
August 2015	Mary Gates Undergraduate Summer Research Symposium. Seattle, WA. "Using Human Lymphocytes as Diagnostic Tools to Predict Anti-Hypertensive Therapeutic Efficacy for Pregnancy-Induced Hypertension." (Poster).
November 2013	Annual Biomedical Research Conference for Minority Students (ABRCMS) Nashville, TN. "Characterizing the Role of the PDZ-Binding Motif of Adrenergic Receptors in vitro." (Poster)
August 2012	Mary Gates Undergraduate Summer Research Symposium Seattle, WA. "Counteracting Antibiotic Resistance with RNA Interference in Prokaryotic Cells." (Poster).

September 2014	First Monash University Virtual International Undergraduate Research Conference Organized by Monash University, Australia. Session Organizer/Moderator.

Teaching Experience

Autumn 2016-Winter 2018	Teaching Assistant. "Pharmacology 401 and 402: General Pharmacology for Pharmacy Students." University of Washington, Seattle, WA.
Winter 2012-2017	Main Guest Lecturer. "Research Experience: A Comprehensive Overview of Molecular Biology and Pharmacology." Archbishop Murphy AP Biology Lecture, Everett WA.
Autumn 2013-June 2015	Assistant Guest Lecturer. "Undergraduate Research and the Undergraduate Research Program." University of Washington Outreach, Seattle, WA.
Autumn 2013-June 2015	Teaching Assistant. "Biology 106: How to Survive and Succeed in the Biology Series." University of Washington, Seattle, WA.
Autumn 2014	Teaching Assistant. "AP Chemistry." Garfield High School, Seattle, WA.
Spring 2014	Invited Talk. "Cockroach Mechanosensory Spine Response to Complex Waveforms." University of Washington Neurobiology 302. Seattle, WA.
Winter 2013	Invited Talk. "Cadmium Chloride Poisoning of the 3rd Nerve in Crayfish." University of Washington Neurobiology 301. Seattle, WA.
Spring 2013	Main Guest Lecturer. "How to Influence Life, A Career in Biomedical Research." Main Guest Lecturer. Archbishop Murphy Career Day, Everett, WA.

University/Laboratory Service

Autumn 2018-Present	Curriculum Committee Member. Restructure the current curriculum for the Pharmacology Ph.D. students as well as bring in alternative teaching opportunities to said students.
Autumn 2016-Present	Autoclave Technician. Monitor the autoclave and its functionality. Organize autoclave times with other laboratories.
Autumn 2016-Present	Laboratory Manager. Responsible for general upkeep of the laboratory, including maintenance of Environmental Health and Safety protocols. Train new undergraduates. Responsible for ordering. Organize and maintain various aspect of the laboratory including plasmids, cells in liquid nitrogen, chemicals, etc.
Winter 2013-Present	Radiation Safety Surveyor. Due to our laboratory performing radioligand binding assays, it is necessary to determine if there is contamination due to the radioactive materials used.

Mentoring Experience

Autumn 2018-Present	Outreaching Grads (OGs) Mentor. Assisted with encouraging potential graduate students to come to the University of Washington. Focus was in the diversity and community for minority students.
Autumn 2017-Present	Graduate Peer Mentor. Mentored incoming graduate students navigate the first year of graduate school and their upcoming general and oral exams.

Autumn 2016-Present	Undergraduate Mentor. Mentored 7 undergraduates that came through the laboratory. Assisted with applications to majors, the McNair Program, and the Undergraduate Research Program. Also assisted with applications and mentoring in regard to medical school, pharmacy school, and graduate school.
Autumn 2015-Present	Inspiring Girls Now in Technology, Engineering, and STEM (IGNITEs). Presented to women from kindergarten through high school about research, science, engineering, technology, and overcoming adversity.
Autumn 2013-Present	Undergraduate Research Program Mentor. As an undergraduate, I interacted with about 500 undergraduate students by giving presentations on how to become involved in research, leading to 100+ newly recruited students. As a graduate student, I present to the Undergraduate Research Leaders (URLs) on graduate school, what to expect, how to prepare, and what life is like as a graduate student. I also assist with administration tasks relating to preparation of the Undergraduate Symposium in May.
Autumn 2014-Summer 2015	Making Connections Mentor. One-on-one mentor with a high school student to assist with tutoring, applications to college, and guidance through high school and into college.

Publications and Manuscripts in Review

Janezic EM, **Harris DA**, Dinh D, Lee KS, Marsh N, Hinds TR, Hsu PL, Zheng N, Hague C (2019). "Structure-function analyses reveal Scribble PDZ4 stabilizes α1D-AR in cell membranes." J Biol Chem. In review.

Harris DA, Park JM, Lee KS, Xu C, Stella N, Hague C (2017). "Label-free dynamic mass redistribution reveals low-density, pro survival alpha1B-adrenergic receptors in human SW480 colon carcinoma cells." J Pharmacol Exp Ther 361(2): 219-228.

Kountz TS, Lee KS, Aggarwal-Howarth S, Curran E, Park JM, **Harris DA**, Stewart A, Hendrickson J, Camp ND, Wolf-Yadlin A, Wang EH, Scott JD, Hague C (2016). "Endogenous N-terminal domain cleavage modulates alpha1D-adrenergic receptor pharmacodynamics." J Biol Chem 291(35):18210-21.

Camp ND, Lee KS, Cherry A, Wacker-Mhyre JL, Kountz TS, Park JM, **Harris DA**, Estrada M, Stewart A, Stella N, Wolf-Yadlin A, Hague C (2016). "Dynamic Mass Redistribution Reveals Diverging Importance of PDZ-ligands for G Protein-coupled Receptor Pharmacodynamics." Pharmacological Research 105: 13-21.

O'Connor S, Bess J, Cooper B, Cordova-Danchez A, **Harris DA**, Jeong C, Stella N, Mendez S (2016). Concerning Cannabis-Infused Edibles: Factors That Attract Children to Foods. Prepared for the Washington State Liquor and Cannabis Board.

Camp ND, Lee KS, Wacker-Mhyre JL, Kountz TS, Park JM, **Harris DA**, Estrada M, Stewart A, Wolf-Yadlin A, Hague C (2015). "Individual Protomers of a G Protein-coupled Receptor Dimer Integrate Distinct Functional Modules." Cell Discov. Cell Discovery 1: 15011.

Harris DA, Karlova Y, Hague C (2015). "Using Human Lymphocytes as Diagnostic Tools to Predict Anti-Hypertensive Therapeutic Efficacy for Pregnancy-Induced Hypertension." The McNair Scholars Journal of the University of Washington, 15.

Harris DA, Estrada M, Hague C (2014). "Characterizing the Role of the PDZ-Binding Motif of Serotonin Receptors *in vitro*." The McNair Scholars Journal of the University of Washington, 14.

Honors and Awards

September 2018-June 2019	Graduate Opportunities and Minority Participation (GO-MAP) Dissertation Year Funding (Tuition and Stipend)
June 2016- June 2018	Pharmacological Sciences Training Grant (Tuition and Stipend)
September 2015-June 2016	GO-MAP Introductory Year Funding (Tuition and Stipend)
September 2014-June 2015	Ronald E. McNair Undergraduate Diversity Fellowship ($2,500/quarter)
September 2013-June 2015	Washington State Opportunity Scholarship
September 2011-June 2015	Walton Family Foundation Scholarship ($12,000 over 4 years)
September 2011-June 2015	Everett Rotary Scholarship for Aspiring Scientists ($15,000 over 4 years)
September 2011-June 2015	Jimmy Dean Military Memorial Scholarship – 4 Time Winner (2,000/year)
September 2011-June 2014	Initiative for Maximizing Student Diversity (IMSD) BootCamp (2 week college prep), TeachLab (laboratory assistant prep), and Summer Internship (Housing and Stipend)

Technical Experience

Molecular Genetics and Biochemistry: Cloning, DNA Purification, Protein Purification, CRISPR/Cas 9 Technology, RNAi Experience.

Tissue Culture: Stable cell line generation, transfections, cell maintenance, ICC, EPIC Dynamic Mass Redistribution, Cell imaging, Matrigel Technology, Spheroid Microplate.

Behavior: Forced swim test, intraperitoneal injections, perfusions, rat surgeries.

Professional Societies

September 2015-Present	Science and Engineering Business Association (SEBA), Member
September 2011-Present	Women in Science and Engineering (WiSE), Member

September 2013-June 2015	Grey Matters Undergraduate Neuroscience Journal, Editor/Photographer/Event Planner
September 2011-June 2015	Louis Stokes Alliances for Minority Participation (LSAMP), Member

Volunteer Experience

Summer 2010-Present	Veterans of Foreign Wars (VFW) Ladies Auxiliary Lifetime Member. Assisted with setting up and taking down of Veteran's Affairs. Visited veterans in hospitals. Presented on VA benefits and how to get involved. Assisted in organizing and setting up parties (Christmas/4 of July) for soldiers and their families.